

- I. THE HEPTACYANOMOLYBDATE(III) ION: SPECTROSCOPIC AND MAGNETIC PROPERTIES AND CHEMICAL REACTIVITY.
- II. SPECTROSCOPIC AND MAGNETIC STUDIES OF MONOMERIC AND DIMERIC  $d^5$  SYSTEMS.
- III. SPECTROSCOPIC AND MAGNETIC STUDIES OF POLYMERIC OXO- AND HYDROXOBRIDGED SYSTEMS.

Thesis by  
George Robert Rossman

In Partial Fulfillment of the Requirements  
for the Degree of  
Doctor of Philosophy

California Institute of Technology  
Pasadena, California  
1971

(Submitted February 26, 1971)

## ACKNOWLEDGMENT

The contributions of numerous members of the Caltech community are appreciated and are specifically referenced at various points in the text. A particularly large contribution to this work has come from H. J. Schugar, who, while supplying compounds, effort, data, steaks, and Tootsie Rolls, has worked closely with the author in the accumulation and interpretation of the data relating to the  $d^5$  systems. The keen interest and ideas of Professor H. B. Gray have likewise had major impact during the course of these investigations. The National Science Foundation is acknowledged for providing Graduate fellowship support throughout the period of this work.

## ABSTRACT

Heptacyanomolybdate(III), isolated as the potassium salt,  $K_4Mo(CN)_7 \cdot 2H_2O$  has been studied by infrared, raman, ESR, magnetic susceptibility, optical spectral, and x-ray techniques. Solutions of the ion have been identified as having a seven-coordinate pentagonal bipyramidal structure, while the structure in the solid potassium salt has been proposed to be a capped trigonal prism. The anhydrous potassium salt,  $K_4Mo(CN)_7$ , and the hydrated cesium salt,  $Cs_4Mo(CN)_7 \cdot xH_2O$  also assume the pentagonal bipyramidal geometry. The molecule is chemically reactive, combining readily in solution with oxygen to form  $[Mo(CN)_7OH_2]^{4-}$  and with halogens to form products which when isolated are waxy and presumably polymeric.

Optical spectra have been obtained for four-, five-, six-, and seven-coordinate manganese(II) and iron(III) compounds. These are used as a basis of comparison for interpretation of the detailed optical and magnetic data obtained on the oxobridged iron(III) dimer  $enH_2[(FeHEDTA)_2O] \cdot 6H_2O$ .

The occurrence of simultaneous pair electronic excitations in the dimer is described, and evaluation of the relative merits of the spin-coupling and molecular orbital models for oxobridged dimers is presented. A dihydroxobridged ferric dimer is described as well as a series of dialkoxobridged iron(III) and aluminum dimers derived from metal acetylacetonate and dipivaloylmetane complexes. The extent of antiferromagnetic coupling between the two iron atoms in the dihydroxo-

and the dialkoxobridged iron dimers has been found to be nearly identical through variable temperature magnetic susceptibility studies. The magnetic and infrared studies are extended to include a variety of metal oxides, oxy-hydroxides, and natural and synthetic minerals which have various forms of oxo- and hydroxobridging. The OH infrared bands are identified and in some instances, the LN<sub>2</sub> temperature positions of the band are compared to the room temperature position. Ferritin models and ferritin micelles are compared to these iron polymers, and the similarity of the infrared spectrum of ferric hydroxide to ferritin micelles is discussed.

## TABLE OF CONTENTS

<u>SECTION</u>	<u>TITLE</u>	<u>PAGE</u>
I.	THE HEPTACYANOMOLYBDATE(III) ION: SPECTROSCOPIC AND MAGNETIC PROPERTIES AND CHEMICAL REACTIVITY	
A.	<u>Physical Characterization Studies</u>	1
1.	<u>Introduction</u>	2
	a. Synthesis	2
	b. Physical Measurements	4
3.	<u>Infrared and Raman Spectra</u>	5
4.	X-Ray Structural Studies	17
5.	Magnetic and Electronic Spectral Properties	18
	a. Magnetism	18
	b. ESR	19
	c. Electronic Spectra	19
6.	Tabular Summary of Data	26
7.	References	29
B.	<u>Chemical Characterization Studies</u>	30
1.	Introduction	30
2.	Oxidation of $\text{Mo}(\text{CN})_7^{4-}$	31
3.	pH Dependence of $\text{Mo}(\text{CN})_7^{4-}$ Solutions	35
4.	Photochromism of Aqueous Solutions of $\text{K}_4\text{Mo}(\text{CN})_7 \cdot 2\text{H}_2\text{O}$	36
5.	Oxidative Additions to $\text{Mo}(\text{CN})_7^{4-}$	39
6.	References	42

<u>SECTION</u>	<u>TITLE</u>	<u>PAGE</u>
C.	<u>Appendix--Cyanomolybdate Data</u>	43
D.	<u>Electron Paramagnetic Resonance Spectral Study of Potassium Heptacyanomolybdate(III) Dihydrate</u>	51
II.	SPECTROSCOPIC AND MAGNETIC STUDIES OF MONOMERIC AND DIMERIC $d^5$ SYSTEMS	
A.	<u>Electron Spectral Studies of Iron(III) in a Tetrahedral Oxide-Donor Field</u>	57
B.	<u>Oxobridged Iron(III) Dimers</u>	64
C.	<u>A Dihydroxobridged Iron(III) Dimer</u>	104
D.	<u>Synthesis and Characterization of Dimeric Dialkoxobridged Iron(III) Dimers</u>	113
E.	<u>Simultaneous Pair Electronic Excitations in a Binuclear Iron(III) Complex</u>	139
F.	<u>Electronic Spectra of <math>d^5</math> Manganese(II) and Iron(III) Compounds</u>	147
1.	<u>Introduction</u>	147
2.	<u>Manganese(II)</u>	148
3.	<u>Six-coordinate Iron(III) Compounds</u>	151
4.	<u>Iron(III) EDTA-Type Chelates-- Seven-Coordination</u>	158
5.	<u>References</u>	165

<u>SECTION</u>	<u>TITLE</u>	<u>PAGE</u>
III.	SPECTROSCOPIC AND MAGNETIC STUDIES OF POLYMERIC OXO- AND HYDROXO- BRIDGED SYSTEMS	
	A. <u>Extended Lattice Hydroxobridged Fe(III)</u>	166
	1. <u>Introduction</u>	166
	2. <u>Synthesis of Model Hydroxy-minerals</u>	166
	3. <u>Magnetic Susceptibility Studies</u>	167
	4. <u>Infrared Spectra</u>	168
	5. <u>References</u>	174
	B. <u>Metal Oxides and Hydrous Oxides</u>	175
	1. <u>Introduction</u>	175
	2. <u>Source of Materials</u>	175
	3. <u>Infrared Spectra</u>	176
	4. <u>Relationship of Ferritin to Hydrous Iron to Hydrous Iron Oxides</u>	183
	5. <u>References</u>	192
	C. <u>Optical Spectra of Selected Iron Polymers with an Eye for SPE Transitions</u>	193
IV.	PROPOSITIONS	
	1. The Synthesis of a Vanadium(IV) Dimer for Experimental Testing of Theories of Simultaneous Pair Electronic Excitations	200

<u>SECTION</u>	<u>TITLE</u>	<u>PAGE</u>
2.	An Investigation of the Structural Status of OH in Extended Lattice Compounds	204
3.	An Investigation of the Color Effects in Potassium and Cesium Tetrafluoroborate Solutions	207
4.	Molybdenum Cyanide Sulfide Complexes	209
5.	An Examination of Infrared Intensities of Coordination Compounds	213



# I. THE HEPTACYANOMOLYBDATE(III) ION: SPECTROSCOPIC AND MAGNETIC PROPERTIES AND CHEMICAL REACTIVITY

## A. Physical Characterization Studies

### 1. Introduction

Potassium heptacyanomolybdate(III) dihydrate,  $K_4Mo(CN)_7 \cdot 2H_2O$ , was first reported by Young in 1932,<sup>(1)</sup> but the structure of the compound has remained undetermined and its chemistry has yet to be characterized. The formulated stoichiometry of the compound suggests that it may contain the  $[Mo(CN)_7]^{4-}$  ion and thus be a member of the uncommon class of seven-coordinate compounds. Few seven-coordinate compounds have been prepared that are molecular species which are ligated by a single kind of ligand, and those which have been prepared have been exclusively fluoride complexes such as  $IF_7$ ,  $NbF_7^{3-}$ , etc., which are  $d^0$  or  $d^{10}$  systems, and as such are unavailable for study by a variety of structural techniques. An eight-coordinate formulation,  $[Mo(CN)_7(OH_2)]^{4-}$ , can also be proposed in analogy to the well known  $Mo(CN)_8^{4-}$  and  $Mo(CN)_8^{3-}$  ions. It, however, suffers from the disadvantage of requiring nineteen electrons in outer orbitals and would not be in accord with the eighteen electron "rule". Whatever the coordination number, the possibility of coordination geometry isomerization exists for  $Mo(CN)_7^{4-}$ . Compounds of higher coordination number such as  $Mo(CN)_8^{3-}$ , and particularly  $Mo(CN)_8^{4-}$ , have for some time been known to show this type of isomerization in that they display different geometries in solid and in solution as is evidenced by infrared, raman, and magnetic resonance experiments. The system  $Mo(CN)_7^{4-}$  -

$\text{Mo}(\text{CN})_8^{4-}$  is electronically similar to the chemically reactive and important system  $\text{Co}(\text{CN})_5^{3-} - \text{Co}(\text{CN})_6^{3-}$  and might be expected to display some of the diverse reactions which pentacyanocobaltate(II) undergoes.

To provide a basis for structural discussions of the  $\text{Mo}(\text{CN})_7^{4-}$  ion, the results of infrared, raman, magnetic, and optical data are presented for  $\text{K}_4\text{Mo}(\text{CN})_7 \cdot 2\text{H}_2\text{O}$  and the anhydrous  $\text{K}_4\text{Mo}(\text{CN})_7$ , and preliminary data are included for heptacyanomolybdates of several other cations.

## 2. Experimental

Several batches of  $\text{K}_4\text{Mo}(\text{CN})_7 \cdot 2\text{H}_2\text{O}$  were prepared from  $\text{K}_3\text{MoCl}_6$ ,<sup>(2)</sup> and excess KCN.<sup>(1)</sup> Shiny black flakes of 1-3 mm size and fine, dark olive-green flakes were obtained in various batches. Recrystallization could be accomplished by cooling concentrated solutions in oxygen-free water-ethanol mixtures, and less conveniently by cooling saturated aqueous solutions. Anal. Calcd for  $\text{K}_4\text{Mo}(\text{CN})_7 \cdot 2\text{H}_2\text{O}$ : K, 33.24; Mo, 20.39; C, 17.87; N, 20.84; H, 0.86. Found: K, 33.05; Mo, 20.47; C, 18.05; N, 20.39; H, 0.96.

Anhydrous  $\text{K}_4\text{Mo}(\text{CN})_7$  was prepared from the hydrate by heating it overnight at  $95^\circ$  under high vacuum. It could also be prepared in a finely divided form by lyophilizing aqueous solutions of the dihydrate. Anal. Calcd for  $\text{K}_4\text{Mo}(\text{CN})_7$ : K, 36.00; Mo, 22.08; C, 19.35; N, 22.57; H, 0.00. Found: K, 34.89; Mo, 22.33; C, 19.64; N, 22.22; H, 0.00.

Infrared spectra show that both the hydrated and anhydrous heptacyanides decompose in air to KOH,  $\text{K}_4\text{Mo}(\text{CN})_8$ , and  $\text{K}_2\text{MoO}_4$ .

No evidence for what has been reported<sup>(3)</sup> to be  $\text{KMo}(\text{CN})_5$  has been observed in the oxidation products. Although the solid dihydrate can be briefly exposed to dry air for purposes such as weighing without any sign of decomposition, it was generally handled in a nitrogen purged glovebag and transferred to the appropriate nitrogen-filled containers. In a dry atmosphere, the flakes of the solid readily accumulate static electricity, fly off of spatulas, and stick to nearby objects. The compound is soluble in water and slowly soluble in ethylene glycol but was found to be insoluble in common organic solvents. The solutions are extremely oxygen sensitive. All sample preparations of solutions for physical measurements were done in a high vacuum line. The appropriate amount of degassed water was sublimed onto the solids in the sample vessel and the vessels were then closed either with stop-cocks or by flame sealing under vacuum.

The products of reaction of several cations with  $\text{Mo}(\text{CN})_7^{4-}$  were obtained by simple precipitation reactions. In this manner salts of  $\text{Mn}^{2+}$ ,  $\text{Zn}^{2+}$ ,  $\text{Ag}^+$ , and  $[\text{C}_{10}\text{H}_{21}\text{N}(\text{CH}_2\text{CH}_2)_3\text{NC}_{10}\text{H}_{21}]^{2+}$  were prepared. They are, respectively, black, dirty yellow-green, black, and yellow-green precipitates which have been studied only by infrared spectroscopy. A solution of the barium salt was prepared by the reaction of solutions of a stoichiometric amount of  $\text{Ba}(\text{ClO}_4)_2$  with  $\text{K}_4\text{Mo}(\text{CN})_7$  and centrifugation of the resulting  $\text{KClO}_4$  precipitate near  $0^\circ\text{C}$ . The solution was evaporated to dryness under vacuum to yield a black solid which was redissolved in a minimum volume of lukewarm water and slowly cooled to yield black dendritic crystals. The cesium salt was prepared

by adding water to a 5:1 stiochiometric mixture of solid CsCl and  $K_4Mo(CN)_7 \cdot 2H_2O$  until only a small percentage of the solids remain undissolved. The solution was then warmed slightly until all solids dissolved and cooled at  $4^\circ C$ . The precipitate which looked like largely CsCl was separated from the solution, redissolved in  $H_2O$ , and made to crystallize by the addition of ethanol until the solution was about 30% ethanol by volume and then cooling to  $0^\circ C$ . The dark-green colored fine powder which was obtained was washed with 80% ethanol, ethanol, and ether, and dried briefly under vacuum.

Absorption spectra in the region 210-2500 nm were obtained on a Cary Model 14CMRI spectrophotometer equipped with quartz dewar for immersion of samples into  $LN_2$ .

Infrared spectra were obtained on a Perkin-Elmer 225 spectrophotometer. Pellets and mulls of oxygen-sensitive materials were prepared in nitrogen-purged glovebags in so far as was possible. Solution spectra were obtained from samples dissolved in the vacuum line and transferred to  $N_2$ -filled  $BaF_2$  solution cells with a syringe in a glovebag. Low temperature spectra were obtained in a modified Beckman RIIC VLT-2 unit.

Raman spectra were obtained on a Cary 81 He-Ne laser raman in flame-sealed pyrex solution tubes and with solids on a conical powder holder and protected from slow air oxidation with mineral oil.

Magnetic susceptibility data were taken on a Princeton Applied Research FM-1 vibrating sample magnetometer system equipped with an Andonian Associates variable temperature dewar. System calibrations were performed with  $HgCo(SCN)_4$ .

### 3. Infrared and Raman Spectra

The infrared and raman spectra in the cyanide stretching region of aqueous solutions of  $K_4Mo(CN)_7 \cdot 2H_2O$  both consist of a two-band pattern. The infrared spectra of an approximately 0.2F solution in  $H_2O$  and an approximately 0.12F solution in 0.1F KOH (which helps to prevent photodecomposition) both consist of two bands of near equal intensity ( $\epsilon \approx 900$ ) at 2080 and 2040  $cm^{-1}$  (Figure 1-A). The raman spectrum of aqueous solutions of  $K_4Mo(CN)_7 \cdot 2H_2O$  can be obtained if either cyanide ion or hydroxide ion is added to suppress rapid photodecomposition. These solutions display weak raman emission consisting of two bands of roughly comparable intensity at 2106 and 2063  $cm^{-1}$  (Figure 2-A). The third band at 2079  $cm^{-1}$  in Figure 2-A is emission from the cyanide ion added to suppress photodecomposition and is not present in the spectra of hydroxide-containing solutions which themselves decompose in the laser beam. It is important to note that there are no coincidences between the raman and the infrared bands.

When the number and coincidences of infrared and raman bands of the aqueous solutions are compared with the entries in Table I which lists the predicted number and coincidences of cyanide stretches for various geometries, it is seen that a  $D_{5h}$  pentagonal-bipyramidal structure best explains the experimental data. Two normal stretching modes,  $a_2''$  and  $e_1'$ , are allowed in the infrared, and three modes,  $2a_1'$  and  $e_2'$ , are allowed in the raman. It is only necessary to postulate that two of the three raman bands are very close in energy, or that the missing raman band is of very low intensity. The lack of coincidences

Figure 1. Infrared spectra of the cyanide stretching region of various heptacyanomolybdate(III) salts.

- A)  $\sim 0.2F$   $K_4Mo(CN)_7 \cdot 2H_2O$  in  $H_2O$ , ambient temperature.
- B)  $K_4Mo(CN)_7 \cdot 2H_2O$ . KBr pellet, ambient temperature.
- C)  $K_4Mo(CN)_7 \cdot 2H_2O$ . KBr pellet, near  $80^\circ K$ .
- D)  $K_4Mo(CN)_7$ , anhydrous, KBr pellet, ambient temperature.
- E)  $Cs_4Mo(CN)_7 \cdot xH_2O$ , KBr pellet, ambient temperature.

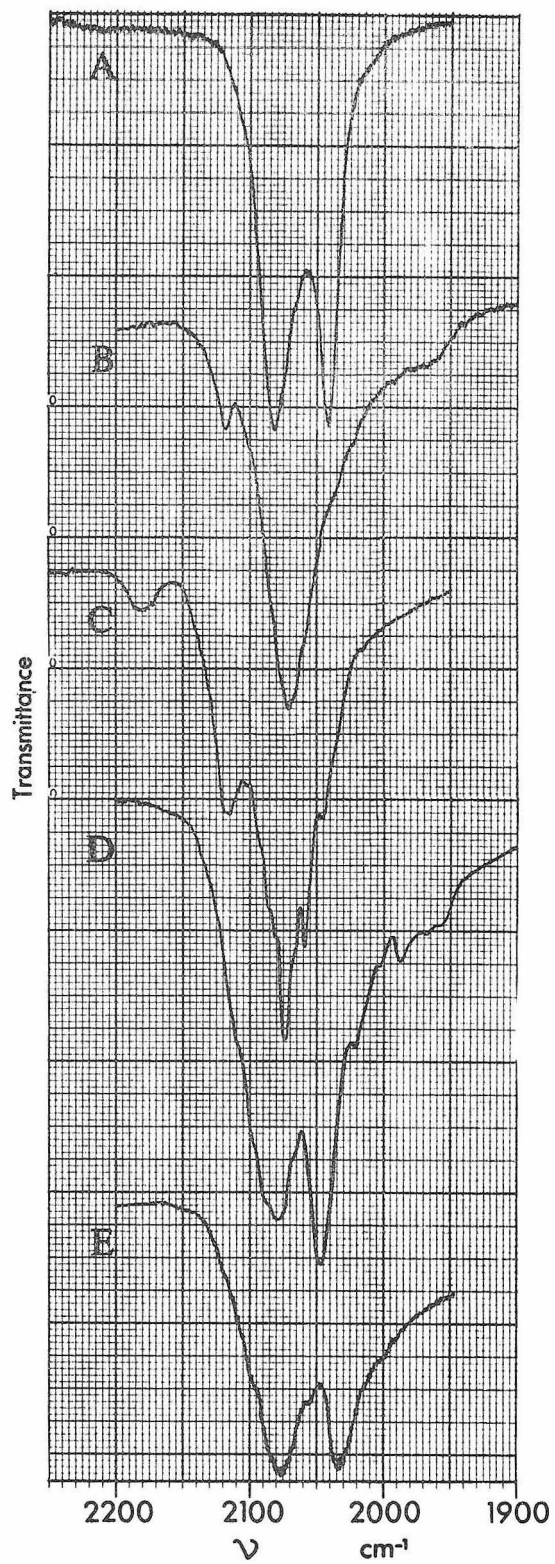


Figure 1

Figure 2. Raman spectra of the cyanide stretching region of potassium heptacyanomolybdate(III).

- A)  $\text{K}_4\text{Mo}(\text{CN})_7 \cdot 2\text{H}_2\text{O}$  estimated to be 0.1F in 0.2F aqueous KCN; ambient temperature. Center band is from  $\text{CN}^-$ .
- B)  $\text{K}_4\text{Mo}(\text{CN})_7 \cdot 2\text{H}_2\text{O}$  solid coarse powder; ambient temperature.



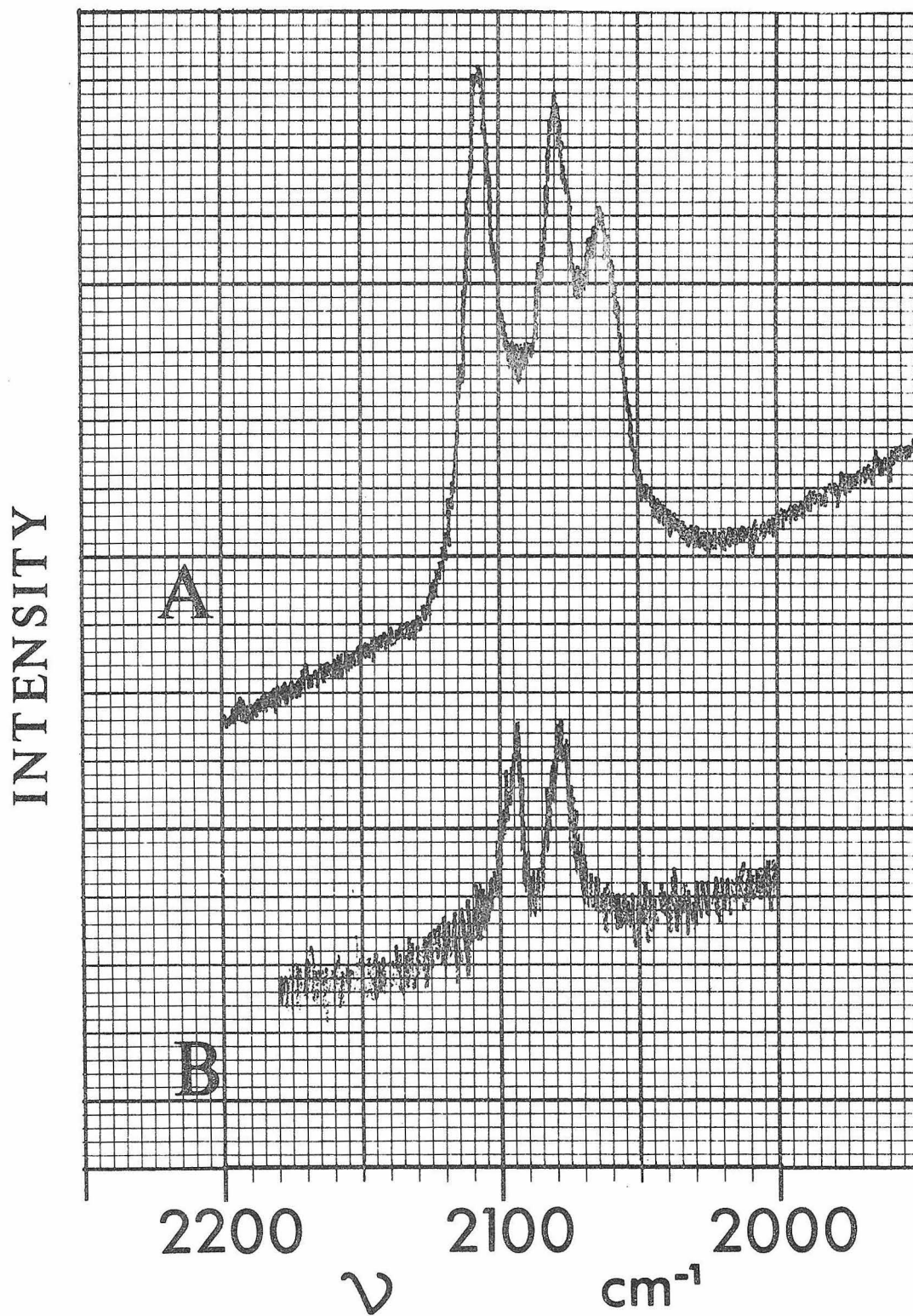









Figure 2

Table I. Predicted Cyanide Stretches in  
Six- and Seven-Coordinated Geometries

	<u>Point Group</u>	<u>Structure</u>	<u>IR</u>	<u>R</u>	<u>Coincidences</u>
six-coordinate	$O_h$		1	2	0
	$D_{3h}$		2	3	1
	$D_{3d}$		2	2	0
seven-coordinate	$D_{5h}$		2	3	0
	$C_{2v}$		6	7	6
	$C_{3v}$		5	5	5
	$C_s$		7	7	7

in particular, as well as the small number of bands, rules out the other seven-coordinate structures.

A six-coordinate octahedral formulation formed from dissociation of  $\text{Mo}(\text{CN})_7^{4-}$  in water to yield  $\text{Mo}(\text{CN})_6^{3-} + \text{CN}^-$  must also be considered particularly since the band at  $2080 \text{ cm}^{-1}$  in the solution infrared is at the frequency of free cyanide ion. The absence of this band in the raman spectrum of  $\text{K}_4\text{Mo}(\text{CN})_7 \cdot 2\text{H}_2\text{O}$  in 0.1F KOH, as well as solution magnetic susceptibility data and ligand field considerations of the optical spectrum to be discussed below, rule out the possibility of the formulation of  $\text{Mo}(\text{CN})_6^{3-}$ . A dimeric cyanobridged formulation can also be eliminated since bridging cyanides would absorb strongly at energies of  $2150 \text{ cm}^{-1}$  or higher.

The infrared spectrum of solid  $\text{K}_4\text{Mo}(\text{CN})_7 \cdot 2\text{H}_2\text{O}$  is essentially identical in mulls and KBr pellets. It consists of four regions of absorption: the water bands near  $3500$  and  $1610 \text{ cm}^{-1}$ , the cyanide stretches near  $2070 \text{ cm}^{-1}$ , and a broad region of absorption extending from  $250$  to  $550 \text{ cm}^{-1}$  corresponding to overlapping metal-carbon stretches, metal-carbon-nitrogen bends, and lattice water. (Figure 3-A).

The water region near  $3500 \text{ cm}^{-1}$  consists of a set of moderately broad, poorly resolved, overlapping bands in both mulls and KBr pellets. At liquid nitrogen temperature, the KBr pellet spectrum develops structure as shown in Figure 3-B. The three most prominent spikes occur at  $3581$ ,  $3498$ , and  $3428 \text{ cm}^{-1}$  with several partially resolved bands and shoulders between them. At room temperature, the water

Figure 3. Infrared spectra of hydrated and anhydrous potassium heptacyanomolybdate(III).

- A)  $\text{K}_4\text{Mo}(\text{CN})_7 \cdot 2\text{H}_2\text{O}$ , 0.67 mg/400 mg KBr pellet, ambient temperature.
- B)  $\text{K}_4\text{Mo}(\text{CN})_7 \cdot 2\text{H}_2\text{O}$ , 0.67 mg/400 mg KBr pellet, near 80°K.
- C)  $\text{K}_4\text{Mo}(\text{CN})_7 \cdot 2\text{H}_2\text{O}$ , 0.67 mg/400 mg KBr pellet; top-ambient temperature; bottom-near 80°K.
- D)  $\text{K}_4\text{Mo}(\text{CN})_7 \cdot 2\text{H}_2\text{O}$ , 7.6 mg/400 mg KBr pellet, ambient temperature.
- E)  $\text{K}_4\text{Mo}(\text{CN})_7$  after having been heated 6 hours at 270°C under vacuum, KBr pellet, ambient temperature.
- F)  $\text{K}_4\text{Mo}(\text{CN})_7$ , anhydrous, Nujol mull, ambient temperature.

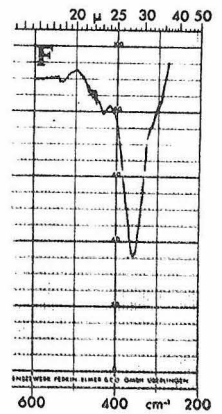
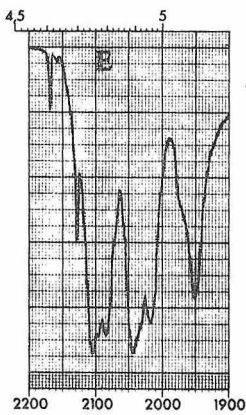
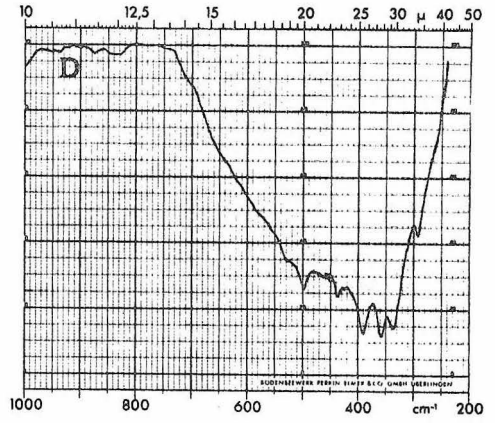
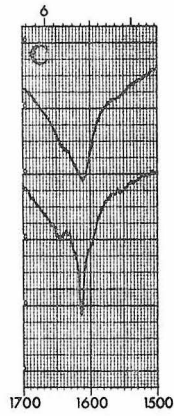
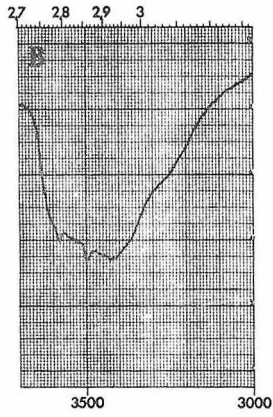
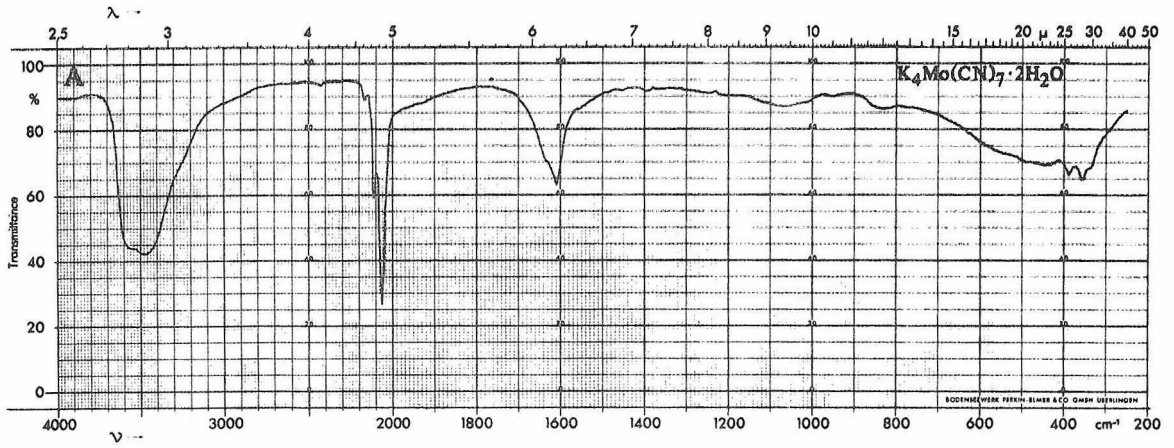


Figure 3

band at  $1610\text{ cm}^{-1}$  has a shoulder at about  $1640\text{ cm}^{-1}$ , whereas near  $78^\circ\text{K}$ , the band system sharpens markedly to a sharp band at  $1613\text{ cm}^{-1}$  and a broader one near  $1646\text{ cm}^{-1}$  (Figure 3-C). In more concentrated pellets at low temperature, the shoulder near  $1600\text{ cm}^{-1}$  also resolves into a band.

The cyanide stretching region in Nujol mulls, significantly different from the aqueous solution spectrum, consists of a strong and somewhat broad band at about  $2064\text{ cm}^{-1}$  and a weaker, but well resolved, side band at  $2111\text{ cm}^{-1}$ . In KBr pellets, these bands appear at  $2070$  and about  $2114\text{ cm}^{-1}$ , respectively. At approximately liquid nitrogen temperature, the resolution improves to reveal a band at  $2059\text{ cm}^{-1}$  and splitting of the  $2114\text{ cm}^{-1}$  band into two components at  $2119$  and  $2115\text{ cm}^{-1}$ . The main peak shifts to  $2074\text{ cm}^{-1}$  and has some poorly resolved structure on the high energy side (Figure 1-B, C).

The region between  $250$  and  $500\text{ cm}^{-1}$  consists of a broad region of absorption with much structure in it. Bands are located at  $498$ ,  $436$ ,  $398$ ,  $356$ ,  $338$ , and  $294\text{ cm}^{-1}$  in Nujol mulls. The bands occur at about the same positions in KBr pellets as is shown in Figure 3-D. Upon partial deuteration of the dihydrate, the band at  $338\text{ cm}^{-1}$  decreases in intensity, but no other changes are apparent in the lower energy region.

The raman spectrum of the black solid is difficult to obtain due to self absorption. From a coarsely ground sample of the solid, two raman bands have been obtained under conditions of high instrument gain at  $2096$  and  $2078\text{ cm}^{-1}$  (Figure 2-B). With the exception of weak

water bands, no other raman frequencies have been observed. While caution must be exercised in accepting the results of a raman experiment that involves shining a focused 60 milliwatt beam of 628 nm light into a black solid whose solutions are known to be photosensitive, it is evident that the raman results support other data which indicate that the solid and the solution contain different forms of the  $\text{Mo}(\text{CN})_7^{4-}$  ion.

More information regarding the nature of solid  $\text{K}_4\text{Mo}(\text{CN})_7 \cdot 2\text{H}_2\text{O}$  may be gained by examining the anhydrous potassium salt,  $\text{K}_4\text{Mo}(\text{CN})_7$ . The salient feature of the infrared spectrum of both mulls and pellets is a pair of bands at about 2078 and 2046  $\text{cm}^{-1}$  which bear a close similarity in both position and shape to the bands of the aqueous solution (Figure 1-D). The remainder of the spectrum simplifies from the loss of the water bands and the appearance of a single medium intensity band at 358  $\text{cm}^{-1}$  and a weaker band at 432  $\text{cm}^{-1}$  (Figure 3-F). The lack of complexity in the low energy region indicates a high degree of molecular symmetry and the cyanide stretch region demonstrates that the anhydrous potassium salt is pentagonal bipyramidal like the aqueous solution. However, the hydrated solid potassium salt is clearly not the same.

The pentagonal bipyramidal pattern has also been obtained from the partially characterized hydrated cesium salt  $\text{Cs}_4\text{Mo}(\text{CN})_7 \cdot x\text{H}_2\text{O}$ . In addition to strong water bands at about 3455 and 1627  $\text{cm}^{-1}$ , two cyanide stretching bands are found at 2077 and 2034  $\text{cm}^{-1}$  (Figure 1-E), and a low energy band at 353  $\text{cm}^{-1}$  similar to the low energy band at 358  $\text{cm}^{-1}$  in anhydrous  $\text{K}_4\text{Mo}(\text{CN})_7$ . The relative ease with which

the coordination geometry of the  $\text{Mo}(\text{CN})_7^{4-}$  ion in the solid, dihydrated potassium salt can be converted into the pentagonal bipyramidal geometry implies that a low energy barrier exists between the two forms.

It will be noted in the spectrum of the anhydrous potassium salt that some structure is present on the  $2078\text{ cm}^{-1}$  band. This structure becomes more pronounced in Nujol mulls and is also evident in the solid cesium salt at liquid nitrogen temperatures. Even more interesting are the bands in the anhydrous potassium salt between  $1950$  and  $2000\text{ cm}^{-1}$ . These bands occurring at energies lower than normally observed for cyanides cannot be simply ascribed to isotopic bands or overtones since after heating anhydrous  $\text{K}_4\text{Mo}(\text{CN})_7$  to  $270^\circ$  for 6 hours under vacuum, the resulting black material has a band at  $1951\text{ cm}^{-1}$  (with a shoulder at about  $1973\text{ cm}^{-1}$ ) that is nearly as intense as the stronger cyanide stretching absorptions between  $2000$  and  $2100\text{ cm}^{-1}$  (Figure 3-E). It is possible to speculate that these bands represent cyanobridging through carbon analogous to carbonyl bridging, as opposed to the  $\text{M}-\text{C}\equiv\text{N}-\text{M}$  bridging commonly found in cyanides. In normal cyanobridged materials, the CN stretch moves to higher frequency whereas in carbonylbridged materials, the CO stretch moves to lower frequency. It is therefore reasonable to expect that cyanobridging through carbon would also cause the stretching mode to move to lower frequency.

The conclusions drawn from the infrared and raman studies are as follows. From the solution studies, a monomeric pentagonal



bipyramidal  $D_{5h}$  structure is indicated. This same  $D_{5h}$  structure also occurs in the anhydrous potassium salt,  $K_4Mo(CN)_7$ , and the hydrated cesium salt. The infrared and raman data clearly indicate that the solid hydrated potassium salt,  $K_4Mo(CN)_7 \cdot 2H_2O$ , has a different structure from the  $D_{5h}$  forms. The data do not allow an assignment of the structure of the  $Mo(CN)_7^{4-}$  ion in the hydrated potassium salt. It is therefore necessary to turn to x-ray and ESR studies to provide additional data.

#### 4. X-Ray Structural Studies

Since the infrared studies have not provided an unambiguous characterization of the structure of the  $K_4Mo(CN)_7 \cdot 2H_2O$ , a single crystal x-ray structural determination was undertaken in cooperation with Dr. Albert Schlueter. Numerous black flakes were examined which had been grown by cooling an ethanol-water solution of the compound. Several flakes that displayed perfect extinction under crossed polarizers and were free from overlapping flakes, were mounted in glass capillaries, evacuated, back-filled with nitrogen, and flame sealed. The crystals held up nicely in the x-ray beam and showed no sign of decomposition after line-up and Weissenberg shots. Unfortunately, at the first level Weissenberg every crystal displayed a complicated form of twinning. Every spot had a satellite, but the relative intensity of the two spots did not appear to vary systematically. For some crystals, the two spots would be blurred together. After several crystals were examined and found to be twinned, the x-ray study was terminated. Although it was possible to choose unit cells

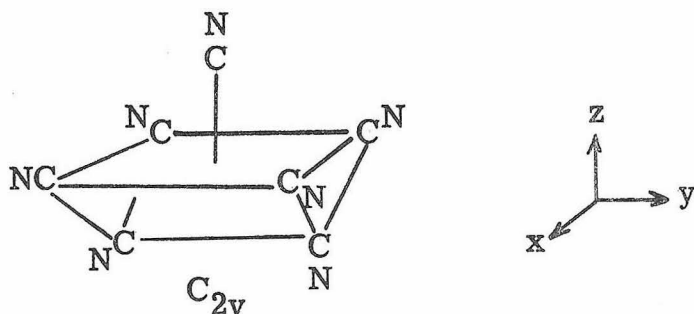
that would give a calculated density in agreement with the experimental value of  $1.96 \text{ gm cm}^{-3}$  (based on the formulation  $\text{K}_4\text{Mo}(\text{CN})_7 \cdot 2\text{H}_2\text{O}$ ), it was impossible to determine the actual unit cell.

### 5. Magnetic and Electronic Spectral Properties

The gram susceptibility of  $\text{K}_4\text{Mo}(\text{CN})_7 \cdot 2\text{H}_2\text{O}$  was found to be  $2.28 \times 10^{-6} \text{ cm}^3 \text{ g}^{-1}$  at  $298^\circ\text{K}$  corresponding to a magnetic moment of 1.73 B.M. Within experimental error, it is constant down to  $90^\circ\text{K}$ , thus essentially confirming the results of a previous determination. <sup>(4)</sup> The magnetic moment of the anhydrous potassium salt has been found to be 1.80 B.M. at  $296^\circ\text{K}$ , and a 0.13F aqueous solution has a magnetic moment of 1.6 B.M. as determined by Evans' NMR method. All of these results indicate low-spin (1 unpaired electron)  $d^3$  configurations. The absence of strong magnetic coupling which would significantly lower the magnetic moments from the spin-only value of 1.7 B.M. rules out the possibility of a dimeric or polymeric formulation employing metal-metal bonds as occur in  $\text{Co}_2(\text{CN})_{10}^{6-}$  or cyanobridging.

A structural proposal for  $\text{K}_4\text{Mo}(\text{CN})_7 \cdot 2\text{H}_2\text{O}$  has come from a low temperature ESR study of the undiluted powder. <sup>(5)</sup> The spectrum was found to be axially symmetric with  $g_{\perp} = 1.973$  and  $g_{\parallel} = 2.103$ . The spectrum has been satisfactorily interpreted in terms of a  $\text{C}_{2v}$  mono-capped trigonal prismatic coordination environment about the central molybdenum (the  $\text{TaF}_7^{2-}$  structure). A low symmetry model is appealing because it is compatible with, in fact demanded by, the multitude of low energy infrared bands. Although six infrared bands are predicted to occur in the CN stretching region for a  $\text{C}_{2v}$  structure,

the axial symmetry indicated by the ESR would mean that the upper face of the trigonal prism, shown below, would be nearly square with the



x and y directions nearly equivalent in this plane, so consequently some of the modes may become nearly degenerate. Note also that while the predicted set of infrared CN stretching modes is not observed at room temperature, the low temperature spectrum (Figure 1-C) shows that the broader absorption observed at room temperature is actually composed of several bands. In aqueous solutions and frozen LiCl glasses, no ESR signal was observed in this region for the  $D_{5h}$  solution form of the  $Mo(CN)_7^{4-}$  ion.

The batch of  $Cs_4Mo(CN)_7 \cdot xH_2O$  which displays the pentagonal bipyramidal pattern in the infrared also has a broad ESR signal at approximately 120°K with g values of about 6.6 (Figure 2, section I-D). While no interpretation is presented for these preliminary results, a thorough study is warranted of the low field region in the ESR of frozen LiCl solutions containing  $D_{5h}$   $Mo(CN)_7^{4-}$  and of a recrystallized and analyzed sample of the cesium salt.

The room temperature electronic absorption spectrum of rigorously deoxygenated aqueous solutions of  $K_4Mo(CN)_7 \cdot 2H_2O$  which

have been prepared in the absence of light of wavelength less than 610 nm is presented in Figure 4-A. Prominent bands are located at 216 and 289 nm, and a prominent shoulder at 402 nm. Shoulders at 320, 260, and 245 nm which are faintly discernible at room temperature show up clearly in spectra taken at low temperatures ( $\sim 90^\circ\text{K}$ ) in glasses formed from solutions of the heptacyanide in concentrated LiCl solutions (Figure 4-B). In these glasses, the 287 nm band undergoes a large increase in intensity at low temperature. Oxidation products and photodecomposition products of the heptacyanide have bands in the region 600-650 nm. Noticeable photodecomposition can occur as a result of the very act of taking the spectrum, particularly in the more highly concentrated solutions. This can be largely prevented by the presence of a large excess of cyanide ion in the solution. The spectrum of a 0.015F solution of the heptacyanide in a 3F KCN solution is essentially identical to that obtained using cyanide-free water as a solvent. In the cyanide containing solutions, no bands with  $\epsilon > 0.5$  are observed in the near infrared and visible at wavelengths greater than 500 nm.

The spectrum of solid  $\text{K}_4\text{Mo}(\text{CN})_7 \cdot 2\text{H}_2\text{O}$  has been obtained both from single crystals and in KBr pellets. Flakes have been obtained which were thin enough to allow spectral studies from the near infrared down to 350 nm at  $\text{LN}_2$  temperature. At room temperature, the only feature down to 420 nm is a band at about 620 nm. When the crystal is cooled to  $78^\circ\text{K}$ , the 620 nm band sharpens and shoulders at about 402,

Figure 4. Electronic spectra of  $\text{K}_4\text{Mo}(\text{CN})_7 \cdot 2\text{H}_2\text{O}$

- A)  $\text{K}_4\text{Mo}(\text{CN})_7 \cdot 2\text{H}_2\text{O}$ , 0.015F aqueous solution, 26°C.
- B)  $\text{K}_4\text{Mo}(\text{CN})_7 \cdot 2\text{H}_2\text{O}$ ,  $\sim 8.5 \times 10^{-3}\text{F}$  in 8:2 saturated  $\text{LiCl}:\text{H}_2\text{O}$  solvent,  $\sim 90^\circ\text{K}$ ,  $\sim 0.10$  mm path.
- C)  $\text{K}_4\text{Mo}(\text{CN})_7 \cdot 2\text{H}_2\text{O}$ , single crystal flake,  $\sim 0.065$  mm thick, 26°C (dashed line) and 78°K (solid line).
- D) Top  $\text{K}_4\text{Mo}(\text{CN})_7$ , anhydrous in KBr pellet, 26°C.  
Center  $\text{K}_4\text{Mo}(\text{CN})_7$ , anhydrous in KBr pellet, 78°K.  
Bottom  $\text{K}_4\text{Mo}(\text{CN})_7 \cdot 2\text{H}_2\text{O}$  in KBr pellet,  $\sim 100^\circ\text{K}$ .

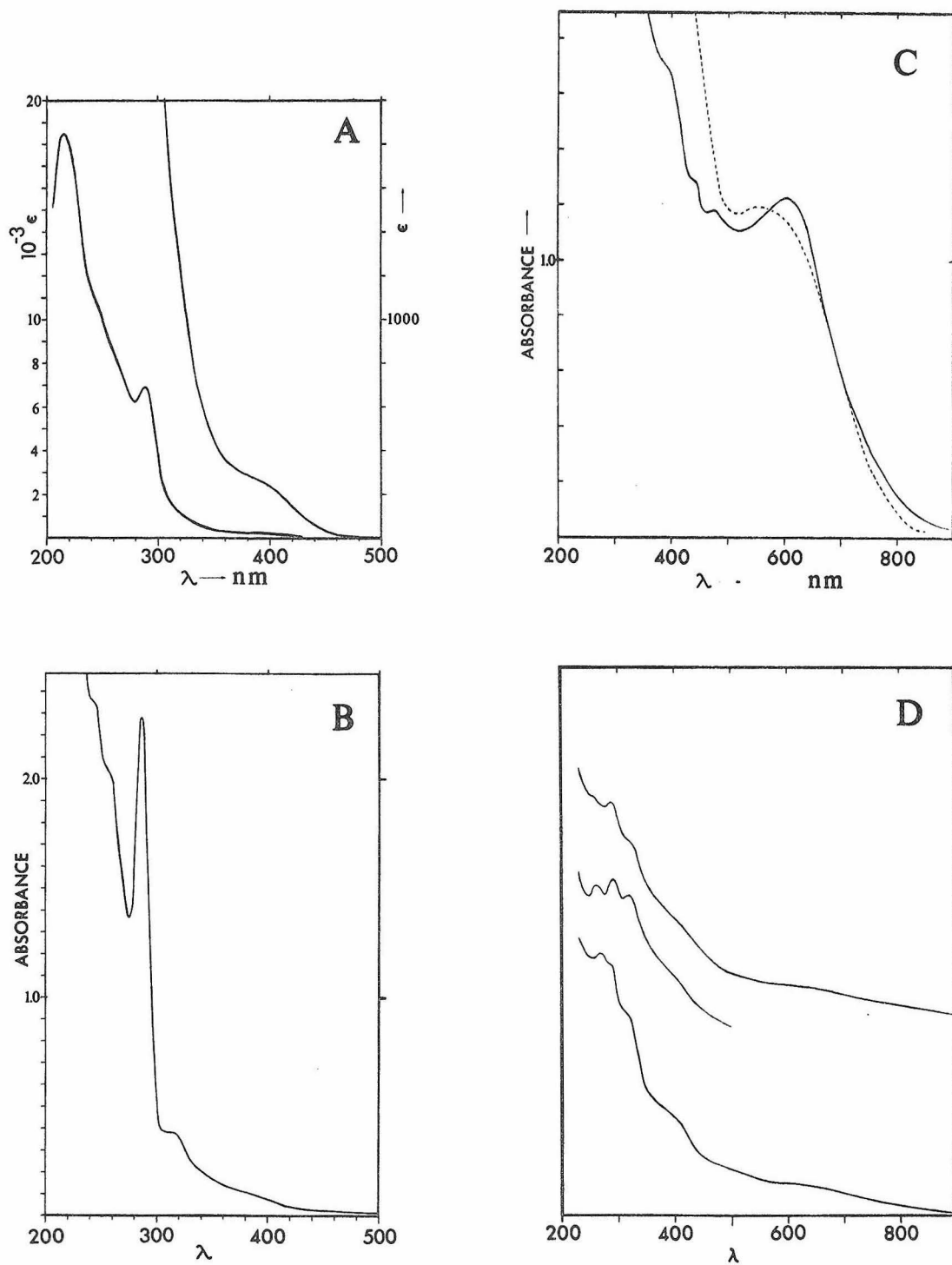


Figure 4

444, and 479 nm are revealed (Figure 4-C). The  $\epsilon$  of the 620 nm band was determined to be approximately 12. This number represents a lower bound on  $\epsilon$  since in the crystal used for this determination there were spots thinner than the measured thickness.

The spectrum of the solid in KBr pellets does not show bands as well defined as the solutions (Figure 4-d). At  $\text{LN}_2$  temperature, shoulders exist at 404, 323, 289, and 269 nm corresponding to the bands and shoulders observed in solution. An additional, but comparatively weak band, is also observed at about 650 nm.

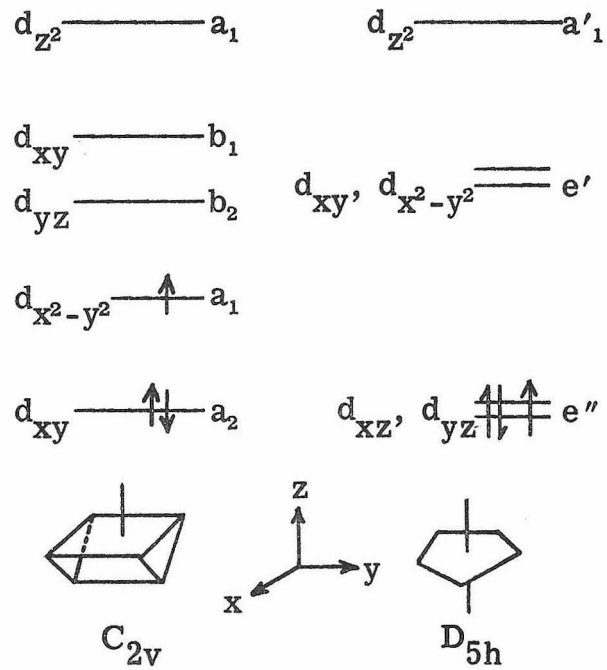
The spectrum of anhydrous  $\text{K}_4\text{Mo}(\text{CN})_7$  in a KBr pellet near 78°K shows a well defined band at 289 nm and other bands and shoulders at 403, 324, and 259 nm. A weak band is also observed near 650 nm (Figure 4-D). In the spectral region observable in the KBr pellets, 225-2000 nm, the principal quantitative differences between the anhydrous and the hydrated materials were the relative intensities of the bands, particularly the 289 nm band, and the apparent shift of the 269 nm band in the hydrate to 259 nm in the anhydrous material.

The electronic spectral studies indicate that there are not large differences between the spectra of the solution and the anhydrous potassium salt, at least in terms of band positions. In the anhydrous potassium salt as in the solution, the most prominent feature is the band at 289 nm. This provides further substantiation of the conclusions reached from the infrared studies regarding the existence of the same coordination geometry in both the solutions and the anhydrous potassium salt.

While differences in the ultraviolet region between the solution and the hydrated potassium salt exist, they are principally differences in relative band intensities. A better comparison is obtained from the spectra of the hydrated and anhydrous potassium salts in KBr pellets (Figure 4-D) which shows that the two spectra are very similar, and therefore suggests that a major reorganization of the coordination environment does not occur in going from the pentagonal bipyramidal form to the proposed  $C_{2v}$  geometry of the dihydrated potassium salt. The band at 620 nm in the crystal spectrum makes it clear that there have occurred enough changes, however, to alter the d-orbital-derived electronic energy levels.

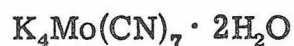
Although detailed calculations of the energies of the states for various electronic configurations in seven-coordinate model systems are not available, the basic features of the optical spectra of the aqueous solution and crystal spectra can be interpreted from orbital energy level diagrams. From the ESR results,<sup>(5)</sup> the d-electron orbital energy levels are arranged in the relative energies indicated below in the  $C_{2v}$  geometry of the solid, hydrated potassium salt. The ordering of the levels in  $D_{5h}$ , also presented below, are similar to those established for  $D_{3h}$  five-coordinate compounds. In each case, the resulting ground state,  ${}^2A_1$  in  $C_{2v}$  and  ${}^2E$  in  $D_{5h}$ , will have one unpaired electron. The first transition in the solid will be the low energy transition of  $d_{xy} \rightarrow d_{x^2-y^2}$  corresponding to the 620 nm band in the hydrated potassium salt. In the aqueous solutions of the  $D_{5h}$  form, the first transitions at 402 and 320 nm will be components of the higher





energy transition  $d_{xz}, d_{yz} \rightarrow d_{xy}, d_{x^2-y^2}$ . The higher energy transitions in both cases will be admixtures of d-d transitions and ligand-to-metal charge transfer bands.

Table II. Summary of Physical Characteristics of



## A) Infrared Spectra, Room Temperature

	$\bar{\nu}$ (cm <sup>-1</sup> )		
Solution:	2080	$\epsilon \approx 900$	
	2040	$\epsilon \approx 900$	
Solid, Nujol mulls:	3566		H <sub>2</sub> O
	3490	shoulder	H <sub>2</sub> O
	3443	shoulder	H <sub>2</sub> O
	2114		CN str.
	2068		CN str.
	1640	shoulder	H <sub>2</sub> O
	1610		H <sub>2</sub> O
	498		
	436		
	390		
	356		
	338		
294			

## B) Raman Spectra, Room Temperature

	$\bar{\nu}$ (cm <sup>-1</sup> )		
Solution	2106	weak	CN str.
	2063	weak	CN str.

Table II (Continued)

Solid	2096	v. weak	CN str.
	2078	v. weak	CN str.

## C) Optical Spectra

	$\lambda$ (nm)	$10^{-3} \bar{\nu}$ ( $\text{cm}^{-1}$ )	$\epsilon$	
Solution	216	46.3	18,400	
	245	40.8		shoulder at $\text{LN}_2$
	260	38.5		shoulder at $\text{LN}_2$
	289	34.6	6900	
	320	31.2		shoulder at $\text{LN}_2$
	402	24.9	230	shoulder
Solid	269	37.2		
	289	34.6		
	323	31.0		
	402	24.9		
	444	22.5		shoulder at $\text{LN}_2$
	479	20.9		shoulder at $\text{LN}_2$
	620	16.1		

## D) Magnetic Moment

Solid 1.73 B. M. at 296°K, Curie law

Solution 1.6 B. M. at ~40°C

## E) ESR

$$g_{\parallel} = 2.103$$

$$g_{\perp} = 1.973$$

Table III. Summary of Physical Characteristics of  
Anhydrous  $K_4Mo(CN)_7$

A) Infrared Spectra, Mineral Oil Mulls, Room Temperature

	$\bar{\nu}$ ( $cm^{-1}$ )	
Solid	2098	shoulder
	2085	shoulder
	2075	
	2046	
	2022	shoulder
	2002	shoulder
	1988	
	1968	shoulder
	432	
	358	

B) Optical Spectra, KBr Pellets, 296°K

$\lambda$ (nm)	$10^{-3} \bar{\nu}$ ( $cm^{-1}$ )
259	38.6
289	34.6
324	30.8
403	24.8

C) Magnetic Moment: 1.80 B. M. at 296°K

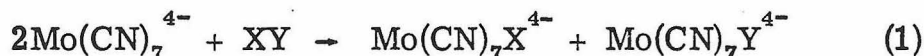
## 7. References

1. R. C. Young, J. Amer. Chem. Soc., 54, 1402 (1932).
2. M. C. Steele, Aust. J. Chem., 10, 490 (1957).
3. M. C. Steele, Aust. J. Chem., 10, 404 (1957).
4. J. Lewis, R. S. Nyholm, and P. W. Smith, J. Chem. Soc., 4590 (1961).
5. For details, see part I-D.

## B. Chemical Characterization Studies

### 1. Introduction

With the exception of the susceptibility of  $K_4Mo(CN)_7 \cdot 2H_2O$  to air oxidation, little has been reported regarding the chemical reactivity of the  $Mo(CN)_7^{4-}$  ion. If truly seven-coordinate, which is likely, it is a seventeen outer-electron system electronically similar to  $Co(CN)_5^{3-}$ . In view of the stability of  $Mo(CN)_8^{4-}$ , analogous to  $Co(CN)_6^{3-}$ , it would be reasonable for  $Mo(CN)_7^{4-}$  to undergo oxidative addition reactions analogous to those of  $Co(CN)_5^{3-}$ , namely:



If a series of monosubstituted heptacyanomolybdate(IV) eight-coordinate complexes could be prepared, they should prove useful in the systematic study of eight-coordination reactions mechanisms in much the same manner that compounds of the type  $Co(CN)_5X^{3-}$  have proven useful in elucidating octahedral substitution mechanisms.

The photochemistry of cyanomolybdates has been an active area of research for several years. Most work has centered about the photoaquation of  $Mo(CN)_8^{4-}$  and occasionally about the photodecomposition of  $Mo(CN)_8^{3-}$ . Not unexpectedly, the oxidation products of  $Mo(CN)_7^{4-}$  have been found to be related to the photochemical products of  $Mo(CN)_8^{4-}$ . Of even greater interest is the unique photochemical behavior of  $Mo(CN)_7^{4-}$  by itself.

In this section are reported the results of the initial studies related to the chemical reactivity and photochemistry of the  $Mo(CN)_7^{4-}$  ion.

## 2. Oxidation of $K_4Mo(CN)_7^{4-}$

Yellow solutions of  $K_4Mo(CN)_7 \cdot 2H_2O$  are readily oxidized by air to short-lived, brown colored solutions which become pink upon dilution. This pink color has been repeatedly mistaken in the literature for the solution color of  $Mo(CN)_7^{4-}$ . After several minutes these solutions turn green and have an optical absorption spectrum which corresponds to a superposition of the spectra of  $Mo(CN)_8^{4-}$  and  $MoO(OH)(CN)_4^{3-}$ . In a period of time ranging from several hours to days depending upon conditions, these solutions ultimately turn yellow and display only the optical spectrum of  $Mo(CN)_8^{4-}$ .

The pink solution is conveniently generated from  $K_4Mo(CN)_7 \cdot 2H_2O$  by dissolving enough of the solid to make a 0.01F solution in ice water saturated with oxygen. The pink color which develops immediately can persist for periods of more than an hour at 0°C.

The principal spectroscopic features of the pink solution are a band at 513 nm and a shoulder near 310 nm (Figure 1). The formation of the pink species has invariably been accompanied by spectroscopically significant amounts of  $Mo(CN)_8^{4-}$  and  $MoO(OH)(CN)_4^{3-}$ . The formation of the pink species can be completely prevented by carrying out the oxidation in the presence of a large excess of cyanide ion. Although the pink solution is reversibly changed to a pale yellow color at pH's greater than 11, the inhibition of the formation of the pink colored solution with cyanide ion is not exclusively a pH effect since cyanide solutions buffered at pH 8 will also destroy the pink color.

Figure 1. Electronic spectra of the pink oxidation product of  $\text{Mo(CN)}_7^{4-}$ .

Solid line--pink product from air oxidation of dilute aqueous solution of  $\text{K}_4\text{Mo(CN)}_7 \cdot 2\text{H}_2\text{O}$ ;  $\sim 0^\circ\text{C}$ .

Dashed line--pink photoaquation product of aqueous  $\text{K}_4\text{Mo(CN)}_8 \cdot 2\text{H}_2\text{O}$  solutions;  $\sim 0^\circ\text{C}$ .

Figure 2. Electronic spectra of a photochromic system consisting of a 0.015F aqueous solution of  $\text{K}_4\text{Mo(CN)}_7 \cdot 2\text{H}_2\text{O}$ .

Dashed line--before exposure to light.

Solid line--steady state formation of photochromic product after three hours exposure to a medium intensity unfiltered short wave uv lamp, 1 cm path, quartz cell,  $\sim 24^\circ\text{C}$ .



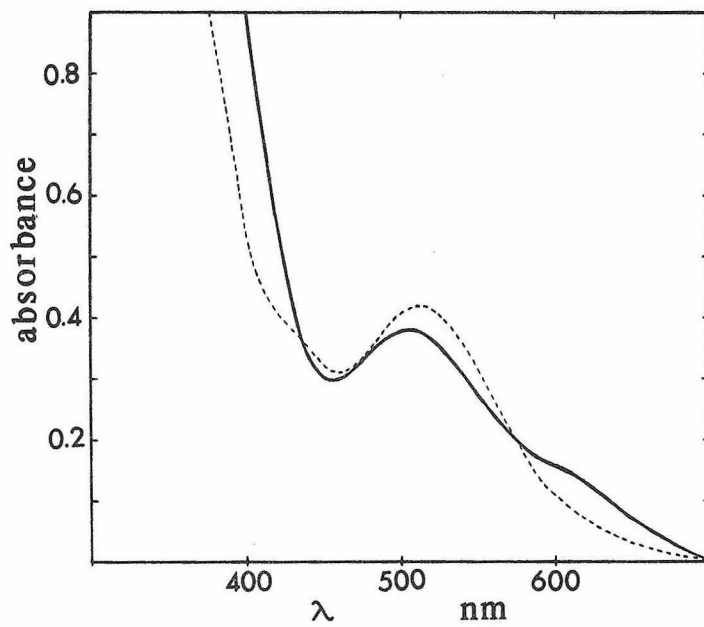


Figure 1

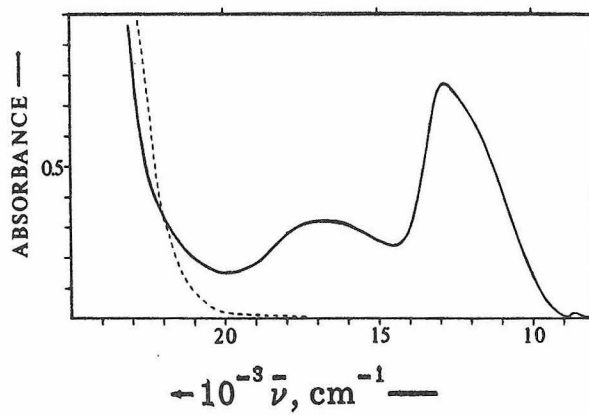
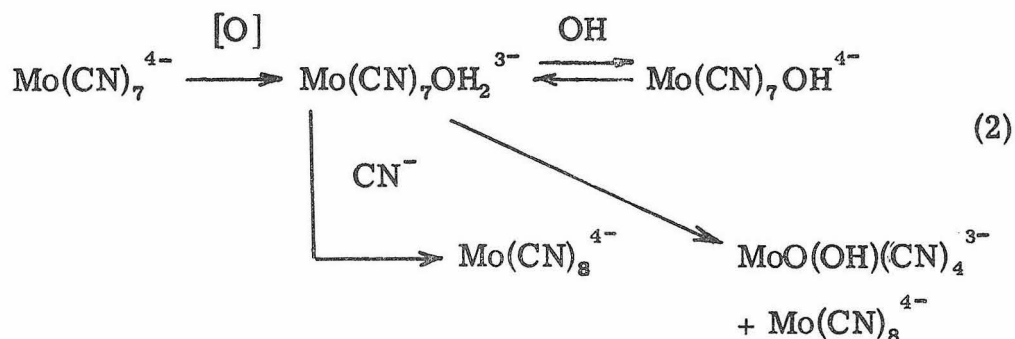


Figure 2

These observations can be explained by the sequence of reactions in equation 2



The first stable species in the oxidation of  $\text{Mo(CN)}_7^{4-}$  is an eight-coordinate Mo(IV) species which has attained the favorable rare-gas shell configuration through incorporation of a solvent molecule into the coordination sphere. The protons are sufficiently acidic so that one can be removed at high pH's to form the yellow heptacyano-hydroxomolybdate(IV) ion. The coordinated water molecule can be displaced with cyanide ion to form octacyanomolybdate(IV) which along with trans-oxo-hydroxotetracyanomolybdate(IV) also is a product of the thermal decomposition of the pink intermediate. Solutions of  $\text{MoO(OH)(CN)}_4^{3-}$  are themselves unstable and ultimately decompose to colorless species.

It has been known for some time that photolysis of  $\text{K}_4\text{Mo(CN)}_8$  in aqueous solution produces a primary pink photoproduct which upon further photolysis goes on to form blue  $\text{MoO(OH)(CN)}_4^{3-}$ . The nature of the pink photoproduct has been formulated both as an aquated product  $[\text{Mo(CN)}_7\text{OH}_2]^{2-}$ , (1) and as a super-complex  $[\text{Mo(CN)}_8(\text{OH}_2)_2]^{4-}$ . (2) This pink photoproduct is also characterized by an absorption band at 513 nm,

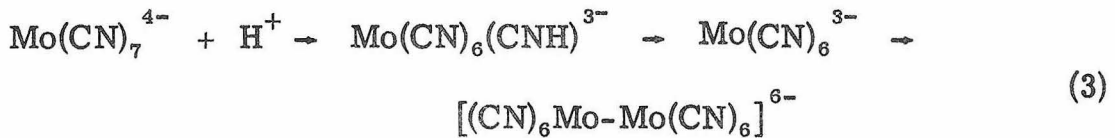
and in fact appears to be identical to the pink oxidation product of  $\text{Mo(CN)}_7^{4-}$  (Figure 1). A red anion was recently isolated from irradiated  $\text{Mo(CN)}_8^{4-}$  in the form of the salt  $\text{Ag}_3[\text{Mo(CN)}_7\text{H}_2\text{O}]$ . (3) The formulation of the common photoproduct of  $\text{Mo(CN)}_8^{4-}$  and oxidation product of  $\text{Mo(CN)}_7^{4-}$  as  $[\text{Mo(CN)}_7\text{OH}_2]^{3-}$  is reasonable whereas the suggestion of a super-complex  $[\text{Mo(CN)}_8(\text{H}_2\text{O})_2]^{4-}$  is not compatible with its immediate formation by the oxidation of  $\text{Mo(CN)}_7^{4-}$ .

The pink intermediate has been formed by a third method. When  $[(n\text{-C}_4\text{H}_9)_4\text{N}]_4\text{Mo(CN)}_8$  (prepared from  $\text{H}_4\text{Mo(CN)}_8$  and  $\text{Bu}_4\text{N}^+\text{OH}^-$ ) was allowed to stand in air for several weeks, it formed a yellow oil which dissolves in ice water to form the pink intermediate. This proved to be a particularly convenient source of the pink species and produced the spectra with the smallest amount of bands arising from other cyanomolybdates.

### 3. pH Dependence of $\text{Mo(CN)}_7^{4-}$ Solutions.

Solutions of  $\text{K}_4\text{Mo(CN)}_7 \cdot 2\text{H}_2\text{O}$  show no color change when they are made alkaline with either cyanide or hydroxide ion. When the solutions are acidified, a deep purple color develops. When one equivalent of  $\text{H}^+$  as  $\text{NaHSO}_4$  is added to a 0.03F solution of  $\text{K}_4\text{Mo(CN)}_7 \cdot 2\text{H}_2\text{O}$ , the purple color develops in about forty seconds. The absorption spectrum in the region 800-350 nm consists of an intense ( $\epsilon \geq 630$ ) single band peaking at 532 nm ( $18.8 \text{ Kcm}^{-1}$ ) with a band width at half-height of  $\sim 5800 \text{ cm}^{-1}$  at  $\sim 15^\circ\text{C}$ . In a period of about 15 minutes, the purple solutions completely decompose to form a yellowish-brown precipitate that has not been characterized. If a large excess of acid is

added to a  $\text{Mo}(\text{CN})_7^{4-}$  solution, the brown gelatinous precipitate forms immediately with only a transient purple color in the solutions. The first step (equation 3) is probably rapid protonation of some of the cyanide ligands followed by slow loss of HCN and immediate reaction of the  $\text{Mo}(\text{CN})_6^{3-}$  with itself to form an unstable dimer (or cluster compound) with strong metal-metal bonding and intense color which ultimately decomposes to uncharacterized materials.



#### 4. Photochromism of Aqueous Solutions of $\text{K}_4\text{Mo}(\text{CN})_7 \cdot 2\text{H}_2\text{O}$ .

Solutions of  $\text{Mo}(\text{CN})_7^{4-}$  are markedly photochromic. A 0.1 F solution which has been stored in darkness is yellow in color. Upon exposure to sunlight, it turns from yellow through dirty green to black in a matter of 2 to 4 minutes. When stored in darkness for a period of 10 to 12 hours, the solution reverts back to its initial yellow color. A sealed system can be cycled repeatedly. One system has been cycled hundreds of times with sunlight, but does show an appreciable build up of  $\text{MoO}(\text{OH})(\text{CN})_4^{3-}$ .

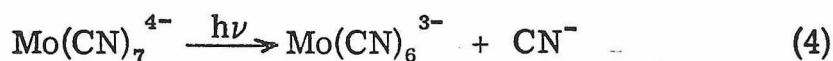
An excess of free cyanide ion (3F  $\text{CN}^-$  to 0.1F Mo) prevents the photoreaction from occurring as does an excess of hydroxide ion. The return to yellow is accelerated by heating the sealed reaction tubes. The forward reaction occurs with both long and short wave uv irradiation.

Spectroscopically, the onset of the photoreaction is indicated by the formation of a band in the near-infrared. As the photoreaction

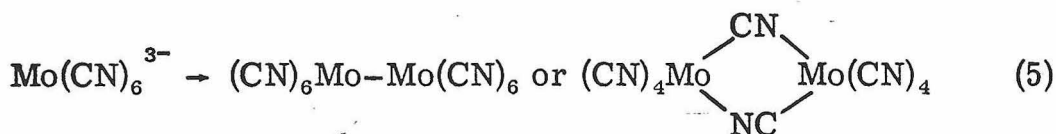
continues, the infrared band grows to reach a maximum on an asymmetric band at 780 nm (Figure 2). A visible band of lower intensity also develops at about 576 nm. In the ultraviolet all of the bands from  $\text{Mo}(\text{CN})_7^{4-}$  decrease in intensity while a new band at 225 nm develops.

A lower bound for the molar absorptivity,  $\epsilon$ , can be placed on the 780 nm band. In a 0.015F solution of  $\text{K}_4\text{Mo}(\text{CN})_7$ , the absorbance of the 780 nm band has been observed to rise to a value which corresponds to an  $\epsilon$  of about 60. Under these conditions, the ultraviolet bands had fallen to about one-half of their normal intensity which means that  $\epsilon_{780}$  is at least 120 and the band arises from a spin-allowed transition.

The cyanide dependence and pH dependence suggest that the initial step in the photoreaction is the loss of cyanide ion analogous to the photocatalyzed exchange of  $\text{CN}^-$  in  $\text{Mo}(\text{CN})_8^{4-}$ . (4)



The  $\text{Mo}(\text{CN})_6^{3-}$  could then conceivably react to form a dimeric (or polymeric) unit containing either Mo-Mo bonds or cyanide bridges:



A monomeric  $\text{Mo}(\text{CN})_6^{3-}$  can be ruled out as a terminal photo-product on the basis of optical and magnetic data. On the basis of ligand field considerations for a  $d^3$ -octahedral Mo(III) hexacyano-complex, the first spin allowed band,  ${}^4A_1 \rightarrow {}^4T_{2g}$ , would be expected

to occur at an energy of at least  $34,000 \text{ cm}^{-1}$ . The low-energy spin-allowed band of the photoproduct, however, occurs at  $12,800 \text{ cm}^{-1}$ .

The study of the magnetism of the  $\text{Mo}(\text{CN})_7^{4-}$  during the photo-reaction should provide a means of discriminating among possible photoproducts. The starting material,  $\text{Mo}(\text{CN})_7^{4-}$ , has one unpaired spin;  $\text{Mo}(\text{CN})_6^{3-}$  should have three spins; a cyanobridged dimer (or polymer) would have reduced magnetism; while a metal-metal bonded dimer should be diamagnetic. Solution NMR magnetic susceptibility measurements on a 0.13F aqueous solution of  $\text{K}_4\text{Mo}(\text{CN})_7 \cdot 2\text{H}_2\text{O}$  gave a magnetic moment for the molybdenum of 1.6 B.M. and did not change when the solution was irradiated with sunlight to produce a black solution. A possible explanation of the failure to observe a change in magnetism is the formation of a small amount of intensely colored material such as a mixed oxidation state compound.

A mixed oxidation state product provides an attractive explanation for the existence of the  $12,900 \text{ cm}^{-1}$  band in the photoproduct. Mixed oxidation state compounds are usually intensely colored and have optical bands in the near infrared. Not only extended lattice compounds such as Prussian blue and Molybdenum blue, but also discrete mixed oxidation state dimers display these characteristics. For example  $[\text{Fe}_2^{\text{II,III}}(\text{CN})_{10}]^5$ , believed to be symmetrically di-cyano bridged, has a high intensity ( $\epsilon = 5500$  per dimer) low energy band at  $7800 \text{ cm}^{-1}$ (5) and  $(\text{NH}_3)_5\text{Ru} \begin{array}{c} \diagup \quad \diagdown \\ \text{O} \\ \diagdown \quad \diagup \end{array} \text{N Ru}(\text{NH}_3)_5^{5+}$  has a band at  $6500 \text{ cm}^{-1}$  with  $\epsilon = 5000$  per dimer. (6)

The photochromic cycle could occur when a small quantity of  $\text{Mo(CN)}_7^{4-}$  is photochemically oxidized, perhaps after first having formed a transient  $\text{Mo(CN)}_6^{3-}$  species (equation 6). The oxidation product would then react with either  $\text{Mo(CN)}_7^{4-}$  or one of its photo-reaction products to form a moderately stable mixed oxidation state compound which is responsible for the color changes. In the back reaction, cyanide ion attack would decompose the mixed oxidation state compound converting it to  $\text{Mo(CN)}_7^{4-}$  and probably a mixture of  $\text{Mo(CN)}_8$  and  $\text{Mo(O)(OH)(CN)}_4^{3-}$  thereby accounting for the slow buildup of oxidation products during the course of repeated photochromic cycling.

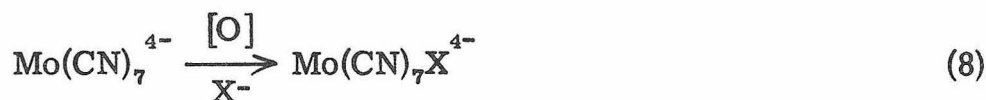
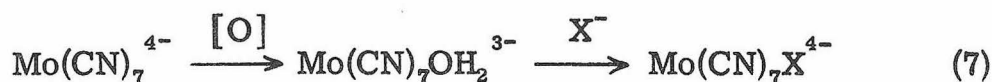


Aqueous solutions of  $\text{KMo(CN)}_7 \cdot 2\text{H}_2\text{O}$  react rapidly with halogens to yield darker colored solutions from which waxy solids can be precipitated with ethanol. Iodine, or solutions of  $\text{I}_3^-$ , react to yield solutions from which a very fine, pale-orange, waxy solid can be precipitated by addition of alcohol. Attempts to recrystallize the compound have yielded only waxy films or fine powders. The prolonged reaction of  $\text{I}_2$  vapor with anhydrous  $\text{K}_4\text{Mo(CN)}_7$  produces a similar product which is characterized by an infrared spectrum consisting of a strong band at  $2112 \text{ cm}^{-1}$  and a moderate band at  $359 \pm 2 \text{ cm}^{-1}$ . Bromine reacts to form dark colored solutions which upon repeated recrystallization attempts yield powders and films which range in color from nearly black to red-brown. Their infrared spectra show a prominent band in

the CN region at about  $2116\text{ cm}^{-1}$  and a shoulder at about  $2152\text{ cm}^{-1}$  which corresponds to the red to dark red product from the reaction of  $\text{K}_4\text{Mo}(\text{CN})_8 \cdot 2\text{H}_2\text{O}$  with aqueous bromine. The spectra invariably display Mo–O bands in the  $700\text{--}1000\text{ cm}^{-1}$  region as well as several bands between  $200$  and  $500\text{ cm}^{-1}$ . The number and intensity of the bands below  $1000\text{ cm}^{-1}$  are variable from sample to sample. Chlorine reacts to form red-brown colored solutions from which a brown, non-crystalline solid can be isolated.

The relatively broad CN-stretching bands as compared to simple monomeric cyanides, the waxy, non-crystalline nature of the compounds, and existence of CN-stretching frequencies above  $2100\text{ cm}^{-1}$  indicate that these products are cyanobridged polymers rather than the anticipated  $\text{Mo}(\text{CN})_7\text{X}^{4-}$  monomers.

A second synthetic route to  $\text{Mo}(\text{CN})_7\text{X}^{4-}$  should be through prior oxidation of  $\text{Mo}(\text{CN})_7^{4-}$  to  $\text{Mo}(\text{CN})_7\text{OH}_2^{3-}$  followed by substitution of the coordinated  $\text{OH}_2$  by a suitable X (equation 6) or through a nearly equivalent route of oxidation of  $\text{Mo}(\text{CN})_7^{4-}$  in the presence of an excess of X (equation 7).



When solutions of  $\text{K}_4\text{Mo}(\text{CN})_7 \cdot 2\text{H}_2\text{O}$  are air oxidized at  $0^\circ\text{C}$  in the presence of large excess of various anions, a variety of colors



develop and persist for periods of several minutes or longer. Iodide produces a deep blue solution with  $\lambda_{\text{max}}$  near 544 nm; thiocyanate, a yellowish brown solution; and nitrite, yellow-orange. No attempt has been made to isolate any of these short-lived products.

## 6. References

1. A. W. Adamson and J. R. Perumareddi, Inorg. Chem., 4, 247 (1965).
2. W. Jakob, A. Samotus, Z. Stasicka, and A. Golebiewski, A. Naturforsch., 21b, 819 (1966).
3. R. P. Mitra, B. K. Sharma, and H. Mohan, Canad. J. Chem., 47, 2317 (1969).
4. A. W. Adamson, J. P. Walker, and M. Volpe, J. Amer. Chem. Soc., 72, 4030 (1950).
5. G. Emschwiller and C. K. Jorgensen, Chem. Phys. Letters, 5, 561 (1970).
6. C. Creutz and H. Taube, J. Amer. Chem. Soc., 91, 3988 (1969).

### C. Appendix. Cyanomolybdate Data

Presented in this section is a collection of data relating to various cyanomolybdate systems that was acquired during the study of  $\text{Mo}(\text{CN})_7^{4-}$ . Infrared and optical data are included for various cyanomolybdates that are common impurities or products of reactions involving  $\text{Mo}(\text{CN})_7^{4-}$ .

Two ions which are common impurities in  $\text{Mo}(\text{CN})_7^{4-}$  preparations are  $\text{Mo}(\text{CN})_8^{4-}$  and  $\text{MoO}(\text{OH})(\text{CN})_4^{3-}$  which arise through the oxidation of the heptacyanide. Their infrared spectra in the CN-stretching region are included in Figure 1. Red  $\text{NaK}_3\text{MoO}_2(\text{CN})_4 \cdot 6\text{H}_2\text{O}$  has been shown by x-ray structural studies<sup>(1)</sup> to be six-coordinate octahedral with trans-oxygens. The CN-stretch spectrum of the undoubtedly isostructural  $\text{K}_4\text{MoO}_2(\text{CN})_4 \cdot 6\text{H}_2\text{O}$  is shown in Figure 1-A. When this compound is dissolved in water, it forms blue  $\text{MoO}(\text{OH})(\text{CN})_4^{3-}$ , a solution spectrum of which appears in Figure 1-D. Blue compounds can be isolated from these solutions as the potassium salts by a variety of techniques. It has been reported previously,<sup>(2)</sup> that infrared spectra of these salts obtained by various authors do not agree. Figure 1, B and C, illustrates this problem with the CN-stretching spectrum of two batches of the compound, presumably  $\text{K}_3\text{MoO}(\text{OH})(\text{CN})_4 \cdot 2\text{H}_2\text{O}$ . Additional study is needed to determine the nature of hydrated and anhydrous salts and the reported<sup>(2)</sup> mixed oxidation state compound,  $\text{K}_6[\text{Mo}_2^{\text{IV}}\text{Mo}^{\text{VI}}(\text{CN})_8\text{O}_6] \cdot 2\text{H}_2\text{O}$ , obtained from these blue solutions. Figures 1-E and 1-F show the solid and solution spectra of  $\text{K}_4\text{Mo}(\text{CN})_8 \cdot 2\text{H}_2\text{O}$ . The difference between the two spectra has long been used as

Figure 1. Infrared spectra in the cyanide stretching region in various cyanomolybdates.

- A)  $\text{K}_4\text{MoO}_2(\text{CN})_4 \cdot 6\text{H}_2\text{O}$ , 0.96 mg/400 mg KBr pellet, ambient temperature.
- B)  $\text{K}_3\text{MoO}(\text{OH})(\text{CN})_4 \cdot 2\text{H}_2\text{O}$ , Nujol mull, ambient temperature.
- C)  $\text{K}_3\text{MoO}(\text{OH})(\text{CN})_4 \cdot 2\text{H}_2\text{O}$ , KBr pellet, different preparation.
- D) 0.1F aqueous solution  $\text{MoO}(\text{OH})(\text{CN})_4^{3-}$ .
- E)  $\text{K}_4\text{Mo}(\text{CN})_8 \cdot 2\text{H}_2\text{O}$ , KBr pellet, ambient temperature.
- F)  $\text{K}_4\text{Mo}(\text{CN})_8 \cdot 2\text{H}_2\text{O}$ , few tenth's formal, ambient temperature.

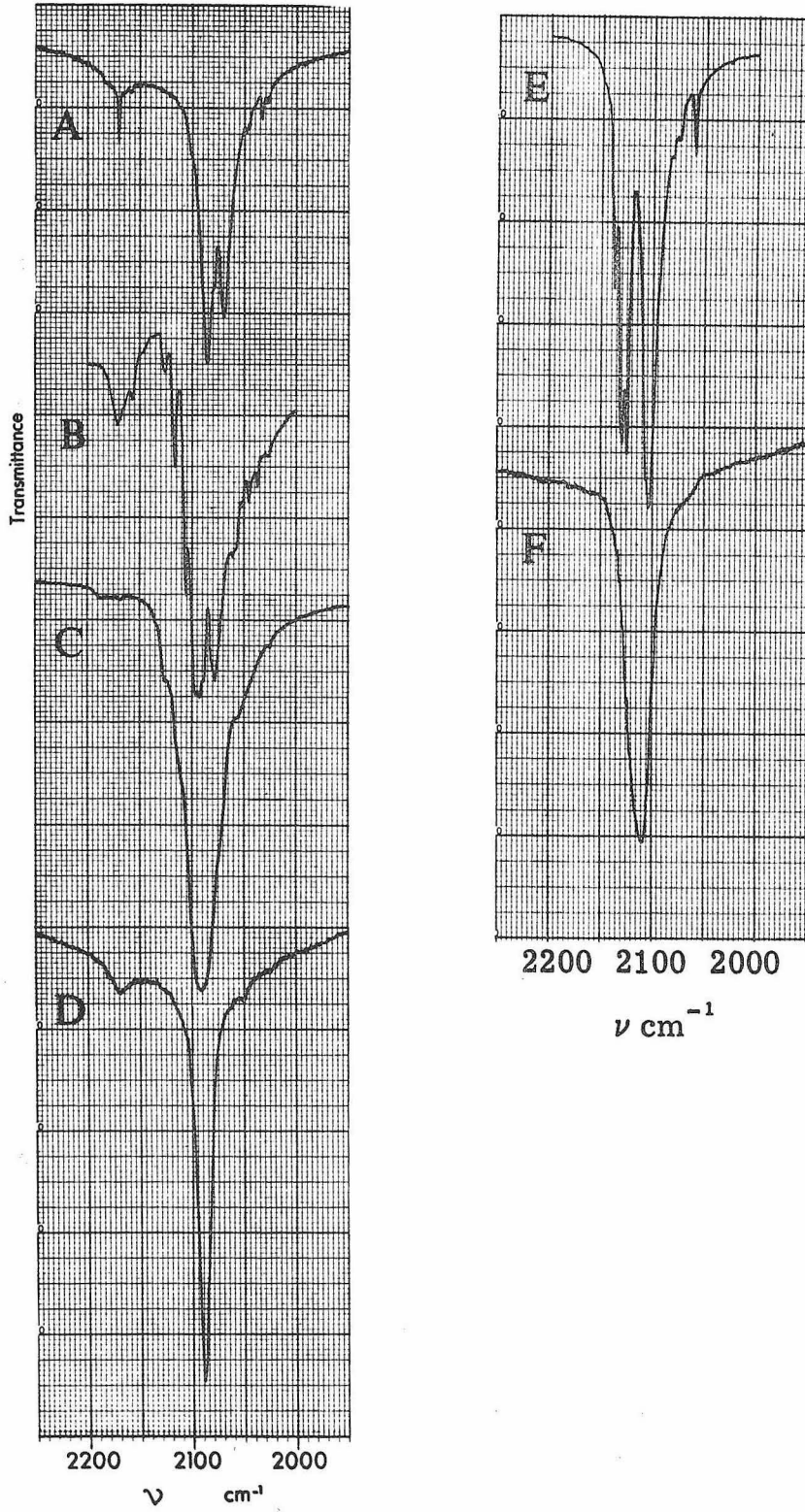


Figure 1

evidence to support the idea of geometrical isomerization between the two phases.

The optical spectra of  $\text{Mo}(\text{CN})_8^{4-}$  and  $\text{MoO}(\text{OH})(\text{CN})_4^{3-}$  are presented in Figure 2. A mixture of these two species is formed when molybdate(VI) is reduced in the presence of cyanide ion. The third common impurity in  $\text{Mo}(\text{CN})_7^{4-}$  systems is the photoproduct whose spectrum is shown in Figure 2-D along with the spectrum of undecomposed  $\text{Mo}(\text{CN})_7^{4-}$  (Figure 2-C).

The optical spectrum of  $\text{K}_4\text{Mo}(\text{CN})_8 \cdot 2\text{H}_2\text{O}$  in 2:1 saturated  $\text{LiCl}:\text{H}_2\text{O}$  at  $78^\circ\text{K}$  is very similar to the room temperature spectrum. The major differences are the development of a weak shoulder at 270 nm and the sharpening of the 282 nm shoulder to a well-defined band at 282 nm. More interesting is the temperature dependence of what is assumed to be  $[(\text{C}_4\text{H}_9)_4\text{N}]_4\text{Mo}(\text{CN})_8$ . Tetrabutylammonium octacyanomolybdate(IV), prepared by adding a stoichiometric quantity of  $\text{HClO}_4$  to a cold  $\text{K}_4\text{Mo}(\text{CN})_8 \cdot 2\text{H}_2\text{O}$  solution, filtering off the  $\text{KClO}_4$ , and titrating the  $\text{H}_4\text{Mo}(\text{CN})_8$  solution with a methanolic  $(\text{C}_4\text{H}_9)_4\text{NOH}$  solution, is sufficiently soluble in EPA to allow variable temperature optical spectra to be taken in this medium. The  $24^\circ\text{C}$  spectrum resembles that of  $\text{K}_4\text{Mo}(\text{CN})_8 \cdot 2\text{H}_2\text{O}$  in  $\text{H}_2\text{O}$  with a shoulder at 442 nm, and bands at 369 and 242 nm. At  $78^\circ\text{K}$  additional bands appear at 398 (with indications of still another band between the 368 and 398 nm bands), 332, 323, and 275 nm regions where there were only hints of shoulders at room temperature.

Figure 2. Optical spectra of aqueous solutions of various cyanomolybdates at  $\sim 24^\circ\text{C}$ . For each compound, the vertical scale for three curves represents, respectively, from left to right  $\epsilon = 0-20,000$ ,  $\epsilon = 0-2000$ , and  $\epsilon = 0-200$ .

- A)  $\text{K}_4\text{Mo}(\text{CN})_8 \cdot 2\text{H}_2\text{O}$ .
- B)  $\text{K}_3\text{MoO}(\text{OH})(\text{CN})_4 \cdot 2\text{H}_2\text{O}$ , 0.02F, pH 7.
- C)  $\text{K}_4\text{Mo}(\text{CN})_7 \cdot 2\text{H}_2\text{O}$ , 0.015F.
- D) Photoproduct from the irradiation of 0.015F  $\text{K}_4\text{Mo}(\text{CN})_7 \cdot 2\text{H}_2\text{O}$ .

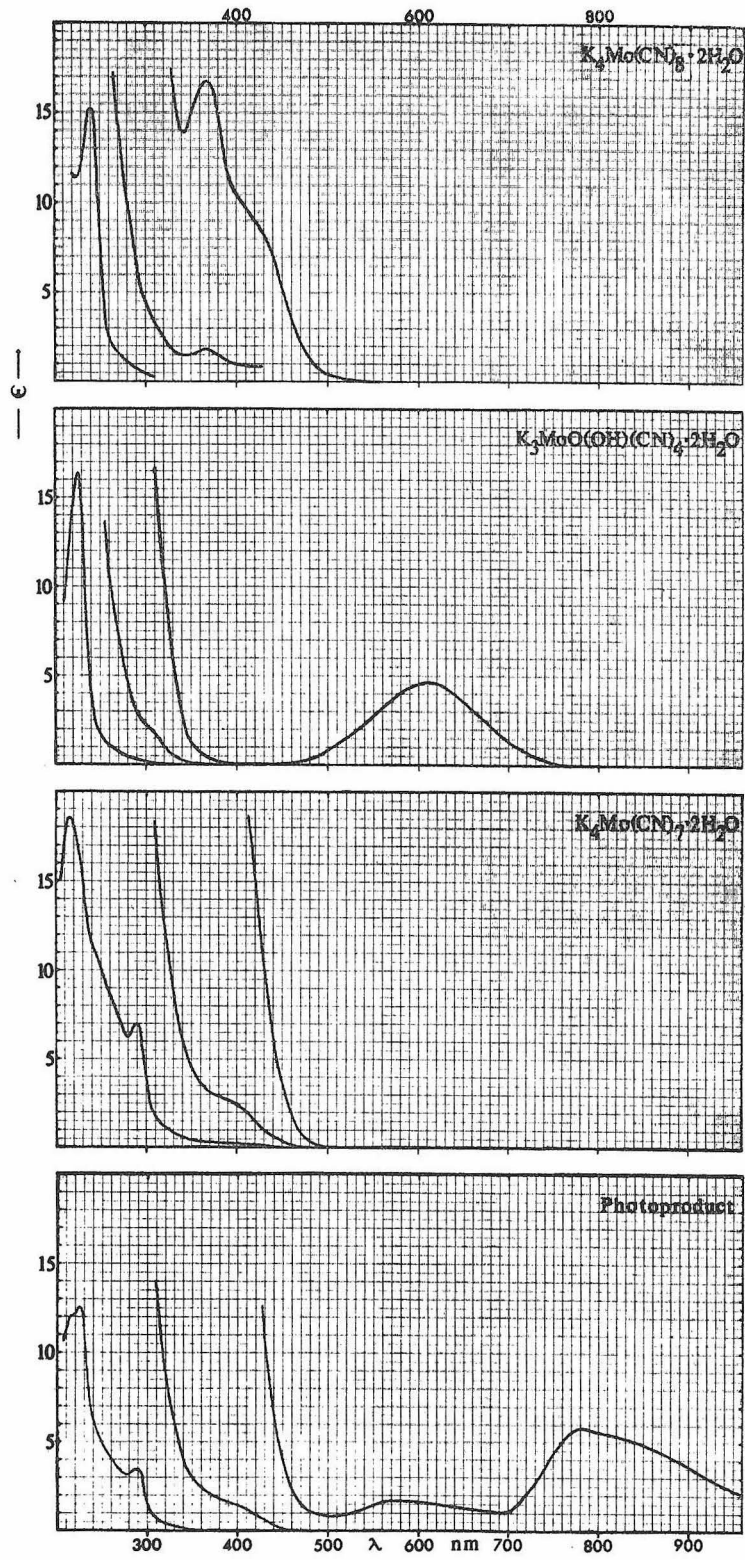


Figure 2



The meaning of these data is not clear, particularly in view of the presently inadequate characterization of the tetrabutylammonium octacyanomolybdate(IV). This material, when freshly prepared, is freely soluble in a variety of organic solvents, but upon standing as the solid for a few days produces sizeable quantities of a yellowish insoluble residue when it is redissolved. One batch, when left exposed to the air for several months, produced the yellow oil which dissolved in water to form pink  $[\text{Mo}(\text{CN})_7(\text{OH}_2)]^{3-}$ .

References

1. V. W. Day and J. L. Hoard, J. Amer. Chem. Soc., 90, 3374 (1968).
2. J. van de Poel and H. M. Neumann, Inorg. Chem., 7, 2086 (1968).

D. Electron Paramagnetic Resonance Spectral Study of Potassium Heptacyanomolybdate(III) Dihydrate

The complex  $K_4Mo(CN)_7 \cdot 2H_2O$  was reported by Young<sup>(1)</sup> in 1932 but to date has remained structurally uncharacterized. The complex anion  $Mo(CN)_7^{4-}$ , having  $S = 1/2$  and simple ligands, should serve as a valuable model for structural studies in the area of seven coordination. Thus we have begun a detailed investigation of the spectroscopic and magnetic properties of  $K_4Mo(CN)_7 \cdot 2H_2O$ . Here we report EPR data that are consistent with a monocapped trigonal prismatic structure for  $Mo(CN)_7^{4-}$  in a polycrystalline sample.

The powder  $K_4Mo(CN)_7 \cdot 2H_2O$  was prepared according to the literature method.<sup>(1)</sup> Our magnetic susceptibility data which give  $\mu_{eff} = 1.73$  B. M. and Curie-law behavior to 77°K are essentially in agreement with those reported earlier.<sup>(2)</sup> The EPR spectra on an undiluted powder sample were obtained at both X-band (9.50 GHz) and K-band (34.8 GHz) frequencies on a Varian-4500 spectrometer using 100 KHz field modulation. The g-values were calculated by comparison with the resonance field of a standard DPPH sample ( $g = 2.0037$ ).

The EPR signal for the sample was observable only below -120°C. The signal linewidth was found to decrease substantially on further lowering of the temperature. This linewidth decrease was accompanied by a concomitant increase in the signal amplitude and the absorption intensity. The X-band and K-band spectra observed at liquid nitrogen temperature are presented in Figure 1, together with those calculated by computer simulation. These spectra are characteristic

Figure 1. ESR spectra. The experimentally observed and computer-simulated EPR spectra for the ion  $\text{Mo}(\text{CN})_7^{4-}$  in an undiluted powder sample of  $\text{K}_4\text{Mo}(\text{CN})_7 \cdot 2\text{H}_2\text{O}$  (broken curves represent the simulated spectra):

A) X-band spectra (9.50 GHz) at 77°K.

B) K-band spectra (34.80 GHz) at 90°K.

Figure 2. ESR spectrum. X-band spectrum (9.33 GHz) at 78°K of undiluted powder sample of  $\text{Cs}_4\text{Mo}(\text{CN})_7 \cdot x\text{H}_2\text{O}$ .

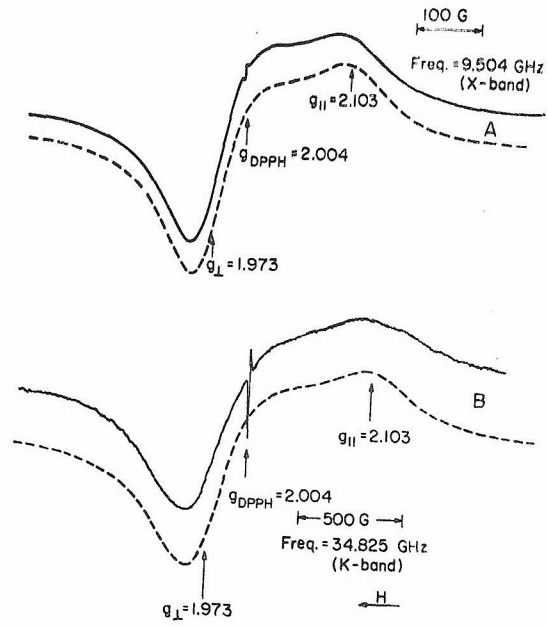


Figure 1

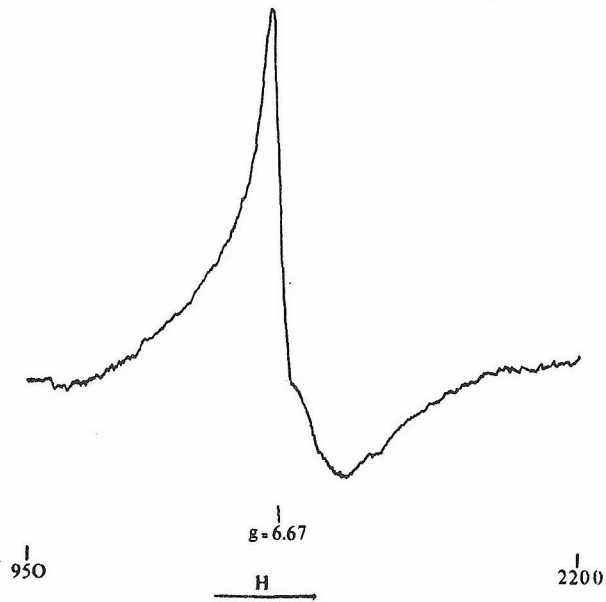


Figure 2

of a polycrystalline sample of an  $S = 1/2$  paramagnetic ion with an axial g-tensor. The observed spectra, which are marked with the resonance peak of a DPPH sample, indicate clearly that  $g_{\parallel} > 2.00$  and  $g_{\perp} < 2.00$  for  $K_4Mo(CN)_7 \cdot 2H_2O$ . The anisotropy in the g-tensor is confirmed by the K-band (34.80 GHz) spectrum in which the separation between the  $g_{\parallel}$  and  $g_{\perp}$  regions is increased by roughly a factor of four over that observed at X-band (9.50 GHz). It is unlikely that the EPR spectra observed for  $Mo(CN)_7^{4-}$  are due to exchange interaction between neighboring Mo(III) species, as no extra resonance attributable to zero-field splitting was observed in the present work. In addition, the EPR absorption intensity observed here was found to increase on decreasing the temperature, which is characteristic of a paramagnetic system. In contrast, antiferromagnetic exchange would lead to a decrease in absorption intensity on lowering the temperature, whereas temperature-independent intensity should accompany ferromagnetic exchange.

Computer simulation of the first derivative lineshapes employing a method described elsewhere<sup>(3)</sup> appears to fit the observed spectra. The best fit is obtained using a Lorentzian lineshape function with the resonance field  $H(\theta)$  calculated from the equation:

$$H(\theta) = [(g_{\parallel}^2 \cos^2 \theta + g_{\perp}^2 \sin^2 \theta)\beta^2]^{-\frac{1}{2}} h\nu \quad (1)$$

where each symbol has its conventional meaning. Terms arising from the nuclear hyperfine interaction were not included in the calculations because the hyperfine structure from  $^{95}Mo$  or  $^{97}Mo$  was not observed

in the present case. The simulated spectra give  $g_{\parallel} = 2.103 \pm 0.005$  and  $g_{\perp} = 1.973 \pm 0.005$  in both X-band and K-band frequencies.

Our EPR data are best accommodated by assuming that the  $\text{Mo}(\text{CN})_7^{4-}$  in  $\text{K}_4\text{Mo}(\text{CN})_7 \cdot 2\text{H}_2\text{O}$  has a  $\text{C}_{2v}$  monocapped trigonal prismatic structure. (4) For this structure the d orbital energy levels are expected to be in the following order:  $d_{z^2}(a_1) > d_{xz}(b_1) \sim d_{x^2-y^2}(a_1) > d_{xy}(a_2)$ , which would give the complex anion a  $(a_2)^2(a_1)^1 = {}^2A_1$  ground state. The observed g-values ( $g_{\parallel} = 2.103$  and  $g_{\perp} = 1.973$ ) may be satisfactorily fit if the ligand field transitions  ${}^2A_1 \rightarrow {}^2B_1, {}^2B_2$  are assigned to the bands at  $30,200 \text{ cm}^{-1}$  and  $25,400 \text{ cm}^{-1}$ , respectively, in the optical absorption spectrum. (5)

The inability to observe an EPR spectrum at room temperature indicates a very short spin-lattice relaxation time. In the present case the effect may arise from rapid intramolecular rearrangement of the  $\text{CN}^-$  ligands, through an intermediate, distorted pentagonal bipyramidal structure. The energy difference between the  $\text{C}_{2v}$  and  $\text{D}_{5h}$  structures should not be large. (6) In fact, in aqueous solution, we have infrared spectral evidence which indicates that the predominant complex species is the  $\text{D}_{5h}$  form of  $\text{Mo}(\text{CN})_7^{4-}$ . (7)

References

1. R. C. Young, J. Amer. Chem. Soc., 54, 1402 (1932).
2. J. Lewis, R. S. Nyholm, and P. W. Smith, J. Chem. Soc., 4590 (1961).
3. F. D. Tsay, H. B. Gray, and J. Danon, J. Chem. Phys., in press.
4. A pentagonal bipyramidal structure ( $D_{5h}$  symmetry) can be ruled out because its  ${}^2E_1[(d_{xz}, d_{yz})^3]$  ground state is incompatible with the observed  $g_{||}$  value.
5. Measured on a KBr pellet of  $K_4Mo(CN)_7 \cdot 2H_2O$  at  $\sim 100^\circ K$ .
6. E. Muetterties, Accounts of Chem. Research, 3, 266 (1970).
7. The ESR data in this section are the result of a study conducted primarily by Fun-Dow Tsay.



## II. SPECTROSCOPIC AND MAGNETIC STUDIES OF MONOMERIC AND DIMERIC $d^5$ SYSTEMS

### A. Electronic Spectral Studies of Iron(III) in a Tetrahedral Oxide-Donor Field

Presently there is a lack of detailed information on the electronic energy levels of tetrahedrally coordinated iron(III) systems. Previous spectroscopic studies of tetrahedral Fe(III) have included  $\text{FeCl}_4^-$ , <sup>(1)</sup> 8-tungstoferrate(III) ion, <sup>(2)</sup> and  $\beta\text{-NaAl}_{1-x}\text{Fe}_x\text{O}_2$ . <sup>(3)</sup> In the first two cases, the important spin-forbidden ligand-field bands are somewhat obscured by intense, low-energy absorption, and in the third case the Fe(III) coordination is significantly distorted from tetrahedral symmetry.

We have performed spectroscopic studies on orthoclase feldspar <sup>(4)</sup> which contains iron(III) in a tetrahedral oxide-donor environment. <sup>(5)</sup> The 295 K absorption spectrum of the sample consists of three prominent bands at 444, 418, and 377 nm, as shown in Figure 1. These bands may be assigned using a level scheme calculated from the energy matrices of Tanabe and Sugano <sup>(6)</sup> for a  $d^5$  system in a cubic ligand field. The diagram presented in Figure 2, which assumes a C/B ratio of 7.83, provides an excellent fit of the experimental data. The spectral bands observed at 444 and 418 nm are due to the transitions  ${}^6A_1 \rightarrow {}^4T_1({}^4G)$  and  ${}^6A_1 \rightarrow {}^4T_2({}^4G)$ , whereas the very sharp peak at 377 nm is logically interpreted as the  ${}^6A_1 \rightarrow ({}^4E, {}^4A_1)$  excitation. A fourth band which is observed at 342 nm in the 85 K spectrum can be assigned to the  ${}^6A_1 \rightarrow {}^4T_2({}^4D)$  transition. In addition, the low-temperature spectrum

**Figure 1.** Electronic absorption spectrum of a specimen of orthoclase feldspar containing Iron(III) in tetrahedral sites.

**Figure 2.** Energy level diagram for Fe(III) in a tetrahedral field. Calculated from the energy matrices of Tanabe and Sugano<sup>(6)</sup> with  $C/B = 7.83$ .

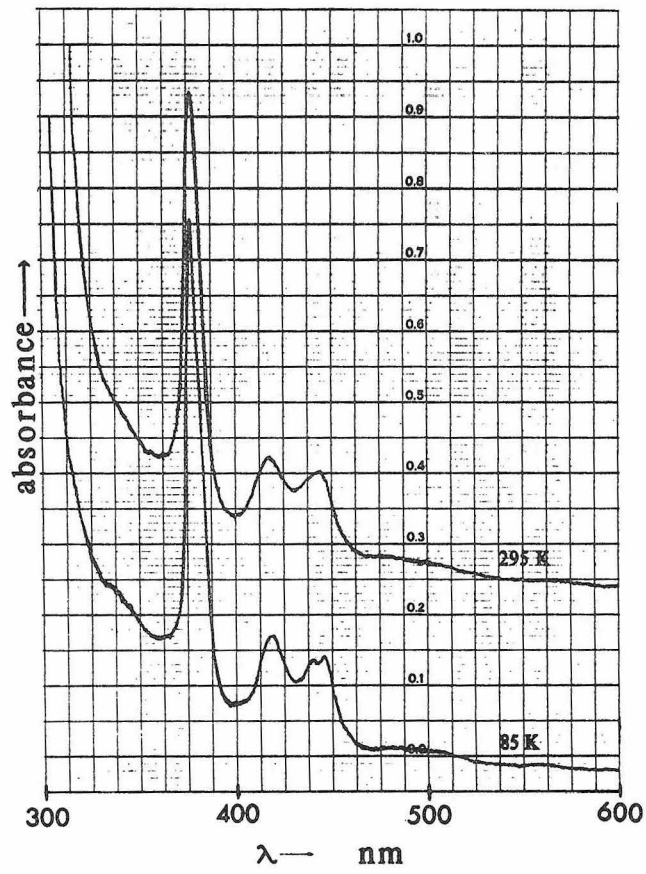


Figure 1

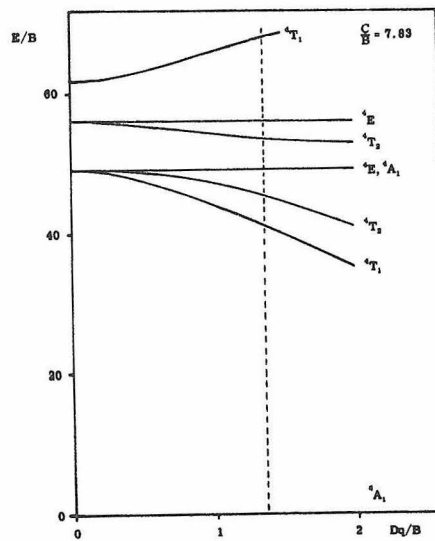


Figure 2

reveals a pronounced splitting of the 444 nm band, as well as a partially resolved shoulder on the 377 nm band. The splittings may reflect a minor low-symmetry component in the ligand field. The shoulder observed on the 377 nm band could also result from a slight energy difference between the  ${}^4A_1$  and  ${}^4E$  states as occurs in hexaquo-manganese(II).<sup>(7)</sup> The spectral data obtained for the  $[\text{Fe(III)O}_4]$  system are summarized in Table I.

The ligand-field parameters,  $\Delta_t$ , B, and C are -7530, 540, and 4230  $\text{cm}^{-1}$ , respectively. For comparison, the spectrum<sup>(8)</sup> of the octahedral complex  $\text{Fe(OH}_2)_6^{3+}$  has been re-analyzed to give B = 945  $\text{cm}^{-1}$ , C = 2950  $\text{cm}^{-1}$ , and  $\Delta_0 = 13,700 \text{ cm}^{-1}$ . The value of  $\Delta_t$  calculated for  $[\text{Fe(III)O}_4]$  is significantly lower than  $\Delta_0$  for  $\text{Fe(OH}_2)_6^{3+}$  as is expected. An interesting point is the much larger C/B ratio in the tetrahedral case. A similarly large ratio has been reported for tetrahedrally coordinated Mn(II) complexes.<sup>(9, 10)</sup>

Finally, we note that comparatively little change occurs in the shape and intensities of the  $[\text{Fe(III)O}_4]$  absorption bands in going from 295 to 85 K. This observation is in accord with the prediction that the intensity-giving mechanism for the spin-forbidden d-d bands in tetrahedral symmetry does not require vibronic coupling.

Table I. Electronic Spectral Data for  
 $[\text{Fe(III)O}_4]$  in Orthoclase Feldspar

${}^6\text{A}_1 \rightarrow$	$\lambda$ (nm)	$\bar{\nu}$ ( $\text{cm}^{-1}$ )	$\epsilon^a$	Calcd <sup>b</sup>
${}^4\text{T}_1$	444	22,500	0.73	22,150
${}^4\text{T}_2$	418	23,900	0.76	24,550
( ${}^4\text{A}_1, {}^4\text{E}$ )	377	26,500	4.1	26,550
${}^4\text{T}_2$	342	29,200	0.1	28,940

<sup>a</sup> Using  $2.57 \text{ g cm}^{-3}$  as the density of orthoclase and 0.83% Fe in sample no. 1273.

<sup>b</sup> For  $\Delta_t = -7350 \text{ cm}^{-1}$ ,  $B = 540 \text{ cm}^{-1}$ ,  $C = 4230 \text{ cm}^{-1}$ .

References

1. H. L. Friedman, J. Amer. Chem. Soc., 74, 5 (1952).
2. D. H. Brown, Spectrochimica Acta, 19, 1683 (1963).
3. T. Birchall, N. N. Greenwood, and A. F. Reid, J. Chem. Soc. (A), 2382 (1969).
4. Orthoclase feldspar, ideally  $\text{KAlSi}_3\text{O}_8$ , has a structure which is based on an infinite three-dimensional silicon-oxygen, aluminum-oxygen framework in which one-fourth of the tetrahedral positions are occupied by aluminum. Specimens have been obtained for which chemical analysis indicates that a small percentage of the aluminum has been replaced by iron.
5. The sample, Caltech Geology reference collection number 1273, was kindly provided by Professor A. L. Albee. Electron microprobe analysis of the clear, light-yellow, gem-quality specimen showed that it contains 0.83% iron by weight, and less than 0.008% manganese. Optical spectra were measured on a Cary 14 RI spectrophotometer. Low-temperature spectra were taken while a  $\text{LN}_2$  cooled gas stream was directed past the sample contained in a quartz dewar. Spectra were taken from 2000 nm to the UV cutoff near 300 nm using sample path lengths ranging from 3.5 to 24 mm.
6. Y. Tanabe and S. Sugano, J. Phys. Soc. Japan, 9, 753 (1954).
7. L. J. Heidt, G. F. Koster, A. M. Johnson, J. Amer. Chem. Soc., 80, 6471 (1959).

8. C. K. Jørgensen, Adv. Chem. Phys., 5, 63 (1962).
9. F. A. Cotton, D. M. L. Goodgame, M. Goodgame, J. Amer. Chem. Soc., 84, 167 (1962).
10. The calculations of the ligand field parameters were performed by Jack C. Thibeault.

## ELECTRONIC STRUCTURE OF OXOBRIDGED IRON(III) DIMERS

Harvey J. Schugar,<sup>1</sup> George R. Rossman,<sup>2</sup> Colin G. Barraclough,<sup>3</sup>  
and Harry B. Gray<sup>2</sup>

Contribution from the Department of Chemistry, Rutgers University,  
New Brunswick, New Jersey 08903, and Contribution No.

from the Arthur Amos Noyes Laboratory of Chemical Physics,  
California Institute of Technology, Pasadena, California 91109

Received

Abstract: Detailed magnetic susceptibility results and electronic, infrared, and Mössbauer spectral data are presented for  $\text{enH}_2[(\text{FeHEDTA})_2\text{O}] \cdot 6\text{H}_2\text{O}$ ,  $\text{Na}_4[(\text{FeEDTA})_2\text{O}] \cdot 12\text{H}_2\text{O}$ ,  $\text{FeHEDTA} \cdot \text{H}_2\text{O}$ , and  $\text{NaFeEDTA} \cdot 3\text{H}_2\text{O}$  (HEDTA = N-hydroxyethylethylenediaminetriacetate, EDTA = ethylenediaminetetraacetate, and  $\text{enH}_2^{2+}$  = ethylenediammonium cation). On the basis of these studies, the dimers are best described as weakly antiferromagnetic ( $S = 5/2$ ,  $5/2$ ) pairs, characterized by  $J = -95$  and  $-99 \text{ cm}^{-1}$ , respectively. The marked intensity enhancement of the ligand field bands and assignment of several UV bands to simultaneous pair electronic (SPE) excitations are discussed in terms of the spin-spin interactions.



## Introduction

There has recently been considerable interest in oxobridged iron(III) dimeric systems. Several complexes of this type have been synthesized and characterized by magnetic susceptibility measurements and Mössbauer spectra.<sup>4-8</sup> Infrared frequencies associated with the oxobridging unit have been identified<sup>4,9</sup> and X-ray structures have been obtained for certain of these oxobridged systems.<sup>10-13</sup> Particular importance can be attached to these systems in view of the presence of dimeric and polymeric species in the aqueous chemistry of iron(III) and the possible occurrence of dimeric iron(III) species in biochemical systems such as the protein hemerythrin.<sup>14</sup> Dimeric ferriporphyrins containing the Fe-O-Fe structural unit have also been characterized.<sup>13,15,16</sup>

In order to present a detailed description of the physical properties of a model oxobridged system, we have chosen to study  $\text{enH}_2[(\text{FeHEDTA})_2\text{O}] \cdot 6\text{H}_2\text{O}$ .<sup>17,18</sup> This compound is of known structure<sup>10</sup> and contains ligands which provide a minimum of interference in the ultraviolet, visible, and infrared spectra. The choice is particularly appropriate because the closely related system  $\text{Na}_4[(\text{FeEDTA})_2\text{O}] \cdot 12\text{H}_2\text{O}$  is available, as well as the monomers  $\text{NaFeEDTA} \cdot 3\text{H}_2\text{O}$  and  $\text{FeHEDTA} \cdot 1\frac{1}{2}\text{H}_2\text{O}$ . The latter complexes provide a reference point for identifying the electronic structural features that are peculiar to the Fe-O-Fe bridging unit. The present paper presents the results of an extensive investigation of the magnetic and spectroscopic properties of the  $\text{enH}_2[(\text{FeHEDTA})_2\text{O}] \cdot 6\text{H}_2\text{O}$  dimer, and related compounds. On the basis of these results we present a critical analysis of the various theoretical models that have been used to describe the electronic structure of oxobridged systems.

### Experimental Section

$\text{enH}_2[(\text{FeHEDTA})_2\text{O}] \cdot 6\text{H}_2\text{O}$ ,  $\text{Na}_4[(\text{FeEDTA})_2\text{O}] \cdot 12\text{H}_2\text{O}$ , and  $\text{NaFeEDTA} \cdot 3\text{H}_2\text{O}$  were prepared as previously described.<sup>17,19</sup>

Solutions of FeHEDTA were prepared by adding 3 equivalents of NaOH to solutions of equimolar amounts of ferric chloride or nitrate and the free ligand.

$\text{FeHEDTA} \cdot 1\frac{1}{2}\text{H}_2\text{O}$  was obtained from the evaporation of salt-free aqueous solutions of the complex prepared from the reaction of equimolar amounts of ferric hydroxide and free ligand at 80-100°C for several minutes. Evaporation of such solutions generally led to the formation of glassy amber films. On occasion, amber crystalline materials could be obtained, and, once in hand, were used to seed additional preparations. Anal. Calcd for  $\text{C}_{10}\text{H}_{18}\text{N}_2\text{O}_{8.5}\text{Fe}$ : C, 33.54; H, 5.07; N, 7.82; Fe, 15.59. Found: C, 33.90; H, 5.42; N, 7.93; Fe, 15.68.

The free ligands,  $\text{H}_3(\text{HEDTA})$  and 99.9% reagent grade  $\text{Na}_2\text{H}_2(\text{EDTA}) \cdot 2\text{H}_2\text{O}$ , used for synthesis and ligand diamagnetism measurements were obtained from M.C. & B. and Baker, respectively, and used as received. Chemical analyses were performed by Schwarzkopf Microanalytical Laboratory.

The large crystals for single crystal studies were grown by evaporation at room temperature in still air of aqueous solutions filtered through 0.22  $\mu\text{m}$  pore size Millipore filters to remove finely dispersed hydrous iron oxides commonly present in preparations of this type. The crystal morphology of  $\text{enH}_2[(\text{FeHEDTA})_2\text{O}] \cdot 6\text{H}_2\text{O}$  is

shown in Figure 1. The relationship of the unit cell axes to the crystal morphology was determined with oscillation and Weissenberg photographs. Selective development of either the rhomboidal (dichroic) or rectangular (non-dichroic) faces occurs. As the Fe-O-Fe unit is directed approximately along  $a^*$ , the electric vector of light normal to the rectangular face always is  $\perp$  to the Fe-O-Fe direction. The electric vector of polarized light normal to the rhomboidal face can be rotated so as to have substantial components perpendicular (orange) or parallel (red) to the Fe-O-Fe axis. Similar dichroism is also observed for the hexagonal face containing the  $a$  axis.

Spectral Measurements. All UV, visible, and NIR spectra were obtained on a Cary 14 RI spectrophotometer. Variable temperature solution studies were conducted employing a 1:1 v/v mixture of filtered, saturated aqueous LiCl and water.<sup>20</sup> The UV spectra were obtained with the solution held as a thin film between two quartz plates. Visible and near infrared spectra were obtained in 0.10 cm and 1.0 cm cells, constructed with rounded edges which minimize the tendency of the glasses to crack at low temperatures.

Polarized spectra were obtained with visible and near infrared sheet polarizers purchased from Cary Instruments.

Infrared spectra were taken on a Perkin Elmer 225 grating spectrophotometer. Solution spectra were taken in 0.05 mm  $\text{BaF}_2$  cells, using deuterium oxide as a solvent. Solids were handled as KBr and TlBr pellets, and Nujol mulls. Low temperature spectra were taken with a modified Beckman RIIC VLT-2 unit. The samples

were run in KBr pellets held in a copper block which fits in the VLT-2. The block temperature was measured with a copper/constantan thermocouple. To minimize heating of the pellets, the source was operated at 75% of normal intensity as measured by the source intensity meter of the instrument.

Magnetic Susceptibility Measurements. Magnetic susceptibility measurements were made with a Princeton Applied Research FM-1 vibrating sample magnetometer equipped with an Andonian Associates LHe dewar which allows control of temperature from room temperature down to LHe. Room temperature data were calibrated with  $\text{HgCo}(\text{SCN})_4$ .<sup>21</sup>

For variable temperature runs, the sample is fitted at the end of a sample rod assembly which contains a Cu/constantan thermocouple which fits into the sample holder. The sample temperature is determined by the power in a heater which boils the coolant liquid ( $\text{LN}_2$  or LHe) and warms the resulting gas which flows by the sample. Variable temperature data are taken by automatically reducing the power to the heater so that the sample slowly cools. Magnetometer output (proportional to the susceptibility of the material in the sample region) is continuously plotted versus thermocouple reading on an X-Y recorder. The cooling curves are done in two parts. First  $\text{LN}_2$  is used as a coolant while the sample is cooled from  $300^\circ\text{K}$  to about  $80^\circ\text{K}$ . A second run is later made using LHe as the coolant and covering the range  $120^\circ\text{K}$  and lower. The cooling rates-- $1\frac{3}{4}$  hours for  $\text{LN}_2$  and  $1\frac{1}{2}$  hours for LHe--were chosen to be slow enough so that the thermocouple

and sample are in thermal equilibrium with each other. The raw data were corrected for the diamagnetism of the sample holder and the effects of the density changes of the gaseous coolant and then calibrated with the room temperature values of the compounds. The thermocouples which have been calibrated with LN<sub>2</sub>, LH<sub>2</sub>, and LHe, rapidly lose sensitivity below 30°K. Below 15°K thermometric inaccuracies of 5°K may be possible. The sample size was 0.33 cm<sup>3</sup> of material.

The molar diamagnetic corrections used for enH<sub>2</sub>[(FeHEDTA)<sub>2</sub>O] · 6H<sub>2</sub>O and Na<sub>4</sub>[(FeEDTA)<sub>2</sub>O] · 12H<sub>2</sub>O are  $-399 \times 10^{-6}$  and  $-522 \times 10^{-6}$  cgs, respectively. The molar diamagnetic corrections used for NaFeEDTA(OH<sub>2</sub>) · 2H<sub>2</sub>O and for FeHEDTA · H<sub>2</sub>O are  $-187 \times 10^{-6}$  and  $-157 \times 10^{-6}$ . The respective magnetic moments at 25°C are 5.90 and 5.85 B. M. These figures are obtained from the measured values of the gram susceptibilities of H<sub>3</sub>(HEDTA) ( $\chi_g = -0.490 \times 10^{-6}$ ) and Na<sub>2</sub>H<sub>2</sub>(EDTA) · 2H<sub>2</sub>O ( $\chi_g = -0.475 \times 10^{-6}$ ), and from published values for ethylenediamine<sup>22</sup> and Pascal's constants.<sup>23</sup>

Mössbauer Spectra. The Mössbauer spectra were obtained by Professor R. H. Herber at Rutgers University. The compounds were finely ground and contained within aluminum foil supports whose spacing was less than 1 mm. The spectrometer and processing of data have been described elsewhere.<sup>24</sup>

## Results and Discussion

Infrared Spectra. The infrared spectra of enH<sub>2</sub>[(FeHEDTA)<sub>2</sub>O] · 6H<sub>2</sub>O contained in KBr and TlBr pellets at 300°K are presented in Figure 2. KBr pellets and mineral oil mulls of this compound gave

equivalent results. The band associated with the antisymmetric stretch of the Fe-O-Fe unit was studied in D<sub>2</sub>O solution and in KBr pellets at two temperatures (Figure 3). Low energy spectra for the dimers and monomers taken in TlBr pellets are presented in Table I. Comparable results were obtained in KBr pellets and mineral oil mulls. Referring to the infrared spectrum of  $\text{enH}_2[(\text{FeHEDTA})_2\text{O}] \cdot 6\text{H}_2\text{O}$  presented in Figure 2, the band located at  $837.5 \text{ cm}^{-1}$  is characteristic of oxobridged ferric ions.<sup>4</sup> The shoulder at  $867.8 \text{ cm}^{-1}$  appears to be associated with the Fe-O-Fe band in the solid (see Figure 3). High energy shoulders have been observed by other workers in solid state IR spectra.<sup>13</sup>

The characteristic Fe-O-Fe absorption is also present in the spectrum of a concentrated D<sub>2</sub>O solution, thereby substantiating the presence of dimer in solution. When a sample of the dimer in a KBr pellet is cooled to 89°K, the Fe-O-Fe band at  $837.5$  moves to  $844.2 \text{ cm}^{-1}$ . This shift of  $6.7 \text{ cm}^{-1}$  is larger than typical shifts for ligand bands. (For example, the ligand band at  $969.8 \text{ cm}^{-1}$  shifts  $2.6 \text{ cm}^{-1}$  to  $972.4 \text{ cm}^{-1}$  at 89°K.) The Fe-O-Fe band of  $\text{Na}_4[(\text{FeEDTA}_2\text{O})] \cdot 12\text{H}_2\text{O}$  at  $851.2 \text{ cm}^{-1}$  shifts  $5.1 \text{ cm}^{-1}$  to  $856.3 \text{ cm}^{-1}$  when the temperature is lowered to 98°K. Other bands in this spectrum typically shift 2.3 to  $2.5 \text{ cm}^{-1}$ . The larger blue shift of the Fe-O-Fe band on cooling has also been reported by Reiff, Long, and Baker.<sup>6</sup> Possible interpretations of this observation will be considered later.

The infrared spectra characteristic of the oxobridged unit in both linear and bent transition metal dimers have been recently reviewed.<sup>25</sup> As the Fe-O-Fe bond angle in  $(\text{FeHEDTA})_2\text{O}^{2-}$  was found

to be  $165^\circ$ , this system most closely approximates the linear case. Such systems characteristically display IR absorption at  $\sim 850 \text{ cm}^{-1}$  which is associated with the antisymmetric stretch of the M-O-M unit. The symmetric stretching mode gives rise to a second characteristic band at  $\sim 230 \text{ cm}^{-1}$ .

The low energy IR bands for the Fe-O-Fe dimers, related monomers, and ligands studied here are listed in Table I. A comparison of the absorptions of the monomers and dimers in this region does not reveal any band unique to the dimeric compounds. Thus, we are unable to pinpoint the symmetric Fe-O-Fe stretching mode.

Electronic Absorption. The UV spectrum of  $(\text{FeHEDTA})_2\text{O}^{2-}$  presented in Figure 4 differs in relative band intensity from the previously reported spectrum<sup>19</sup> as a result of using more concentrated solutions in very short path length cells. Under the latter experimental conditions, only a negligible amount of monomeric  $[\text{FeHEDTA}(\text{OH})]^-$  is present. When cooled to  $78^\circ\text{K}$ , the 272 nm band almost completely disappears, and the shoulder near 400 nm develops into a band at 393 nm. The other two UV bands do not undergo large intensity changes at low temperatures.

Not shown here is the very similar spectrum of  $(\text{FeEDTA})_2\text{O}^{4-}$ . The UV absorption of a 0.04 F aqueous solution of the monomeric  $\text{NaFeEDTA} \cdot 3\text{H}_2\text{O}$  consists of a single band at 257 nm ( $\epsilon \approx 10,000$ ), and that of  $\text{FeHEDTA} \cdot 1\frac{1}{2}\text{H}_2\text{O}$  also consists of a single band at 248 nm ( $\epsilon \approx 7700$ ). The respective deprotonated monomeric species,  $[\text{FeEDTA}(\text{OH})]^{2-}$  and  $[\text{FeHEDTA}(\text{OH})]^-$  have absorptions at 260 nm ( $\epsilon \approx 7500$ ) and 238 nm ( $\epsilon \approx 8300$ ), respectively.

The visible spectrum of an aqueous solution 0.05 F in the ferric HEDTA chelate (distributed mainly as  $(\text{FeHEDTA})_2\text{O}^{2-}$ ) consists of an overlapping pair of bands at 465 and 475 nm and a shoulder at 543 nm. No significant change in the spectrum occurs when a 50% saturated LiCl solution is used as the solvent. When this LiCl solution containing  $(\text{FeHEDTA})_2\text{O}^{2-}$  is cooled to 16°K, the 475 nm band disappears, leaving a band peaking at 469 nm, and the shoulder gains intensity (Figure 5). In 0.2F aqueous solution, the above band splitting is less pronounced and  $\epsilon$  increases slightly, in part reflecting the concentration dependency of the monomer-dimer equilibrium. In this work,  $\epsilon$ , the molar absorptivity, is expressed per mole of Fe(III).

Band splitting is not observed in the single crystal spectrum; only a single, well-defined band at 475 nm is present. The band at 530 nm is absent in the non-dichroic face, while in the dichroic face it is strongly polarized along the Fe-O-Fe direction. While the 475 nm band does not appear to be polarized, interference by both the 530 nm band and higher energy absorptions allows only a tentative conclusion on this point.

A dominant feature of the NIR spectrum of an aqueous solution of  $(\text{FeHEDTA})_2\text{O}^{2-}$  is a broad, weak ( $\epsilon = 3$ ) band at 894 nm (Figure 6). In the crystal, the band appears structured and displays the temperature dependence shown in Figure 7. This band (and the  $\text{H}_2\text{O}$  overtone at 971 nm) are strongly polarized along the Fe-O-Fe direction, being almost completely absent in the non-dichroic crystal face ( $\epsilon < 0.3$ ).

A search for a lower energy ligand field (LF) absorption was conducted beyond 1300 nm. Since this region cannot be studied in



aqueous solution; single crystals were again employed. Two weak bands at 1480 and 1575 nm were observed, but unlike the 894 nm band, they develop the characteristic appearance of vibrational overtones when the crystal was cooled to 25°K. The remainder of the low energy NIR is comprised of vibrational overtone absorptions which display a significant improvement in resolution as the temperature is lowered. The corresponding monomers display several low intensity, incompletely resolved bands in VIS-NIR region. Spectral data for the monomers are collected in Table II.

The four observed ligand field bands of these dimers are located in the spectral range 400-900 nm (Figures 5-7). Absorption at lower energies appears to be entirely due to infrared overtones. Apart from the enhanced band intensities, the LF spectra of the dimers are similar to the LF spectra of typical six-coordinate  ${}^6A_1$  ferric ion complexes<sup>26, 27</sup> such as ferric alum,  $Fe(H_2O)_6^{3+}$ , and  $Fe(malonate)_3^{3-}$ . (Specifically, we observe two broad bands at low energy followed by a sharper band and a shoulder at higher energies.) This similarity is reasonable because the relatively weak spin-spin coupling of the ferric ions ( $J \cong -95 \text{ cm}^{-1}$ ) via the bridging oxide ion is small in comparison to the energies of the d-d transitions (11,000-25,000  $\text{cm}^{-1}$ ). Thus the first four electronic absorption bands of the ferric dimers given in Tables III and IV are assigned as the four lowest LF transitions of an approximately octahedral, high-spin  $d^5$  complex ( ${}^6A_1$  ground state):  ${}^6A_1 \rightarrow {}^4T_1 ({}^4G)$ ,  ${}^4T_2 ({}^4G)$ ,  $[{}^4A_1, {}^4E] ({}^4G)$ ,  ${}^4T_2 ({}^4D)$ .

We have determined the polarizations for three of the LF absorptions in  $(\text{FeHEDTA})_2\text{O}^{2-}$ . The two low energy bands are strongly polarized along the Fe-O-Fe direction. The next band does not appear to be significantly polarized. Since this compound crystallizes in the monoclinic system (bi-axial), the polarization data cannot differentiate between magnetic and electric dipole excitations.

The LF spectra of  $(\text{FeHEDTA})_2\text{O}^{2-}$  and  $(\text{FeEDTA})_2\text{O}^{4-}$  are surprisingly intense for transitions from  ${}^6A_1$  ground states to quartet excited states. However, similarly enhanced band intensities have been found for  $\text{MnCl}_2$ ,  $\text{MnF}_2$ ,<sup>28</sup>  $\text{KMnF}_3$ ,<sup>29</sup> and  $\text{MnS}$ .<sup>30</sup> While all of these compounds represent examples of infinitely extended, bridged metal ion systems (i. e., magnetically concentrated), the nearest neighbor antiferromagnetic interactions are probably the most important. It is observed that the spin (and parity) "forbidden" bands are a factor of 10-50 more intense than the corresponding absorptions of their magnetically dilute counterparts (e.g.,  $\text{MnCl}_2 \cdot 4\text{H}_2\text{O}$ ). We believe that  $(\text{FeHEDTA})_2\text{O}^{2-}$  is a special case of this phenomenon; that is, a system of isolated, magnetically-interacting metal ion pairs. Although much remains to be learned about the mechanism of intensity enhancement in these systems, recent proposals by Ferguson *et al.*<sup>31</sup> and McClure *et al.*<sup>28</sup> are reasonable. Adopting the formalism of Ferguson *et al.*,<sup>31</sup> we include a brief discussion of this effect here.

The ground state of the ferric dimers is described by  $S = (5/2, 5/2)$  interacting pairs. A single ion electronic excitation leads to a  $S = (3/2, 5/2)$  pair. In the spin-spin coupling model based on

Heisenberg-type exchange ( $-2J\underline{S}_1 \cdot \underline{S}_2$ ), the ground state and excited state pairs are described in terms of the respective spin manifolds (5, 4, 3, 2, 1, 0) and 4\*, 3\*, 2\*, 1\*), where the integers refer to the allowed values of the total spin multiplicity, i. e.,  $S_{\text{Total}} = (S_1 + S_2) \dots (S_1 - S_2)$ , where  $S_1 \geq S_2$ . This formalism leads to a model in which transitions such as 1-1\*, 2-2\*, etc. are spin-allowed.

We next turn to a discussion of the UV spectra of  $(\text{FeEDTA})_2\text{O}^{4-}$  and  $(\text{FeHEDTA})_2\text{O}^{2-}$ . The bands in this region are too intense to be entirely due to the higher energy, one-center LF transitions (Fig. 4). We have suggested,<sup>32</sup> therefore, that absorption in the UV is dominated by simultaneous pair electronic (SPE) transitions. In brief, a single UV photon simultaneously excites a d-d transition on each ferric ion in the Fe-O-Fe unit. Since these ferric ions are only weakly coupled, UV absorptions are expected at energies corresponding closely to sums of individual ferric ion transitions. This is apparent from the data and calculated energy sums listed in Tables III and IV.

The model we use to describe the SPE excitation process is related to the model for intensity enhancement of the LF bands. Namely, the pair of excited ferric ions may be described as an interacting  $S = (3/2, 3/2)$  system which generates the spin manifold [3\*, 2\*, 1\*, 0\*]. Transitions of these metal ion pairs between manifold levels of identical spin-multiplicity are now allowed. The magnetic interaction results in a substantial reduction in paramagnetism at room temperature (see discussion of magnetism below). Thus the 0 → 0\* transition is expected to be the predominant one.

This model suggests one reason why the SPE bands are considerably more intense than the LF bands. Namely, the 0 → 0\* transition is absent

for single ion excitation of the ferric ion pairs. While this simple model predicts an inverse temperature effect for the LF bands, it provides no insight towards the thermal behavior of the SPE bands. We observed that the bands at 272 cooled out while those at 235 and 308 nm gained intensity at low temperatures (Figure 4). The shoulder near 400 nm also gained intensity developing into a band at 393 nm.

The above model also suggests that all of the LF band intensities should diminish at low temperature. Referring to Figures 5 and 7, only the band at 894 nm behaved this way. The bands at 550 and 393 nm intensify at low temperature.

SPE bands were first observed by Dieke and co-workers in  $\text{PrCl}_3$ <sup>33, 34</sup> and later by Ferguson *et al.*<sup>35</sup> There are no obvious reasons why SPE bands should not be commonly present in polynuclear metal complexes.<sup>36</sup> It should be noted that Hansen and Ballhausen<sup>37</sup> have already proposed that the "extra" band present in the spectrum of  $[\text{Cu}(\text{CH}_3\text{CO}_2)_2\text{H}_2\text{O}]_2$  results from the simultaneous excitation of  $\text{Cu}^{2+}$  ion pairs.

Magnetic Susceptibility. The magnetic susceptibility data over the temperature range 10-300°K for  $\text{enH}_2[(\text{FeHEDTA})_2\text{O}] \cdot 6\text{H}_2\text{O}$  and  $\text{Na}_4[(\text{FeEDTA})_2\text{O}] \cdot 12\text{H}_2\text{O}$  are listed in Table V and presented graphically in Figure 8. The results can be fitted by the usual spin-spin interaction model, i. e., taking the Hamiltonian for the interaction as  $H = -2J\mathbf{S}_1 \cdot \mathbf{S}_2$ . We have assumed that  $S_1 = S_2 = 5/2$ ,  $g = 2.00$ , and that  $J = -95 \text{ cm}^{-1}$  for  $\text{enH}_2[(\text{FeHEDTA})_2\text{O}] \cdot 6\text{H}_2\text{O}$  and  $J = -99 \text{ cm}^{-1}$  for  $\text{Na}_4[(\text{FeEDTA})_2\text{O}] \cdot 12\text{H}_2\text{O}$ . The calculated results are shown in Figure 9 where it can be

seen that they fit the data (Table III) well. The rise in  $\chi_g$  at very low temperatures has been observed previously.<sup>6</sup>

For each of the above compounds and other related materials containing the Fe-O-Fe structural unit, it is found that the data can be fitted equally well with either the  $S = (5/2, 5/2)$  or  $S = (3/2, 3/2)$  models. In no case has the  $S = (\frac{1}{2}, \frac{1}{2})$  model proved satisfactory.<sup>6, 38</sup> Unfortunately, magnetic susceptibility measurements on these systems ( $J \cong -100 \text{ cm}^{-1}$ ) have been unable to provide a basis for choosing between the former two models. This is because the additional spin levels which are unique for the  $S = (5/2, 5/2)$  model are not appreciably populated below 300°K. A definitive choice between the  $S = (5/2, 5/2)$  and  $S = (3/2, 3/2)$  models can be made by inspection of electronic spectra, which clearly show that the energy levels of the system are derived from  $S = 5/2$  ferric ions. Therefore, the  $S = (5/2, 5/2)$  model is the correct choice. It does not appear unreasonable to suggest that this conclusion applies equally well to the Fe-O-Fe systems that contain nonbridging ligands such as phen, bipy, and salen. Although most of the ligand field bands are obscured by intense intraligand and charge transfer absorption, a broad, weak ( $\epsilon \sim 3-7$ ) band is observed<sup>7</sup> in these compounds at about  $10,000 \text{ cm}^{-1}$  and probably corresponds to the first LF band in  $(\text{FeHEDTA})_2\text{O}^{2-}$ . While two of these other dimers contain five- and seven-coordinate iron, the Fe-O-Fe unit apparently dominates their magnetic behavior; the observed similarities in the magnetic data are probably not accidental.

A recent e. s. r. measurement<sup>39</sup> supports our use of  $g = 2.00$  (a value consistent with  ${}^6A_1$  ferric ions) and also indicates that any

zero-field splitting must be very small. Our calculated results also assume the absence of temperature independent paramagnetism (T. I. P.). This assumption is supported by the data for  $\text{Na}_4(\text{FeEDTA})_2\text{O} \cdot 12\text{H}_2\text{O}$ . The lowest observed susceptibility is  $\chi_m = 130 \times 10^{-6}$  cgs units, which fixes the upper limit for the T. I. P. Similar upper limits of the T. I. P. have been obtained by others.<sup>6, 38</sup>

The spin-spin interaction probably occurs by superexchange through the bridging oxide ion, since the two Fe(III) atoms are too far apart for direct overlap of their wavefunctions. In fact, this molecule is almost exactly the model situation discussed by Owen and Thornley<sup>40</sup> in their review of the Anderson mechanism of superexchange. They considered two  $d^5$  cations with a bridging oxygen anion, the three atoms being in a linear arrangement. It was shown that  $J$  should be negative and of the order of magnitude that we observe.

Mössbauer Data. Mössbauer parameters were measured at 295 and 77°K for  $\text{enH}_2[(\text{FeHEDTA})_2\text{O}] \cdot 6\text{H}_2\text{O}$ ,  $\text{Na}_4[(\text{FeEDTA})_2\text{O}] \cdot 12\text{H}_2\text{O}$ ,  $\text{NaFeEDTA} \cdot 3\text{H}_2\text{O}$  and  $\text{FeHEDTA} \cdot 1\frac{1}{2}\text{H}_2\text{O}$ . The results are listed in Table VI. Mössbauer measurements have been reported by other workers on a variety of dimers containing the Fe-O-Fe structural unit.<sup>4-8</sup> We will restrict the discussion here to those cases where data exist for the corresponding high-spin monomeric ferric complexes. Ideally, the coordination environment in the monomers and dimers should also be as similar as possible. Accordingly, Table VI contains data obtained by us, along with selected measurements reported by others.

Regarding the structural relationships of the compounds reported here,  $(\text{FeHEDTA})_2\text{O}^{2-}$  and  $(\text{FeEDTA})_2\text{O}^{4-}$  display nearly identical optical spectra and presumably have similar coordination environments (distorted octahedral). While the corresponding monomers contain  ${}^6\text{A}_1$  ferric ion, seven-coordination has been found in  $\text{RbFeEDTA} \cdot 3\text{H}_2\text{O}$ <sup>41</sup> and presumably also is present in  $\text{NaFeEDTA} \cdot 3\text{H}_2\text{O}$ . The detailed structure of  $\text{FeHEDTA} \cdot 1\frac{1}{2}\text{H}_2\text{O}$  is unknown, and a case can be made for either six or seven coordination. The complexes  $(\text{FeSalen})_2\text{O} \cdot 2\text{py}$  and  $\text{FeSalenCl} \cdot (\text{CH}_3\text{NO}_2)_x$  have both been characterized by single crystal X-ray diffraction studies.<sup>11, 42</sup> These compounds are a typical Fe-O-Fe antiferromagnet ( $J = -90 \text{ cm}^{-1}$ ) and a high-spin complex, respectively. Each compound contains five-coordinate ferric ion located slightly above the base of a distorted square pyramidal ligand environment. Neither the pyridine nor nitromethane is coordinated to the ferric ion. The terpyridyl complexes  $[(\text{Feterpy})_2\text{O}](\text{NO}_3)_4 \cdot \text{H}_2\text{O}$  and  $\text{Fe}(\text{terpy})\text{Cl}_3$  have been studied by Reiff and co-workers.<sup>6</sup> The compounds are, respectively, an antiferromagnet ( $J = -105 \text{ cm}^{-1}$ ) and a high-spin complex. Although the former compound most likely contains an Fe-O-Fe structural unit, no additional structural conclusions can be drawn at this time.

All of the compounds listed in Table V are characterized by approximately the same isomer shift ( $0.78 \pm 0.13 \text{ mm/sec}$ ). It has been stated that isomer shift values in this range unequivocally establish the ferric ions as being in a sextet spin state and rule out a quartet state.<sup>8</sup> Although the isomer shift criterion for  ${}^6\text{A}_1$  ferric ion is reasonable, its utility will not be established until more ferric compounds with spin quartet ground states are synthesized and fully characterized.

Examination of data in Table V reveals that the monomer-dimer pairs display substantial differences in their  $\Delta E_Q$  values. However, the  $\Delta E_Q$  differences in these systems do not follow a set pattern and thus their electronic structural significance is not at all clear.

Heisenberg Spin-Spin Coupling and Delocalized Molecular Orbital Models for Fe-O-Fe Systems. Magnetic susceptibility measurements show that the ground state of all known Fe-O-Fe systems is diamagnetic. Two models have been frequently used to account for this ground state diamagnetism. As a phenomenological treatment of spin-spin coupling, the Heisenberg model has invariably allowed a close fit of the experimental data. Associated with this spin-spin coupling theory is the hypothesis of super-exchange as an interpretation of the mechanism of paramagnetic and/or ferromagnetic interaction between metal ions bridged by diamagnetic ligands. Both subjects have been recently reviewed by Martin.<sup>43</sup>

An alternative approach based on MO theory has been proposed by Dunitz and Orgel.<sup>44</sup> Applied to the Fe-O-Fe systems, delocalized, three-center MO's are formed via the appropriate overlap of the metal ion  $d\pi$  orbitals with the  $p\pi$  orbitals of the bridging oxide group. Lewis and co-workers have recently commented on the applicability of this model to oxobridged transition ion dimers in general.<sup>38</sup> Although cases are known where the magnetic data and the predictions of the MO model appear to be at odds, such instances are complicated by the neglect of spin-orbit coupling in the simple MO treatment, departures from  $O_h$  symmetry, and other factors.

Perhaps the evidence which best sustains this model (and a major consideration by Dunitz and Orgel) is the fact that unusually



short metal-oxygen distances are found in the bridging units. In a variety of systems whose structures are accurately known from single-crystal X-ray diffraction studies, the metal-bridging oxide distances are typically 0.1-0.3 Å shorter than reference terminal M-O (metal-OH<sub>2</sub>, metal-OH, etc.) distances. Such results have been interpreted in terms of multiple bonding between the metal ion and the oxide bridge. Results in the recent structural report of an Al-O-Al system by Kushi and Fernando,<sup>45</sup> suggests that the multiple-bonding picture may be overemphasized. The Al<sup>3+</sup> ions are five coordinate, the ligation of the neutral dimer being completed by four 2-methyl-8-quinolinol anions. The Al-O distances in the Al-O-Al unit (1.68 Å) are unusually short. Although three-center  $\pi$  bonds involving the relatively high energy, empty d-orbitals of Al<sup>3+</sup> are not impossible, this system underscores the point that trivalent (and tetravalent) metal ions may enjoy shortened bond distances to oxide ions for simple electrostatic reasons. However, it must be noted that the position of the IR band associated with the Fe-O-Fe unit ( $\sim 850 \text{ cm}^{-1}$ ) shows a greater temperature dependence than the other IR bands of the dimers. It may be argued that this IR band should display special sensitivity towards the extent of antiferromagnetic interaction, which is related to the temperature and perhaps the extent of "multiple bonding". On the other hand, it is difficult to assess the relationship between bond order and band position. In fact, while the MO model predicts different bond orders for dimeric units composed of  $\underline{d}^3$ ,  $\underline{d}^4$ , and  $\underline{d}^5$  pairs, nearly all such materials exhibit a strong IR absorption at about  $850 \text{ cm}^{-1}$ .<sup>25</sup> This survey includes selections from the first, second, and third-row

transition series. An alternative hypothesis for the band shifts described above is that any changes in crystal packing forces might be expected to be accentuated in the linkage that holds the individual ferric complexes together.

We believe that a reasonable choice between the MO and spin-spin coupling model may be made for the Fe-O-Fe dimers because the MO model is not consistent with either the spectral or magnetic data. The MO model can be constructed in accord with the symmetry of  $(\text{FeHEDTA})_2\text{O}^{2-}$  (approximately  $C_2$ ) or that of the Fe-O-Fe unit ( $C_{2v}$ ). In this manner the ground state triplet predicted by the MO model is split. Three observations do not support this scheme. First, the temperature dependence of the magnetic susceptibility seems far too small to accommodate anything but an unreasonably miniscule degree of MO splitting. Secondly, independent of the ferric ion coordination number (5, 6, or 7) and symmetry, the extent of antiferromagnetism nicely corresponds to  $J = -95 \pm 10 \text{ cm}^{-1}$ . Finally, the LF spectra of ground state ( $T \leq 30^\circ\text{K}$ )  $(\text{FeHEDTA})_2\text{O}^{2-}$  and  $(\text{FeEDTA})_2\text{O}^{4-}$  are still those of  ${}^6A_1$ -type ferric ions. A ground state of the type predicted by the MO model should give rise to a drastically different spectrum since the number and energies of the excited states must be different. For these reasons, the spin-spin coupling model is highly preferable as a means of describing the electronic structures of Fe-O-Fe systems.

Acknowledgments. The authors wish to thank Professor R. Herber for obtaining the Mössbauer data and Professor J. Potenza for performing the X-ray diffraction studies related to the single crystal

spectral measurements. We appreciate their interest and helpful discussions. Work at Rutgers was supported by the Rutgers Research Council and a Petroleum Research Fund Starter Grant. Work at the California Institute of Technology was supported by the National Science Foundation.

References

- (1) Rutgers University.
- (2) California Institute of Technology.
- (3) On leave from the University of Melbourne, Melbourne, Australia.
- (4) A. V. Khedekar, J. Lewis, F. E. Mabbs, and H. Weigold, J. Chem. Soc. (A), 1561 (1957).
- (5) A. V. D. Bergen, K. S. Murray, and B. O. West, Austral. J. Chem., 21, 1505 (1968).
- (6) W. M. Reiff, G. J. Long, and W. A. Baker, Jr., J. Amer. Chem. Soc., 90, 6347 (1968).
- (7) W. M. Reiff, W. A. Baker, Jr., and N. E. Erickson, J. Amer. Chem. Soc., 90, 4794 (1968).
- (8) R. R. Berrett, B. W. Fitzsimmons, and A. A. Osusu, J. Chem. Soc. (A), 1575 (1968).
- (9) D. J. Hewkin and W. P. Griffith, J. Chem. Soc. (A), 472 (1966).
- (10) S. J. Lippard, H. J. Schugar, and C. Walling, Inorg. Chem., 6, 1825 (1967).
- (11) M. Gerloch, E. D. McKenzie, and A. D. C. Towl, J. Chem. Soc. (A), 2850 (1969).
- (12) E. B. Fleisher and S. Hawkinson, J. Amer. Chem. Soc., 89, 720 (1967).
- (13) E. B. Fleisher and T. S. Srivastava, J. Amer. Chem. Soc., 91, 2403 (1969).
- (14) M. Y. Okamura, I. M. Klotz, C. E. Johnson, M. R. C. Winter, and R. J. P. Williams, Biochem., 8, 1951 (1969).

(15) N. Sadasivan, H. I. Berspaccher, W. H. Fuchsman, and W. S. Caughey, Biochem., 8, 534 (1969).

(16) I. A. Cohen, J. Amer. Chem. Soc., 91, 1980 (1969).

(17) H. J. Schugar, C. Walling, R. B. Jones, and H. B. Gray, J. Amer. Chem. Soc., 89, 3712 (1967).

(18) Abbreviations used in this paper include: phen = 1,10-phenanthroline; bipy = 2,2'-bipyridine; terpy = 2,2',2''-terpyridine; Salen = N,N'-ethylenebis(salicylideneimine).

(19) H. J. Schugar, A. T. Hubbard, F. C. Anson, and H. B. Gray, J. Amer. Chem. Soc., 91, 71 (1969).

(20) Aqueous LiCl solutions have proven satisfactory as a glass forming solvent for use at liquid helium temperatures. Saturated aqueous LiCl and a mixture of two parts saturated LiCl solution and one part water both form clear glasses containing few or no cracks in one centimeter cells when rapidly cooled by immersion into liquid helium. The 1:1 saturated LiCl:H<sub>2</sub>O mixture employed in this work formed a crack-free glass when slowly cooled to 25°K.

(21) B. N. Figgis, R. S. Nyholm, J. Chem. Soc., 4190 (1958).

(22) "Handbook of Chemistry and Physics," 46th Edition, Chemical Rubber Company, Cleveland, Ohio, 1965, p. E-102.

(23) E. König in "Magnetic Properties of Coordination and Organometallic Transition Metal Compounds," Landolt-Börnstein, New Series, Vol. 2, Ed., K. H. Hallwege, Springer-Verlag, Berlin, 1966, pp. 1-16 to 18.

(24) R. Herber in "The Mössbauer Effect and Its Application in Chemistry," Advances in Chemistry Series No. 68, American Chemical Society, Washington, D.C., 1967, pp. 1-20.

(25) R. M. Wing and K. P. Callahan, Inorg. Chem., 8, 871 (1969).

(26) S. Holt and R. Dingle, Acta Chem. Scand., 22, 1091 (1968)

and references therein.

(27) H. L. Schläfer, Z. Physik Chem., NF, 4, 116 (1955).

(28) L. L. Lohr, Jr., and D. S. McClure, J. Chem. Phys., 49, 3516 (1968).

(29) J. Ferguson, H. J. Guggenheim, and Y. Tanabe, J. Phys. Soc. Japan, 21, 692 (1966).

(30) D. R. Huffman, J. Appl. Phys., 40, 1334 (1969).

(31) J. Ferguson, H. J. Guggenheim, and Y. Tanabe, J. Chem. Phys., 45, 1134 (1966).

(32) H. J. Schugar, G. R. Rossman, J. Thibeault, and H. B. Gray, Chem. Phys. Lett., 6, 26 (1970).

(33) F. L. Varsanyi and G. H. Dieke, Phys. Rev. Lett., 7, 442 (1961).

(34) G. H. Dieke and E. Dorman, Phys. Rev. Lett., 11, 17 (1963).

(35) J. Ferguson, H. J. Guggenheim, and Y. Tanabe, Phys. Rev., 161, 207 (1967).

(36) SPE bands are present in solutions containing  $[\text{FeNTA}(\text{OH})]^-$  and  $[\text{FeEDDA}(\text{OH})]^0$  where NTA = nitrilotriacetate and EDDA = sym-ethylenediaminediacetate. A substantial reduction of paramagnetism is found for these systems, and most of the ferric ion is undoubtedly present as Fe-O-Fe dimers. We have also observed what may be SPE bands in DMSO solutions of a dimer whose probable structure is  $[(\text{phen})_2\text{FeCl}]_2\text{O}^{2+}$ . The bipy and Salen ferric dimers display UV spectra completely dominated by intraligand and/or charge transfer absorption bands.

- (37) A. E. Hansen and C. J. Ballhausen, Trans. Far. Soc., 61, 631 (1965).
- (38) J. Lewis, F. E. Mabbs, and A. Richards, J. Chem. Soc. (A), 1044 (1967).
- (39) M. Y. Okamura and B. M. Hoffman, J. Chem. Phys., 51, 3128 (1969).
- (40) J. Owen and J. H. M. Thornley, Rept. Prog. Physics, 29, 675 (1966).
- (41) M. L. Lind, M. J. Harmor, T. A. Harmor, and J. L. Hoard, Inorg. Chem., 3, 34 (1964).
- (42) M. Gerloch and F. E. Mabbs, J. Chem. Soc. (A), 1598 (1967).
- (43) R. L. Martin in "New Pathways in Inorganic Chemistry," E. Ebsworth et al., Editors, Cambridge, 1968.
- (44) J. D. Dunitz and L. E. Orgel, J. Chem. Soc., 2594 (1953).
- (45) Y. Kushi and Q. Fernando, J. Amer. Chem. Soc., 92, 91 (1970).

Table I. Low Energy Infrared Spectral Data

$\text{Na}_4[(\text{FeEDTA})_2\text{O}] \cdot 12\text{H}_2\text{O}$	$\text{Na}[\text{FeEDTA}(\text{OH}_2)] \cdot 2\text{H}_2\text{O}$	$\text{enH}_2[(\text{FeHEDTA})_2\text{O}] \cdot 6\text{H}_2\text{O}$	$\text{FeHEDTA} \cdot 1\frac{1}{2}\text{H}_2\text{O}$
595 $\text{cm}^{-1}$ w <sup>a</sup>	578 $\text{cm}^{-1}$ m <sup>a</sup>	526 $\text{cm}^{-1}$ w <sup>a</sup>	592 $\text{cm}^{-1}$ w <sup>a</sup>
555 w, sh	511 w	475 w-m	572 m
518 m	491 w	439 w	558 w
471 m	473 m	407 w	526 w-m
440 w	441 w-m	386 w-m	478 m
401 w, sh	418 w, sh	367 w	470-430 b
388 m-s	407 s	341 m	393 s 88
370 w, sh	388 w	311 w-m	345 m
313 s	350 s	273 sh	330 s
261 s	311 s	260 s	315 m
	286 m-s		282 w-m
	262 s		263 s
	221 m		255 s
			232 m
			221 m

<sup>a</sup>w, weak; m, medium; s, strong; sh, shoulder.

<sup>b</sup>Several overlapping bands.



Table II. Spectral Data for Monomeric Complexes

Compound	conc.	pH	$\lambda_{\max}$ (nm)	$\epsilon$
Fe(HEDTA)(OH <sub>2</sub> )	$2 \times 10^{-4}$ F	4.8 <sup>a</sup>	248	7700
[Fe(HEDTA)(OH)] <sup>-</sup>	$2 \times 10^{-4}$ F	6.6 <sup>a</sup>	238	8300
[Fe(EDTA)(OH <sub>2</sub> )] <sup>-</sup>	$2 \times 10^{-4}$ F	7.0 <sup>b</sup>	266	8200
NaFe(EDTA) · 3H <sub>2</sub> O	single crystal		881	0.3
[Fe(EDTA)(OH)] <sup>2-</sup>	$2 \times 10^{-4}$ F	9.0 <sup>b</sup>	260	7500

<sup>a</sup>  $6 \times 10^{-4}$ F NaCl.

<sup>b</sup>  $6 \times 10^{-4}$ F NH<sub>4</sub>Cl.

Table III. Solution Electronic Spectral Data and Band Assignments for  $\text{enH}_2[(\text{FeHEDTA})_2\text{O}] \cdot 6\text{H}_2\text{O}^a$ 

$\lambda$ (nm)	296°K <sup>a, b</sup>		Low Temperature		Assignment	Calcd Sums
	$\bar{\nu} \times 10^{-3} \text{ cm}^{-1}$	$\epsilon$	$\lambda$ (nm)	$\bar{\nu} \times 10^{-3} \text{ cm}^{-1}$		
894	11.2	2.6	c, d	--	${}^6\text{A}_1 \rightarrow {}^4\text{T}_1$	--
544	18.4	~40	537	18.6	${}^6\text{A}_1 \rightarrow {}^4\text{T}_2$	--
477	21.0	~25	469	21.3	${}^6\text{A}_1 \rightarrow ({}^4\text{A}_1, {}^4\text{E})$	--
455	22.0	~2				
403	24.8	~120	397 <sup>e</sup>	25.2	${}^6\text{A}_1 \rightarrow {}^4\text{T}_2$	--
343	29.2		337	29.7	$({}^6\text{A}_1 \rightarrow {}^4\text{T}_1) + ({}^6\text{A}_1 \rightarrow {}^4\text{T}_2)$	29.6
307	32.6		305	32.8	$({}^6\text{A}_1 \rightarrow {}^4\text{T}_1) + ({}^6\text{A}_1 \rightarrow {}^4\text{T}_2)$	32.2
273	36.6		f	--	$({}^6\text{A}_1 \rightarrow {}^4\text{T}_2) + ({}^6\text{A}_1 \rightarrow {}^4\text{T}_2)$	36.8
235	42.6		234	42.7	$({}^6\text{A}_1 \rightarrow {}^4\text{T}_2) + ({}^6\text{A}_1 \rightarrow {}^4\text{T}_2)$	43.2
					$({}^6\text{A}_1 \rightarrow {}^4\text{A}_1, {}^4\text{E}) + ({}^6\text{A}_1 \rightarrow {}^4\text{A}_1, {}^4\text{E})$	42.0

Dq = 1090  $\text{cm}^{-1}$ , B = 950  $\text{cm}^{-1}$ , C = 2300  $\text{cm}^{-1}$ g

Table III. (Continued)

- a All  $\epsilon$ 's are based on moles of iron(III), not moles of dimer, and are obtained by visually estimating and subtracting out the contribution of overlapping bands.
- b 0.20F soln. in  $H_2O$ .
- c Infrared overtones prevented accurate determination of this band position.
- d 0.05F soln in 1:1 satd  $LiCl:H_2O$  at 16 °K.
- e 0.29F soln in 1:1 satd  $LiCl:H_2O$  at 78 °K, thin film.
- f 273 nm band almost completely disappears at low temperatures.
- g Ref. 32.

Table IV. Electronic Spectral Data and Band Assignments for  $\text{Na}_4[(\text{FeEDTA})_2\text{O}] \cdot 12\text{H}_2\text{O}$ .

$\lambda$ max	$\bar{\nu}$ ( $\text{cm}^{-1} \times 10^{-3}$ )	$\epsilon$	Assignment	Calcd Sums
888 <sup>a</sup>	11.3	3.1	${}^6\text{A}_1 \rightarrow {}^4\text{T}_1$	--
543	18.4	~50	${}^6\text{A}_1 \rightarrow {}^4\text{T}_2$	--
477	21.0	~35	${}^6\text{A}_1 \rightarrow ({}^4\text{A}_1, {}^4\text{E})$	--
464	21.6	~2		
405 <sup>b</sup>	24.7	~100	${}^6\text{A}_1 \rightarrow {}^4\text{T}_2$	--
344	29.1	c	$({}^6\text{A}_1 \rightarrow {}^4\text{T}_1) + ({}^6\text{A}_1 \rightarrow {}^4\text{T}_2)$	29.7
309	32.4	c	$({}^6\text{A}_1 \rightarrow {}^4\text{T}_1) + ({}^6\text{A}_1 \rightarrow {}^4\text{A}_1, {}^4\text{E})$	32.3
272	36.8	c	$({}^6\text{A}_1 \rightarrow {}^4\text{T}_2) + ({}^6\text{A}_1 \rightarrow {}^4\text{T}_2)$	36.8
246	40.7	c	$({}^6\text{A}_1 \rightarrow {}^4\text{T}_2) + ({}^6\text{A}_1 \rightarrow {}^4\text{A}_1, {}^4\text{E})$	39.4
			$({}^6\text{A}_1 \rightarrow {}^4\text{A}_1, {}^4\text{E}) + ({}^6\text{A}_1 \rightarrow {}^4\text{A}_1, {}^4\text{E})$	42.0

<sup>a</sup> 0.10F solution in 1:1 satd LiCl:H<sub>2</sub>O; 296°K.

<sup>b</sup> 0.01F solution in 1:1 satd LiCl:H<sub>2</sub>O; 296°K.

<sup>c</sup>  $\epsilon$  values of overlapping bands are on the order of  $10^3$ .

Table V. Magnetic Susceptibility Data and Calculated Magnetic Moment per Ferric Ion for  $\text{enH}_2[(\text{FeHEDTA})_2\text{O}] \cdot 6\text{H}_2\text{O}$  and  $\text{Na}_4[(\text{FeEDTA})_2\text{O}] \cdot 12\text{H}_2\text{O}$ .

Temp	$\text{enH}_2[(\text{FeHEDTA})_2\text{O}] \cdot 6\text{H}_2\text{O}$		$\text{Na}_4[(\text{FeEDTA})_2\text{O}] \cdot 12\text{H}_2\text{O}$	
	$10^6 \chi_g (\text{cm}^3 \cdot \text{g}^{-1})$	$\mu(\text{B. M.})$	$10^6 \chi_g (\text{cm}^3 \cdot \text{g}^{-1})$	$\mu(\text{B. M.})$
10	--	--	2.14	0.33
14	1.55	0.31	--	--
26.5	0.713	0.33	0.19	0.27
39.5	-0.110	0.22	-0.29	0.19
49.5	-0.210	0.21	-0.30	0.21
58.5	-0.104	0.27	-0.40	0.17
73.0	0.347	0.45	-0.06	0.37
96.1	1.29	0.76	0.70	0.69
115	1.77	0.93	1.30	0.92
149	2.38	1.20	1.73	1.16
186	2.73	1.42	1.97	1.37
235	3.00	1.67	2.22	1.61
257	3.10	1.76	2.31	1.72
288	3.16	1.88	2.43	1.85
297.3	3.194	1.92	--	--
299.7	--	--	2.46	1.90

Table VI. Mössbauer Parameters of Selected Pairs of Monomers and Oxobridged Dimers.

Compound	Isomer Shift ( $\delta$ )		Quadrupole Splitting	
	295°K	77°K	295°K	77°K
$\text{enH}_2[(\text{FeHEDTA})_2\text{O}] \cdot 6\text{H}_2\text{O}^{\text{b}}$	0.63	0.74	1.69	1.75
$\text{FeHEDTA} \cdot 1\frac{1}{2}\text{H}_2\text{O}$	0.68	0.69	0.80	0.83
$\text{Na}_4[(\text{FeEDTA})_2\text{O}] \cdot 12\text{H}_2\text{O}$	0.66	0.70	1.82	1.94
$\text{Na}[\text{FeEDTA}] \cdot 3\text{H}_2\text{O}$	0.66	0.73	0.75	0.76
$[(\text{Feterpy})_2\text{O}](\text{NO}_3)_4 \cdot \text{H}_2\text{O}$	0.79	0.94	1.93	2.35
$\text{Fe terpy Cl}_3$	0.69	0.81	0.54	0.54
$(\text{Fe Salen})_2\text{O} \cdot \text{py}_2$	0.71	0.79	0.92	0.88
$\text{Fe SalenCl} \cdot (\text{CH}_3\text{NO}_2)_x$	0.70	--	1.34	--

<sup>a</sup>All data expressed in min/sec relative to a  $\text{Na}_2\text{Fe}(\text{CN})_5\text{NO} \cdot 2\text{H}_2\text{O}$  absorber; 0.35 mm/sec added to the original isomer shift data of the latter four materials which were measured relative to iron foil.<sup>6,7</sup>

<sup>b</sup>At 298°K, values of 0.75 and 1.63 min/sec for  $\delta$  and  $\Delta E_Q$  were found by Okamura et al.<sup>14</sup>

Figure Captions

- 1) Crystal morphology of  $\text{enH}_2[(\text{FeHEDTA})_2\text{O}] \cdot 6\text{H}_2\text{O}$ . The Fe-O-Fe unit is oriented approximately along  $a^*$  (1 to b and c), and its projection onto the crystal faces is indicated by the arrows.
- 2) Infrared spectra of  $\text{enH}_2[(\text{FeHEDTA})_2\text{O}] \cdot 6\text{H}_2\text{O}$ . High energy spectrum: 0.37 mg in 400 mg KBr pellet. Low energy spectrum: 1.44 mg in 400 mg TlBr pellet.
- 3) Behavior of the infrared antisymmetric Fe-O-Fe stretch band of  $\text{enH}_2[(\text{FeHEDTA})_2\text{O}] \cdot 6\text{H}_2\text{O}$ .
  - a) KBr pellet at  $310^\circ\text{K}$ .
  - b) KBr pellet at  $\sim 100^\circ\text{K}$ .
  - c)  $\text{D}_2\text{O}$  solution.
- 4) UV spectra of  $\text{enH}_2[(\text{FeHEDTA})_2\text{O}] \cdot 6\text{H}_2\text{O}$  at 296 and  $78^\circ\text{K}$  in a 1:1 mixture of satd LiCl and  $\text{H}_2\text{O}$ : 0.29F, thin film.
- 5) Visible spectra of  $\text{enH}_2[(\text{FeHEDTA})_2\text{O}] \cdot 6\text{H}_2\text{O}$  at 296 and  $16^\circ\text{K}$  in a 1:1 mixture of satd LiCl and  $\text{H}_2\text{O}$ : 0.050 F, path 0.1 cm.
- 6) Near IR spectrum of  $\text{enH}_2[(\text{FeHEDTA})_2\text{O}] \cdot 6\text{H}_2\text{O}$  at  $296^\circ\text{K}$  in saturated LiCl; 0.20 F, path 1.0 cm.
- 7) Near IR spectra of the dichroic (rhomboidal) face of  $\text{enH}_2[(\text{FeHEDTA})_2\text{O}] \cdot 6\text{H}_2\text{O}$ , 0.32 mm thick.
  - a)  $296^\circ\text{K}$ .
  - b)  $89^\circ\text{K}$ .
  - c)  $25^\circ\text{K}$ .

Figure Captions (continued)

8) Gram susceptibility of oxo-bridged dimers.



9) Comparison of the measured (line) and calculated (points) temperature dependence of the magnetic moment per ferric ion of oxo-bridged iron dimers.



$$S = (5/2, 5/2), g = 2.0, J = -95 \text{ cm}^{-1}, \text{T.I.P.} = 0.$$



$$S = (5/2, 5/2), g = 2.0, J = -99 \text{ cm}^{-1}, \text{T.I.P.} = 0.$$



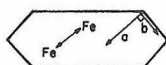
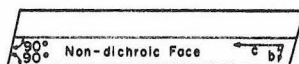
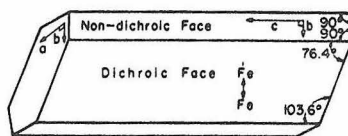


Figure 1

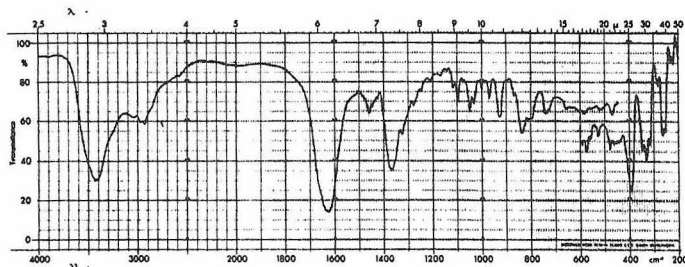


Figure 2

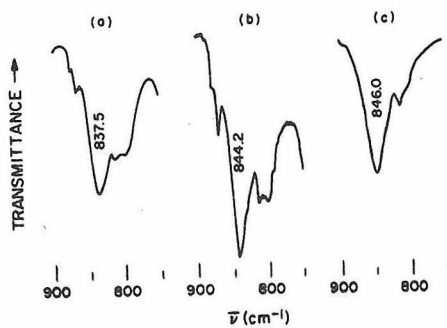


Figure 3

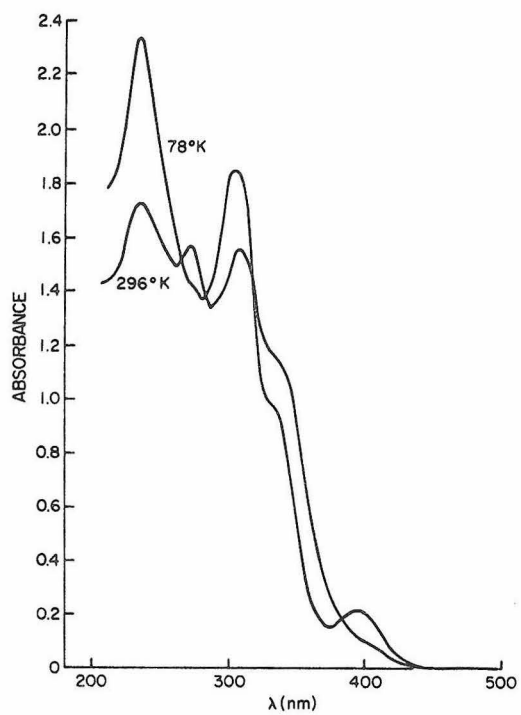


Figure 4

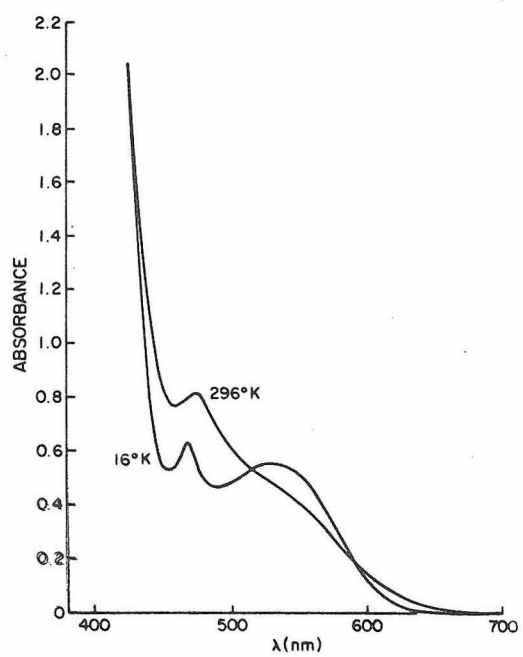


Figure 5

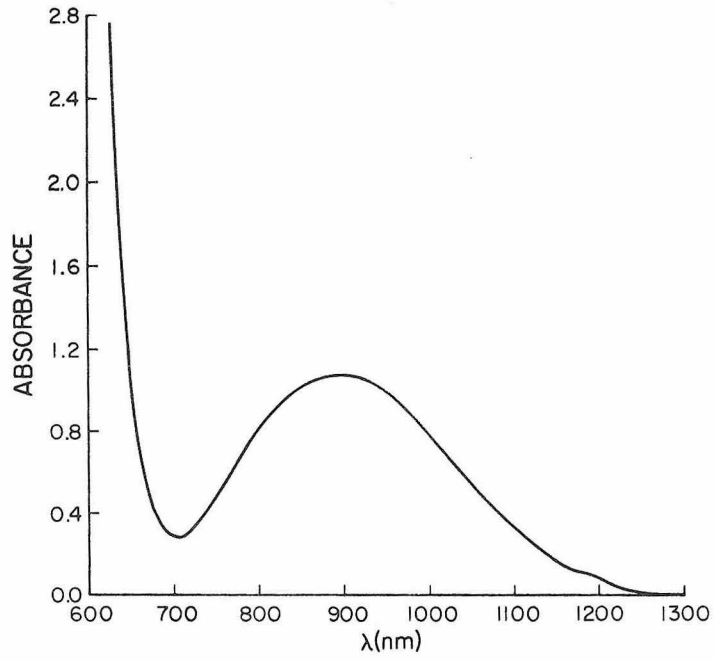


Figure 6

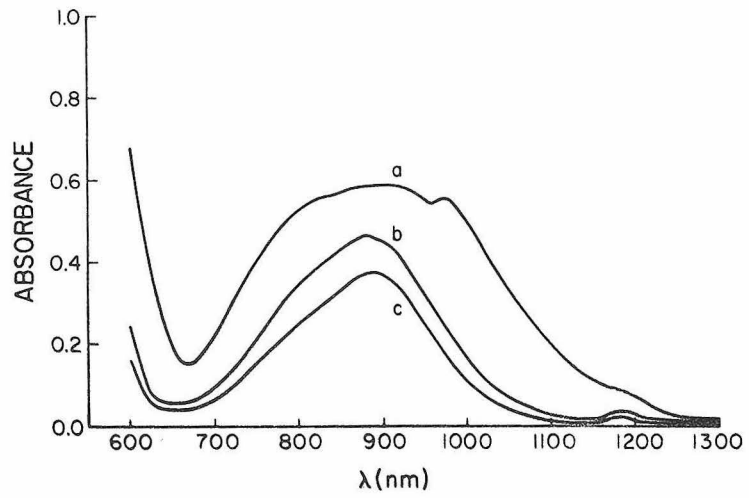


Figure 7

100/101-102-103

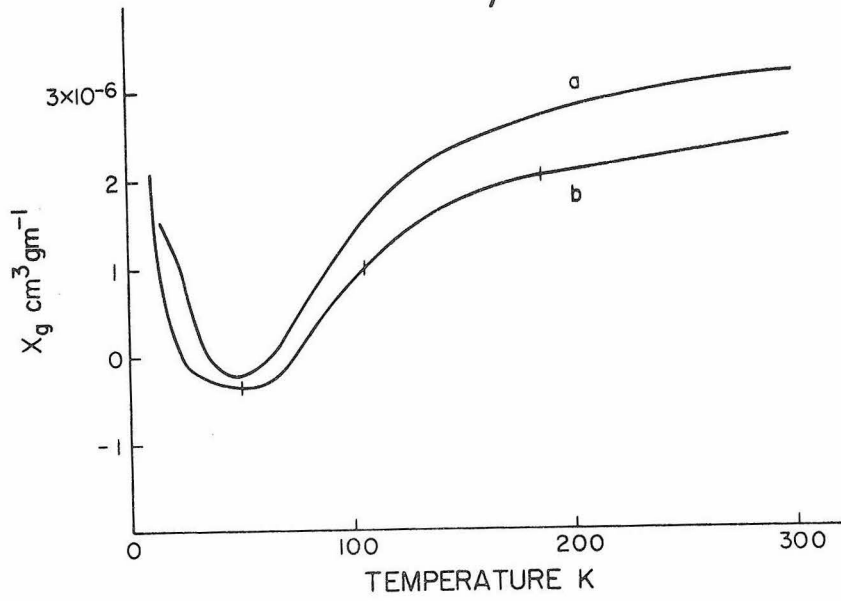


Figure 8

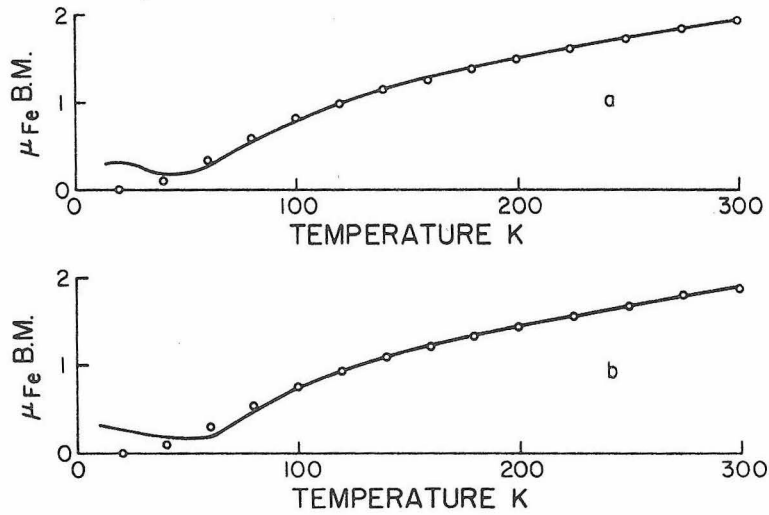


Figure 9

### C. A Dihydroxobridged Ferric Dimer

Recent investigations have produced<sup>(1-3)</sup> a large number of dimeric complexes containing the oxobridged structural unit  $\text{Fe}_2\text{O}^{4+}$ . Here we report the isolation and characterization of  $[\text{Fe}(\text{pic})_2\text{OH}]_2$ , which apparently is the first example of a crystalline iron(III) dimer which utilizes dihydroxobridging in its coordination structure.

Anderegg has previously demonstrated<sup>(4)</sup> by redox potentiometry that ferric ion forms 1:1 and 1:2 complexes with picolinate; the latter complex hydrolyzes to  $[\text{Fe}(\text{pic})_2\text{OH}]$ , which dimerizes at relatively low chelate concentrations ( $> 10^{-4}\text{M}$ ). We have isolated the dimer as a yellow-green microcrystalline powder by raising the pH of fairly concentrated chelate solutions to about 4 with  $\text{HCO}_3^-$  ( $\text{Fe}^{3+}$ :Picolinic acid: $\text{HCO}_3^- = 1:2:3$  with  $[\text{Fe}^{3+}] > 0.1\text{M}$ ). The preferred method of preparation utilizes slow base generation from the hydrolysis of urea. A typical preparation involved heating a solution of 0.01 mole  $\text{FeCl}_3 \cdot 9\text{H}_2\text{O}$ , 0.02 mole picolinic acid, and 0.01 mole urea in 200 ml water at  $90-95^\circ$  for one day. The resulting yellow-green prismatic needles were separated from the hot solution, washed with water, and dried at  $100^\circ$  (yield 60-70%)<sup>(5)</sup>; the crystals become contaminated with a red substance if a stoichiometric amount of urea is used and/or heating is continued for a period of several days. The dimeric complex is only very slightly soluble in water and in common organic solvents such as acetone, methanol, and chloroform.

The structure of dimeric complex may be inferred from infrared spectral data. The infrared spectrum of  $[\text{Fe}(\text{pic})_2\text{OH}]_2$  (KBr pellet or

mineral oil mull) reveals a broad, weak absorption at  $950\text{ cm}^{-1}$  that is not present in the spectrum of the monomeric complex  $[\text{Fe}(\text{pic})_2(\text{OH}_2)\text{Cl}]$ . Secondly, no band between  $800$  and  $850\text{ cm}^{-1}$  attributable<sup>(1,6,7)</sup> to an oxobridged structural unit is observed in  $[\text{Fe}(\text{pic})_2\text{OH}]_2$ . Finally, the similarity in the absorption peaks due to the picolinate ligand in both  $[\text{Fe}(\text{pic})_2(\text{OH}_2)\text{Cl}]$  and  $[\text{Fe}(\text{pic})_2\text{OH}]_2$  rules against any type of picolinate bridging in the dimer. We therefore conclude that the  $950\text{ cm}^{-1}$  band in  $[\text{Fe}(\text{pic})_2\text{OH}]_2$  is due to a vibrational mode associated with the  $\text{Fe}_2(\text{OH})_2^{4+}$  structural unit. Consistent with this assignment, the  $950\text{ cm}^{-1}$  band is not observed in a sample of  $[\text{Fe}(\text{pic})_2\text{OD}]_2$ , which was prepared by precipitating the complex from  $\text{D}_2\text{O}$ . It is reasonable to assume that the band in question has shifted in the dideuterioxobridged complex to substantially lower frequency and is hidden under the strong absorption due to the coordination picolinate groups.

Our interpretation of the structure of the dimeric complex derives additional support from the fact that crystals of  $[\text{Cr}(\text{pic})_2\text{OH}]_2$ , which we have prepared and fully characterized,<sup>(8)</sup> are isomorphous with crystals of  $[\text{Fe}(\text{pic})_2\text{OH}]_2$ ; the infrared band in  $[\text{Cr}(\text{pic})_2\text{OH}]_2$  due to the  $[\text{Cr}_2(\text{OH})_2]^{4+}$  unit is observed at  $970\text{ cm}^{-1}$ .

Magnetic susceptibility data in the range 16 to 299 K for  $[\text{Fe}(\text{pic})_2\text{OH}]_2$ ,  $[\text{Fe}(\text{pic})_2(\text{OH}_2)\text{Cl}]$ , and the known<sup>(1)</sup> oxobridged dimer  $[(\text{FeHEDTA})_2\text{O}]^{2-}$  are shown in Figure 1. The formulation of  $[\text{Fe}(\text{pic})_2\text{OH}]_2$  as a hydroxobridged dimer is consistent with the extent of its antiferromagnetic behavior, which is considerable relative to the reference monomeric complex but is not in the range typical<sup>(1-3)</sup> of

Figure 1. Temperature profiles (16-299 K) of the effective magnetic moments of monomeric, hydroxobridged, and oxobridged Iron(III) complexes.

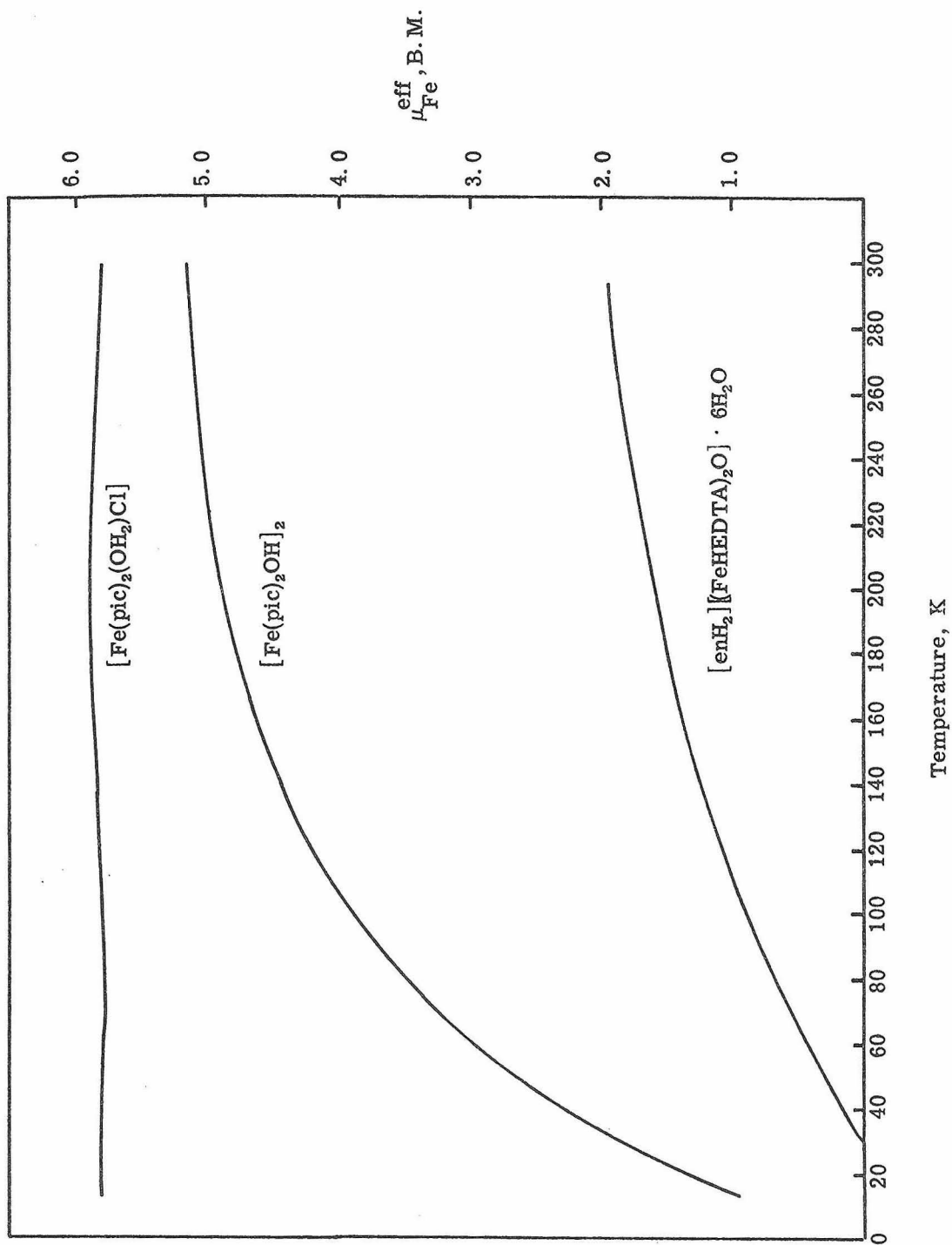


Figure 1



oxobridged structures. Assuming a spin-spin coupling model with  $g = 2.00$ , an excellent fit of the magnetic data is obtained for  $J = -8 \text{ cm}^{-1}$  in the case of  $[\text{Fe}(\text{pic})_2\text{OH}]_2$  and  $J = -86 \text{ cm}^{-1}$  for  $[(\text{FeHEDTA})_2\text{O}]^{2-}$ . It may be hoped that the large difference in the magnetic behavior of the two types of model compounds will prove useful in making structural assignments in other dimeric ferric complexes.

The Mössbauer spectra of  $[\text{Fe}(\text{pic})_2\text{OH}]_2$  and  $[\text{enH}_2][(\text{FeHEDTA})_2\text{O}] \cdot 6\text{H}_2\text{O}$  are also substantially different. The quadrupole splitting constant for the former complex at 80 K is  $1.00 \text{ mm sec}^{-1}$ , whereas for the oxobridged complex it is  $1.7 \text{ mm sec}^{-1}$ . Although the quadrupole splitting is not as large for the dihydroxobridged complex, nevertheless its magnitude indicates a substantially asymmetric coordination environment.

Finally, we turn to a comparison of magnetic and spectral data for  $[\text{Fe}(\text{pic})_2\text{OH}]_2$  and the dimer formed upon base hydrolysis of aqueous ferric nitrate or perchlorate, which has previously been formulated<sup>(1, 4, 9)</sup> as a dihydroxobridged species. Anderegg has pointed out<sup>(4)</sup> that  $[\text{Fe}(\text{pic})_2\text{OH}]_2$  and the aquo dimer must have a similar bridging structure, because they exhibit similar electronic spectral bands at 342 and 335 nm, respectively. Our proof here that  $[\text{Fe}(\text{pic})_2\text{OH}]_2$  is a dihydroxobridged species would thus appear to confirm that the aquo dimer is in fact  $\text{Fe}_2(\text{OH})_2^{4+}$ . We note, however, that the room temperature magnetic moment which has been estimated<sup>(1)</sup> for the aquo dimer is substantially lower than that measured directly for the

crystalline  $[\text{Fe}(\text{pic})_2\text{OH}]_2$  model complex and further work on the former system is needed.

Figure 2. Infrared spectra of hydroxobridged dimers, ambient temperature.

- A)  $[(\text{pic})_2\text{FeOH}]_2$ , KBr pellet.
- B)  $[(\text{pic})_2\text{FeCl}(\text{OH}_2)]$ , 1.40 mg/ 400 mg KBr pellet.
- C)  $[(\text{pic})_2\text{FeOD}]_2$ , KBr pellet.
- D)  $[(\text{pic})_2\text{CrOH}]_2$ , 1.5 mg/400 mg KBr pellet.
- E)  $[(\text{pic})_2\text{CrOD}]_2$ , 1.6 mg/400 mg KBr pellet.

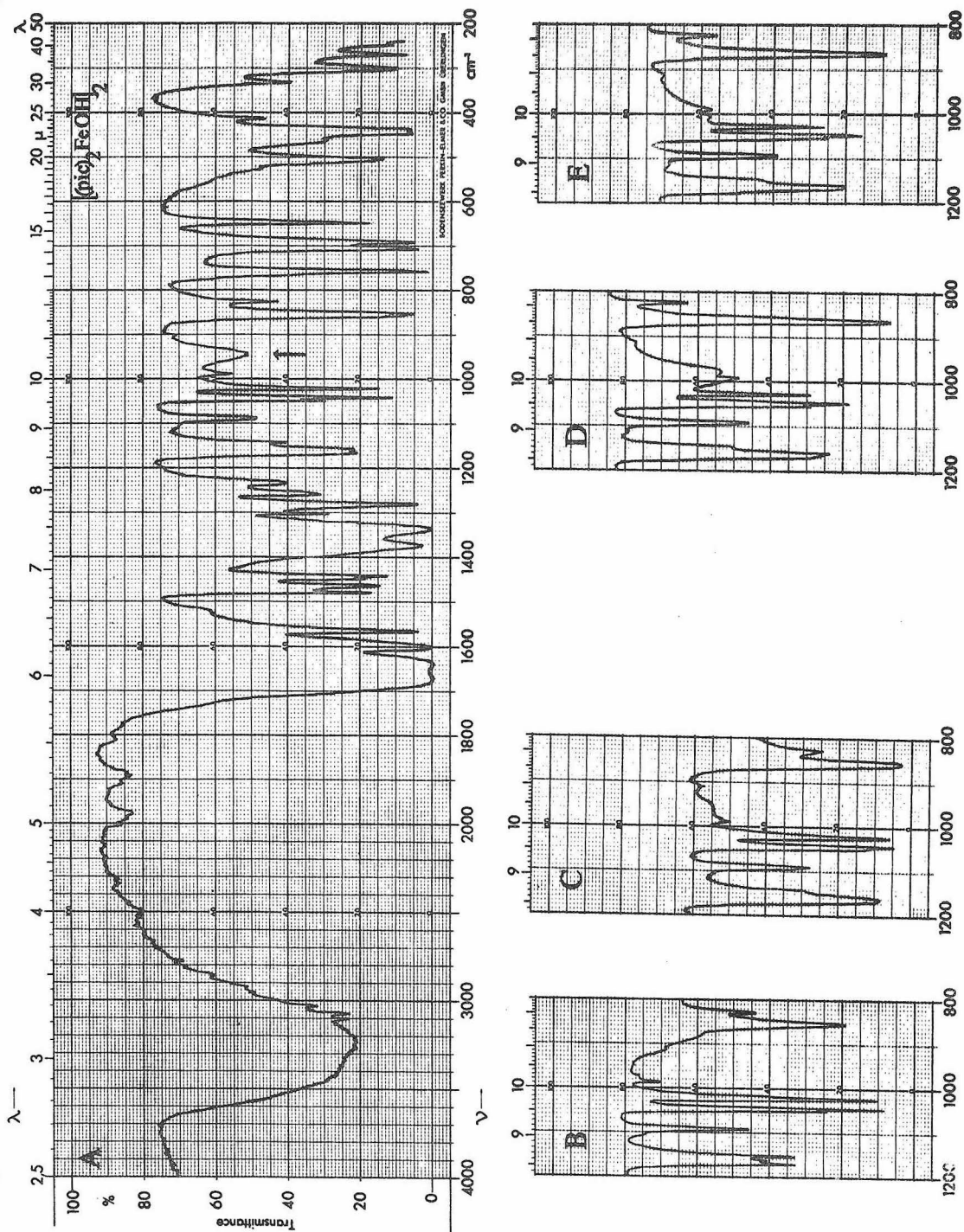


Figure 2

References

1. H. Schugar, C. Walling, R. B. Jones, and H. B. Gray, J. Amer. Chem. Soc., 89, 3712 (1967); and references therein.
2. W. M. Reiff, W. A. Baker, Jr., and N. E. Erickson, J. Amer. Chem. Soc., 90, 4794 (1968); and references therein.
3. J. Lewis, F. E. Mabbs, and A. Richards, J. Chem. Soc. (A), 1014 (1967).
4. von G. Anderegg, Helv. Chim. Acta, 43, 1530 (1960).
5. Satisfactory elemental analyses have been obtained for all new compounds reported here.
6. F. A. Cotton and R. M. Wing, Inorg. Chem., 4, 867 (1965).
7. D. J. Hewkin and W. P. Griffith, J. Chem. Soc. (A), 472 (1966).
8. Magnetic susceptibility data for  $[\text{Cr}(\text{pic})_2\text{OH}]_2$  in the range 16-300 k give  $J = -6 \text{ cm}^{-1}$  for  $g = 2.00$ , which falls in the range  $J = -4$  to  $-7 \text{ cm}^{-1}$  found for dihydroxobridged Cr(III) dimers [see A. Earnshaw and J. Lewis, J. Chem. Soc., 396 (1961)].
9. L. N. Mulay and P. W. Selwood, J. Amer. Chem. Soc., 77, 2693 (1955).

D. Chelates of  $\beta$ -Diketones. VI. Synthesis and Characterization of Dimeric Dialkoxobridged Iron(III) Complexes with Acetylacetone and 2,2,6,6-Tetramethylheptane-3,5-dione (HDPM)

Chin-Hua S. Wu, George R. Rossman,<sup>(1)</sup> Harry B. Gray, George S. Hammond, and Harvey J. Schugar<sup>(2)</sup>

Contribution No. \_\_\_\_\_ from the Arthur Amos Noyes Laboratory of Chemical Physics, California Institute of Technology, Pasadena, California 91109, and the School of Chemistry, Rutgers University, New Brunswick, New Jersey, 08903

1. Abstract

A series of compounds assigned the structure  $[L_2FeOR]_2$  where L is the enolate of acetylacetone or dipivaloylmethane (HDPM) and R is  $CH_3-$ ,  $C_2H_5-$ , and isopropyl have been prepared and characterized. They are obtained by the oxidation of ferrous compounds in alcoholic solutions containing free ligand and bases or directly from ferric compounds. These dimers are weakly antiferromagnetic ( $-J \cong 10 \text{ cm}^{-1}$ ). Their infrared and optical spectroscopic properties are reported.

## 2. Introduction

In the course of a study of the mechanism of oxidation of iron(II) chloride in nonaqueous solvents, <sup>(3, 4)</sup> we observed large enhancement in the rates of oxygen consumption upon addition of  $\beta$ -diketones, such as HDPM, and amines. In a typical experiment the rate of oxidation of a 0.1 M solution of iron(II) chloride in methanol at 30° was increased at least three-hundredfold by addition of 0.3 M each of HDPM and piperidine. Furthermore, a golden yellow product precipitated from the solution almost immediately. Initially, we suspected that the material might be an intermediate in the oxidation process, for example  $(\text{DPM})_2\text{FeOOFe}(\text{DPM})_2$ . However, an exhaustive search for evidence for a peroxide structure, or unusual oxidizing properties, proved to be negative. We then found that the same material could be formed from iron(III) chloride, HDPM, and piperidine in methanol solution. The alternative method of preparation, in conjunction with properties reported in this paper, led to assignment of the structure as  $[(\text{DPM})_2\text{FeOCH}_3]_2$ . The analogous dimer containing ethoxy groups is produced if the reactions are carried out in ethyl alcohol.

Similar materials resulting from the oxygenation of other ferrous chelates have been reported by other workers. Emmert and co-workers <sup>(5)</sup> have produced a variety of alkoxobridged ferric  $\beta$ -diketones by a similar procedure. For example, the oxygenation of  $(\text{acac})_2\text{Fe}(\text{pyridine})_2$  in various alcohols yielded crystalline materials of composition  $(\text{acac})_2\text{FeOR}$ . These products were characterized only

by melting point and elemental analysis although we presume that the structures are analogous to those that we have studied. More recently, Lever, Lewis, and Nyholm have reported that the oxygenation of (picolinate N-oxide)<sub>2</sub> Fe(H<sub>2</sub>O)<sub>2</sub> in CH<sub>3</sub>OH yields a crystalline product of composition (picolinate-N-oxide)<sub>2</sub> FeOCH<sub>3</sub>.<sup>(6)</sup> They proposed a polymeric structure to account for its reduced effective moment of 5.09 B. M. (spin-only  $\mu_{\text{eff}} = 5.92$  B. M. for  $S = 5/2$ ).

We report here the synthesis and spectroscopic and magnetic characterization of dimeric dialkoxobridged iron(III) chelates with DPM or acac as the nonbridging ligand.

### 3. Experimental

#### Preparation of Compounds

[(acac)<sub>2</sub>Fe(OC<sub>2</sub>H<sub>5</sub>)]<sub>2</sub>. This compound was prepared by the procedure of Emmert et al.<sup>(5)</sup> Orange crystals were obtained and recrystallized from anhydrous ethanol (m. p. 158°, lit. 159°C).

A simpler preparation results from the reaction of sodium ethoxide with an equimolar amount of the readily available Fe(acac)<sub>3</sub>. An instantaneous reaction occurs with either concentrated ethanolic solutions or slurries of Fe(acac)<sub>3</sub>. The dimeric product is less soluble than its precursor and approximately 75% yields of the crude material are obtainable by filtration of the cooled (~0°C) reaction mixtures. The product is dried under vacuum at room temperature, or in a stream of dry N<sub>2</sub>. The crude product was purified as above and is identical with the material obtained by Emmert's method.



This procedure appears to be general for the production of related dimers from the appropriate tris- $\beta$ -diketonate and alkoxide salt. (7)

$[(\text{acac})_2\text{Al}(\text{OC}_2\text{H}_5)]_2$ . This compound was prepared from  $\text{Al}(\text{acac})_3$  and sodium ethoxide following the procedure used for  $[(\text{acac})_2\text{Fe}(\text{OC}_2\text{H}_5)]_2$ ; m. p.  $154^\circ\text{C}$ . An alternative preparation involving the reaction of  $\text{Al}(\text{OC}_2\text{H}_5)_3$  with two moles of ligand has been described by Mehrotra and Mehrotra. (8) This material has been reported to be dimeric in boiling benzene. (9) Both preparations give material having identical melting points and infrared spectra.

$[(\text{acac})\text{Fe}(\text{OCH}_3)_2]_x$ . Following the procedure of Emmert and co-workers, (5) the oxygenation of a methanolic solution of  $(\text{acac})_2\text{Fe}(\text{pyridine})_2$  results in a bright yellow product. The material is presumably polymeric since it is essentially insoluble in boiling polar organic solvents such as  $\text{CH}_3\text{OH}$ ,  $\text{CHCl}_3$ , and acetone, and chars without melting. A similar yellow powder can be formed from the reaction of a methanolic solution of  $\text{Fe}(\text{acac})_3$  with two equivalents of methoxide ion.

$\text{Fe}(\text{DPM})_3$  and  $[(\text{picolate-N-oxide})_2\text{Fe}(\text{OCH}_3)]_2$ . These compounds were prepared according to literature methods. (3, 6)

$[(\text{DPM})_2\text{Fe}(\text{OR})]_2$  R =  $\text{CH}_3$ ,  $\text{C}_2\text{H}_5$ , and  $i\text{-C}_3\text{H}_7$ .

1) By the oxidation of ferrous chloride in an alcohol in the presence of DPM.

Fifteen ml of the appropriate dry alcohol 0.3 M in both HDPM and piperidine was saturated at 1 atm and  $30^\circ\text{C}$  with oxygen. To this

solution solid  $\text{FeCl}_2 \cdot 2\text{H}_2\text{O}$  ( $1.75 \times 10^{-3}$  moles,  $\sim 0.12$  M) was added with stirring. Immediate  $\text{O}_2$  consumption and product precipitation occurred. After 30 minutes the reaction was nearly complete with 20 ml ( $0.8 \times 10^{-3}$  mole) of  $\text{O}_2$  absorbed. When the solution was stirred another 30 minutes, less than one additional ml of  $\text{O}_2$  was absorbed. The suspended orange precipitate was collected, thoroughly washed with alcohol in small portions, and dried at room temperature in vacuum over  $\text{P}_2\text{O}_5$  (yield 75%). If water is added to the red filtrate,  $\text{Fe}(\text{DPM})_3$  forms. The same product is formed when the ratio of  $\text{FeCl}_2$  and DPM is varied between 1:2 and 1:3.

2) From iron(III) chloride, HDPM, piperidine, and ROH.

To a filtered dry solution of ferric chloride in the appropriate alcohol (e. g. ,  $1.6 \times 10^{-3}$  mole in 20 ml alcohol) was added a solution of  $3.2 \times 10^{-3}$  moles of freshly distilled HDPM and  $6 \times 10^{-3}$  mole purified piperidine in 5 to 10 ml of the same alcohol. The solution was stirred at room temperature. The product precipitated immediately and was collected by filtration, thoroughly washed with numerous portions of the alcohol, and dried over  $\text{P}_2\text{O}_5$  in vacuum at room temperature. Yields were 90%, 70%, and 12% from methanol, ethanol, and isopropanol, respectively.

The dimeric iron(III) alkoxide complexes are stable in the absence of moisture. The moisture sensitivity of the solids is such that inert atmospheric techniques are not required in low humidity environments. However, solutions of these dimers are readily decomposed by moisture to yield the tris- $\beta$ -diketonates as a major product

along with insoluble residues. In addition, heating of the apparently anhydrous solutions often results in disproportionation to the tris-chelates and unidentified materials.

### Physical Measurements

Molecular weights were determined in  $\text{CHCl}_3$  by vapor phase osmometry (Hewlett-Packard 301 A). Infrared spectra were obtained on a model 225 Perkin-Elmer spectrophotometer using KBr pellets, mineral oil mulls on CsI plates, and freshly prepared  $\text{CHCl}_3$  solutions. Optical spectra were measured on a Cary 14 RI spectrophotometer in  $\text{CHCl}_3$  and cyclohexane solutions and in KBr pellets. Variable temperature magnetic susceptibility data were obtained on a PAR FM-1 vibrating sample magnetometer. Melting points were measured with a DuPont 900 DTA and in melting point capillary tubes with conventional techniques. Elemental analyses were performed by Schwarzkopf Microanalytical Laboratories. Selected physical constants and analytical data are summarized in Table I.

## 4. Results and Discussion

### Structural Formulation and Infrared Spectra

The molecular weight data given in Table I establish the dimeric nature of the  $(\beta\text{-diketonate})_2\text{Fe}(\text{OR})$  complexes. The infrared spectra of representative dimers are shown in Figure 1. For purposes of comparison, the spectrum of  $\text{Fe}(\text{DPM})_3$  is included. As all significant spectral features of the tris-monomeric chelates are present in the spectra of the corresponding dimeric materials, we have chosen to

Table I. Physical Constants and Analytical Data

Compound	m. p. °C	Mol wt at 37°C		Calcd			Found			corr. μ <sup>298°K</sup> , B. M.
		Calcd	Found	C	H	Fe	C	H	Fe	
$[(DPM)_2Fe(OCH_3)]_2$	208-213 <sup>a</sup>	906.8	911	60.92	9.11	12.31	61.01	9.02	12.13	5.09
$[(DPM)_2Fe(OC_2H_5)]_2$	226-230 <sup>a</sup>	934.9	872	61.66	9.29	11.95	61.47	8.90	12.39	5.02
$[(DPM)_2Fe(O-i-C_3H_7)]_2$	216-220 <sup>a</sup>	962.9	921	62.36	9.42	11.60	62.15	9.46	11.86	5.09
$Fe(DPM)_3$	163	605.6	605	65.44	9.48	9.22	65.10	9.25	9.31	5.90
$[(acac)_2Fe(OC_2H_5)]_2$	158 <sup>a</sup>	598.2	479	--	--	--	--	--	--	4.94
$[(acac)_2Al(OC_2H_5)]_2$	154	540	b	--	--	--	--	--	--	diamagnetic
$[(pic-N-O)_2Fe(OCH_3)]_2$	--	726.2	insol	--	--	--	--	--	--	5.14

<sup>a</sup> Melts with decomposition.<sup>b</sup> dimeric, Reference 9

Figure 1. Infrared spectra:

- A)  $\text{Fe}(\text{DPM})_3$
- B)  $[(\text{DPM})_2\text{Fe}(\text{OCH}_3)]_2$  (insert near  $500\text{ cm}^{-1}$  shows the improvements in resolution at  $\sim 78^\circ\text{K}$ ).
- C)  $[(\text{acac})_2\text{Fe}(\text{OC}_2\text{H}_5)]_2$
- D)  $[(\text{acac})_2\text{Al}(\text{OC}_2\text{H}_5)]_2$
- E)  $[(\text{DPM})_2\text{Fe}(\text{O-}\underline{\text{i}}\text{-C}_3\text{H}_7)]_2$

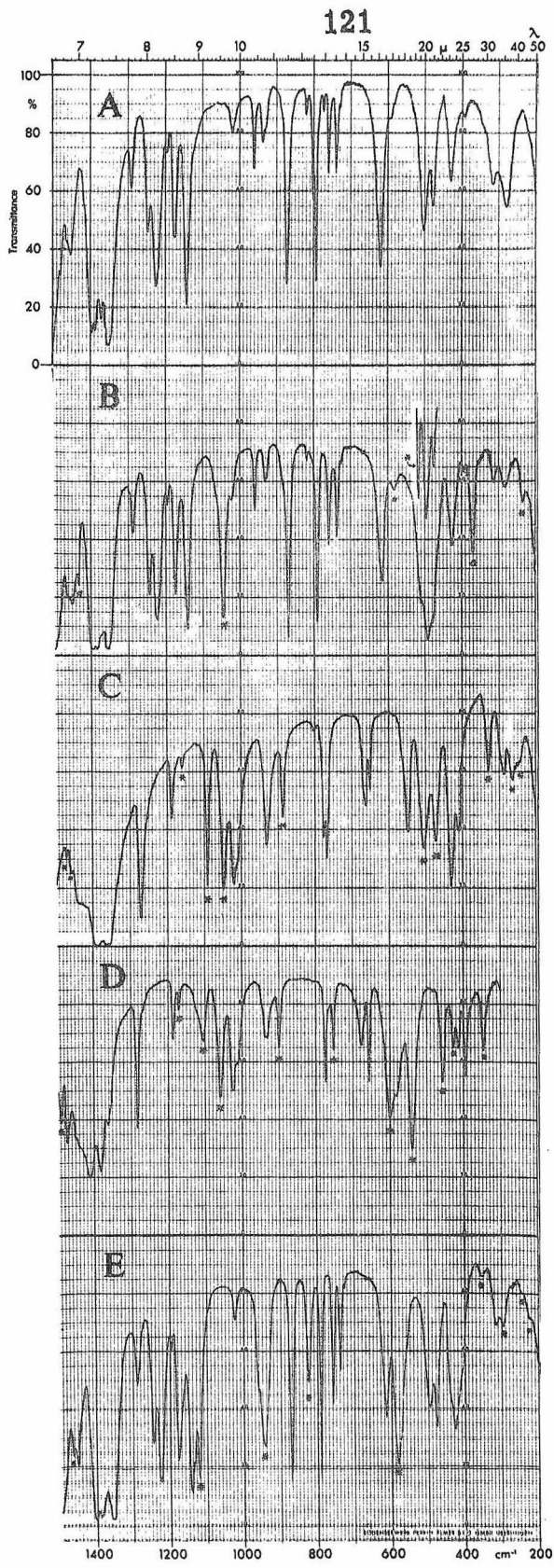


Figure 1

summarize the data by listing only the new absorption bands of the dimeric chelates (Table II).

The first point to note is that the absorption peaks associated with the ligated acac and DPM are essentially identical in both the monomeric and corresponding dimeric materials. Thus the structures of the dimeric complexes are probably as shown in Figure 2, in which the  $\beta$ -diketonates are nonbridging ligands. As discussed below, the magnetic measurements are also in accord with the suggested structure.

The dominant feature among the new infrared absorptions (Table II) is the appearance of one or more strong bands in the region  $800\text{-}1200\text{ cm}^{-1}$  whose positions depend upon the particular alkoxo group but are relatively independent of both the nature of the nonbridging ligands and central metal ion. In the methoxobridged materials, a single band appears at  $1030\text{-}1050\text{ cm}^{-1}$ . For the ethoxides, three bands located near  $890$ ,  $1050$ , and  $1100\text{ cm}^{-1}$  are prominent spectral features. A fourth band of lower intensity located at about  $330\text{ cm}^{-1}$  is also displayed by all the alkoxides. Both of the isopropoxides studied have significant new bands near  $800$  and  $930\text{ cm}^{-1}$ .

For the simplest case of the methoxodimers, the band at  $\sim 1030\text{-}1050\text{ cm}^{-1}$  corresponds to the C-O stretch typically found near  $1050\text{ cm}^{-1}$  in alcohols.<sup>(10)</sup> For the ethoxobridged dimers, the strong absorption at  $\sim 1050\text{ cm}^{-1}$  is also assigned to a C-O stretch. The neighboring band at about  $1100\text{ cm}^{-1}$  and an additional band at  $\sim 890\text{ cm}^{-1}$  are characteristic of the ethoxo group. For instance, ethanol has

Table II. Infrared Spectra<sup>a</sup>

$[(\text{DPM})_2\text{Fe}(\text{OCH}_3)]_2$	235, 371, 486 s, 580, 1048 s, 1434
$[(\text{picolinate-N-oxide})_2\text{Fe}(\text{OCH}_3)]_2$	312, 392 s, 501 s, 1031 s
$[(\text{acac})\text{Fe}(\text{OCH}_3)_2]_2$	332 s, 1050 s, 1450
$[(\text{DPM})_2\text{Fe}(\text{OC}_2\text{H}_5)]_2$	220, 265 s, 332, 495, 583, 586, 889 s, 1047 s, 1096 s, 1160, 1460
$[(\text{acac})_2\text{Fe}(\text{OC}_2\text{H}_5)]_2$	1460
$[(\text{acac})_2\text{Al}(\text{OC}_2\text{H}_5)]_2$	245, 265, 330, 472 s, 502 s, 885, 1048 s, 1091 s, 1160, 1460, 1471
$[(\text{acac})_2\text{Al}(\text{OC}_2\text{H}_5)]_2$	346, 428, 458, 538 s, 600 s, 751, 898, 1059 s, 1106, 1170, 1489
$[(\text{acac})_2\text{Al}(\text{OC}_2\text{H}_5)]_2$ <sup>b</sup>	150 s, 338, 345, 374, 438, 608, 992 s, 1078, 1177
$[(\text{DPM})_2\text{Fe}(\text{O-i-C}_3\text{H}_7)]_2$	225, 245, 295, 352, 582 s, 825, 945 s, 1120 s, 1462

<sup>a</sup> The only peaks reported are those not found in corresponding monomers; positions in  $\text{cm}^{-1}$ ;  
s = strong band.

<sup>b</sup> Raman spectral data.



Figure 2. Proposed structure of alkoxobridged  $[(\beta\text{-diketonate})_2\text{MOR}]_2$ .

Figure 3. Temperature dependence of the magnetic moments

- A)  $\text{Fe}(\text{DPM})_3 \mu$  vs T
- B)  $[(\text{DPM})_2\text{Fe}(\text{OCH}_3)]_2 \mu$  vs T
- C)  $[(\text{DPM})_2\text{Fe}(\text{O}-i\text{-C}_3\text{H}_7)]_2 \mu$  vs T
- D)  $[(\text{acac})_2\text{Fe}(\text{OC}_2\text{H}_5)]_2 \mu$  vs T
- E)  $[(\text{acac})_2\text{Fe}(\text{OC}_2\text{H}_5)]_2 \chi_g$  vs T

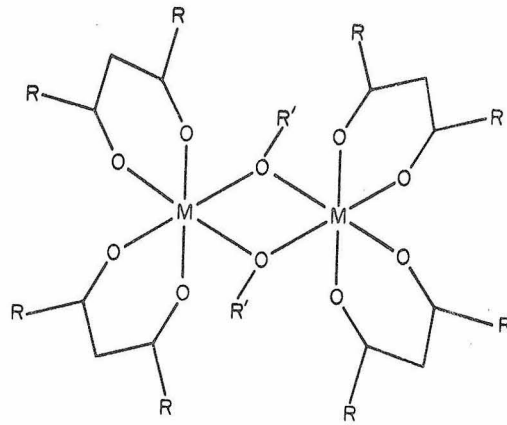


Figure 2

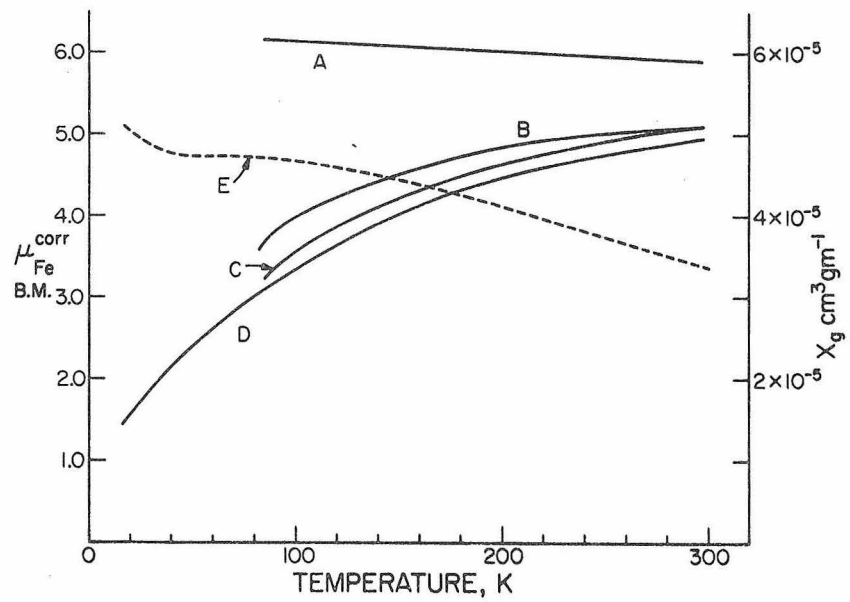


Figure 3

strong absorptions at 1081, 1050, and 876  $\text{cm}^{-1}$  and  $\text{Si}(\text{OC}_2\text{H}_5)_4$  has strong absorptions at 1105 and 1082  $\text{cm}^{-1}$  along with a weak band at 880  $\text{cm}^{-1}$ . For the cases of the polynuclear compounds  $\text{Ti}(\text{OC}_2\text{H}_5)_4$ ,  $\text{Ta}(\text{OC}_2\text{H}_5)_5$ , and  $\text{Nb}(\text{OC}_2\text{H}_5)_5$ , Barraclough *et al.*<sup>(11)</sup> assigned two C-O modes at  $\sim 1030$  and  $1070 \text{ cm}^{-1}$ . As partial hydrolysis of these materials resulted only in the disappearance of the band at  $1030 \text{ cm}^{-1}$ , the two bands were suggested to originate from the bridging and terminal ethoxide groups, respectively.

A variety of isopropoxides display strong absorption at  $\sim 1000 \text{ cm}^{-1}$  that is presumably due to the C-O stretch found at  $1070 \text{ cm}^{-1}$  in isopropanol. Barraclough *et al.*<sup>(11)</sup> have located a band at  $1001\text{-}1036 \text{ cm}^{-1}$  assigned to the C-O frequency for the isopropoxides of Ti(IV), Al(III), Zr(IV), and Ta(V). Similar results for the first two materials have been obtained by Bell *et al.*<sup>(12)</sup> The latter workers also have located an analogous band at  $\sim 1000 \text{ cm}^{-1}$  in  $\text{P}[\text{OCH}(\text{CH}_3)_2]_3$ . (Interestingly, no such absorption was found for the analogous borate.) All the various isopropoxides (and isopropanol itself) show additional absorption features at  $\sim 950$  and  $\sim 840 \text{ cm}^{-1}$ . On this basis we assign the strong band at  $1012 \text{ cm}^{-1}$  to a  $(\text{CH}_3)\text{CH-O}$  stretch for  $[(\text{DPM})_2\text{Fe}(\text{O-}i\text{-C}_3\text{H}_7)]_2$ . Apparently, additional absorptions at  $\sim 950$  and  $\sim 840 \text{ cm}^{-1}$  are also characteristic of the isopropyl group. The bands at  $945$  and  $825 \text{ cm}^{-1}$  exhibited by  $[(\text{DPM})_2\text{Fe}(\text{O-}i\text{-C}_3\text{H}_7)]_2$  are therefore also assigned to the alkoxide groups.

Nakamoto and co-workers<sup>(13)</sup> have recently identified the Fe-O absorption frequencies in  $\text{Fe}(\text{acac})_3$  through isotopic substitution. A

band at  $300.5 \text{ cm}^{-1}$  displayed the maximum shift upon isotopic substitution and was accordingly assigned as the Fe-O stretch. Smaller shifts were observed for the bands appearing at 436, 551, 562, and  $655 \text{ cm}^{-1}$ .

The dialkoxobridged ferric dimers display two or more bands in the low energy region which have appropriate energies for Fe-O stretching modes. However, several ligand modes also are found in this spectral area. Thus a reliable band assignment scheme for the low energy region must await appropriate isotopic substitution data. Also presented without commentary are the Raman bands displayed by  $[(\text{acac})_2\text{Al}(\text{OC}_2\text{H}_5)]_2$  which are not found for  $\text{Al}(\text{acac})_3$ .

The infrared spectrum of  $[(\text{acac})_2\text{Fe}(\text{OC}_2\text{H}_5)]_2$  was also examined at  $\sim 80^\circ\text{K}$ . With the exception of improved band resolution, the most striking spectral feature at  $80^\circ\text{K}$  is the  $12 \text{ cm}^{-1}$  shift to higher energy of the  $502 \text{ cm}^{-1}$  band. Greater than average shifts were also observed for the  $1090$  and  $1048 \text{ cm}^{-1}$  bands ( $5\text{-}6 \text{ cm}^{-1}$ ). Other spectral bands displayed shifts of  $-2$  to  $+3 \text{ cm}^{-1}$ . Therefore the largest shifts in the dimer spectrum all involve bands which are not present in  $\text{Fe}(\text{acac})_3$ . Regarding other ferric dimers, large low temperature shifts are observed<sup>(4)</sup> for the Fe-O-Fe stretch at  $858 \text{ cm}^{-1}$  in  $\text{enH}_2[(\text{HEDTAFe})_2\text{O}] \cdot 6\text{H}_2\text{O}$  (where  $\text{enH}_2^{++}$  is ethylenediammonium and HEDTA is N-hydroxyethylethylenediaminetriacetate)<sup>(15)</sup> and the bridging O-H frequency at  $947 \text{ cm}^{-1}$  in  $[(\text{picolate})_2\text{Fe}(\text{OH})]_2$ .<sup>(16)</sup>

### Magnetic Susceptibility

A feature common to all the dialkoxobridged iron(III) dimers is a room temperature magnetic moment in the range 4.9-5.2 B. M. per iron, a value somewhat lower than the 5.9 B. M. observed for the corresponding tris-monomers and other monomeric, octahedral high-spin Fe(III) complexes (see Table I). Furthermore, Figure 3 shows that all of these dimers display a magnetic moment which decreases with temperature. Such behavior is characteristic of an anti-ferromagnetically coupled system. The magnetic moment per iron vs. temperature curves for  $[(DPM)_2Fe(OCH_3)]_2$  and  $[(picolate-N-oxide)_2Fe(OCH_3)]_2$ <sup>(17)</sup> are nearly identical as are the curves for  $[(DPM)_2Fe(OC_2H_5)]_2$ ,  $[(DPM)_2Fe(O-\underline{n}-C_3H_7)]_2$ ,<sup>(18)</sup> and  $[(acac)_2Fe(OC_2H_5)]_2$ . A representative  $\chi_g$  vs. T curve (for  $[(acac)_2Fe(OC_2H_5)]_2$ ) is also included in Figure 3.

Adopting the standard spin-spin coupling model with a perturbing Hamiltonian  $-2J S_1 \cdot S_2$  and  $S_1 = S_2 = 5/2$ , the experimental data for  $[(acac)_2Fe(OC_2H_5)]_2$ ,  $[(DPM)_2Fe(OC_2H_5)]_2$ , and  $[(DPM)_2Fe(O-\underline{n}-C_3H_7)]_2$  are adequately fit by  $g = 2.0$ ,  $TIP = 0$ , and  $J = -11 \text{ cm}^{-1}$ . Similarly for  $[(DPM)_2Fe(OCH_3)]_2$  and  $[(pic-N-O)_2Fe(OCH_3)]_2$   $J \approx -8.5 \text{ cm}^{-1}$ ; and for  $[(DPM)_2Fe(O-\underline{i}-C_3H_7)]_2$   $J \approx -10 \text{ cm}^{-1}$ . The extent of antiferromagnetic interaction in the dialkoxo dimers is considerably smaller than for oxobridged Fe(III) systems but is comparable to that found in dihydroxobridged Fe(III) dimers ( $J = -8 \text{ cm}^{-1}$ ).<sup>(14-16)</sup> Apparently the antiferromagnetic interaction in systems of the type shown in Figure 2

is primarily characteristic of the  $\text{Fe} \begin{array}{c} \diagup \text{O} \diagdown \\ \diagdown \text{O} \diagup \end{array} \text{Fe}$  structural unit and

relatively insensitive to the nature of  $\text{R}'$  and the nonbridging ligands. Insensitivity to the nature of the nonbridging ligands has also been observed for a series of dimers containing the approximately linear  $\text{Fe-O-Fe}$  structural unit. (14)

### Electronic Spectra

The electronic spectral data are summarized in Table IV and a representative monomer-dimer comparison is shown in Figures 4 and 5 for  $\text{Fe}(\text{DPM})_3$  and  $[(\text{DPM})_2\text{Fe}(\text{OCH}_3)]_2$ . The intraligand and charge transfer bands in the two visible and ultraviolet spectra (Figure 4) are very similar, as would be expected for the structure shown in Figure 2. Two low energy bands (near IR) in each complex are of low intensity and most probably are due to spin-forbidden d-d transitions (Figure 5). Following Piper and Carlin, (19) these bands are assigned to the d-d transitions  ${}^6\text{A}_1 \rightarrow {}^4\text{T}_1$  and  ${}^6\text{A}_1 \rightarrow {}^4\text{T}_2$ , respectively. The somewhat higher energies of the dimer d-d bands as compared to the corresponding monomer could be due to a smaller ligand field strength for bridging alkoxide than for  $\beta$ -diketonate. This conclusion is not firm, however, because small differences in inter-electronic repulsions in the two cases could also lead to shifts of the magnitude observed.

It is important to note that there is no evidence in the electronic spectra of the dialkoxobridged dimers for either substantial intensity enhancements of the spin-forbidden d-d bands or simultaneous pair

Table III. Magnetic Susceptibility Data

	Temp K	$\chi_g$ (cm <sup>3</sup> gm <sup>-1</sup> )	$\mu^{\text{corr}}$ , B. M.
[(acac) <sub>2</sub> Fe(OC <sub>2</sub> H <sub>5</sub> )] <sub>2</sub>	298	33.8 × 10 <sup>-6</sup>	4.95
	252	37.1	4.76
	199	41.2	4.45
	149	44.2	3.99
	101	46.4	3.36
	50.5	47.4	2.41
[(DPM) <sub>2</sub> Fe(OCH <sub>3</sub> )] <sub>2</sub>	298	23.4	5.09
	246	27.4	5.00
	198	31.9	4.84
	149	36.5	4.47
	101	42.5	3.97
	[(DPM) <sub>2</sub> Fe(OC <sub>2</sub> H <sub>5</sub> )] <sub>2</sub>	298	22.0
246		24.7	4.83
199		26.9	4.52
149		29.1	4.06
101		29.9	3.40
[(DPM) <sub>2</sub> Fe(O- <u>n</u> -C <sub>3</sub> H <sub>7</sub> )] <sub>2</sub>		298	20.1
	246	22.6	4.69
	199	25.1	4.44
	149	27.4	4.01
	101	28.4	3.36

Table III (Continued)

	Temp K	$\chi_g$ (cm <sup>3</sup> gm <sup>-1</sup> )	$\mu^{\text{corr}}$ , B. M.
Fe(DPM) <sub>3</sub>	298	23.4	5.89
	246	29.6	6.00
	199	37.1	6.03
	149	50.7	6.08
	91	86.2	6.17
[(picolinate-N-oxide) <sub>2</sub> Fe(OCH <sub>3</sub> )] <sub>2</sub>	298	29.9	5.11
	246	35.1	5.03
	199	40.1	4.83
	149	46.7	4.50
	101	53.5	3.97
[(DPM) <sub>2</sub> Fe(O- <u>i</u> -C <sub>3</sub> H <sub>7</sub> )] <sub>2</sub>	298	21.9	5.09
	246	24.6	4.89
	199	27.2	4.62
	149	30.0	4.19
	101	31.5	3.54



Figure 4. Ultraviolet and visible spectra of  $\text{Fe}(\text{DPM})_3$  (broken line) and  $[(\text{DPM})_2\text{Fe}(\text{OCH}_3)]_2$  in cyclohexane solution.  $\epsilon$  is based on formula weight per iron(III).

Figure 5. Near infrared (ligand field) spectra of  $\text{Fe}(\text{DPM})_2$  (broken line) and  $[(\text{DPM})_3\text{Fe}(\text{OCH}_3)]_2$  in cyclohexane solution.  $\epsilon$  is based on formula weight per iron(III).

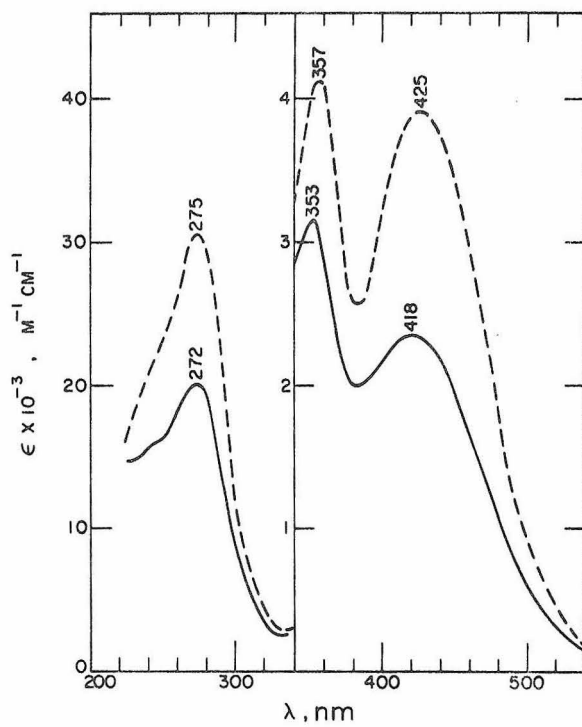


Figure 4

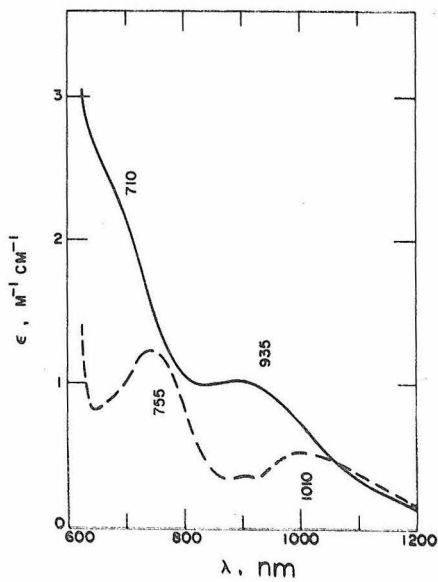


Figure 5

excitations such as found in certain oxobridged Fe(III) dimers. (14, 20)  
Such special spectral features are apparently properties of anti-ferromagnetically coupled systems with J values considerably in excess of  $10 \text{ cm}^{-1}$ .

Table IV. Electronic Spectral Data

Complex	$\lambda_{\text{max}}$ , nm	$10^{-3} \bar{\nu}$ , $\text{cm}^{-1}$	$\epsilon$	Assignment $A_1 \rightarrow$
$\text{Fe}(\text{DPM})_3$	$\sim 1010$	9.90	0.5	${}^4T_1$
cyclohexane solution	$\sim 755$	13.2	1.2	${}^4T_2$
room temperature	425	23.5	3910	a
	357	28.0	4120	a
	275	36.4	30,600	a
$[(\text{DPM})_2\text{Fe}(\text{OCH}_3)]_2$	$\sim 935$	10.7	1.0	${}^4T_1$ 135
cyclohexane solution,	$\sim 710$	14.1	2.0	${}^4T_2$
room temperature	418	23.9	2350	a
	353	28.3	3150	a
	272	36.8	20,000	a
$\text{Fe}(\text{acac})_3$	1025	9.760	0.45	${}^4T_1$
acetone solution,	760	13.160	0.70	${}^4T_2$
room temperature <sup>b</sup>	433	23.12	3400	a
	352	28.41	3250	a

Table IV (Continued)

Complex	$\lambda_{\max}$ , nm	$10^{-3} \bar{\nu}$ , $\text{cm}^{-1}$	$\epsilon$	Assignment $A_1 \rightarrow$
$[(\text{acac})_2\text{Fe}(\text{OC}_2\text{H}_5)]_2$	$\sim 990$	10.1	0.7	${}^4T_1$
$\text{CHCl}_3$ solution	$\sim 725$	13.8	0.7	${}^4T_2$
room temperature	428	23.4	--	a
	352	28.4	--	a
KBr pellet, 78°K	$\sim 950$	10.5	--	${}^4T_1$
	$\sim 735$	13.6	--	${}^4T_2$ 136
	436	22.9	--	a
	355	28.2	--	a

a Intraligand or charge transfer band.

b From reference 19.

5. References

1. National Science Foundation Predoctoral Fellow, 1966-1971.
2. Rutgers University.
3. G. S. Hammond, D. C. Nonhebel, and C.-H. S. Wu, Inorg. Chem., 2, 76 (1963).
4. G. S. Hammond and C.-H. S. Wu, Advances in Chemistry Series, 77, 186 (1968).
5. B. Emmert and W. Seebode, Ber., 71, 242 (1938); and references therein.
6. A. B. P. Lever, J. Lewis, and R. S. Nyholm, J. Chem. Soc., 5262 (1962).
7. Unpublished results of L. Leichter and H. J. Schugar.
8. R. K. Mehrotra and R. C. Mehrotra, Can. J. Chem., 39, 795 (1961).
9. R. C. Mehrotra, Inorg. Chim Acta Reviews, 1, 99 (1967).
10. K. Nakanishi, "Infrared Absorption Spectroscopy," Holden-Day, Inc., San Francisco, 1962, p. 31.
11. C. G. Barraclough, D. C. Bradley, J. Lewis, and I. M. Thomas, J. Chem. Soc., 2601 (1961).
12. J. Bell, J. Heisler, H. Tannenbaum, and J. Goldenson, Anal. Chem., 25, 1720 (1953).
13. K. Nakamoto, C. Udovich, and J. Takemoto, J. Amer. Chem. Soc., 92, 3973 (1970).

14. H. J. Schugar, G. R. Rossman, C. G. Barraclough, and H. B. Gray, to be published.
15. H. J. Schugar, G. R. Rossman, and H. B. Gray, J. Amer. Chem. Soc., 91, 4564 (1969).
16. H. J. Schugar, C. Walling, R. Jones, and H. B. Gray, ibid., 89, 3712 (1967).
17.  $[(\text{picolinate-N-oxide})_2\text{Fe}(\text{OCH}_3)]_2$  is not fully characterized. The magnetic susceptibility data lend support to the tentative dimeric formulation. The insolubility of the compound is not surprising since picolates and related materials are analytical precipitants for ferric ion.
18.  $[(\text{DPM})_2\text{Fe}(\text{O-}n\text{-C}_3\text{H}_7)]_2$ , although not fully characterized, has been prepared using the techniques reported here. The reddish-orange solid melts with decomposition 180-200°C. On the basis of the magnetic susceptibility data it is presumed to be a dialkoxobridged dimer.
19. T. S. Piper and R. L. Carlin, Inorg. Chem., 2, 260 (1963).
20. H. J. Schugar, G. R. Rossman, J. Thibeault, and H. B. Gray, Chem. Phys. Lett., 6, 26 (1970).

E. Simultaneous Pair Electronic Excitations in a Binuclear Iron(III) Complex

Harvey J. Schugar, Department of Chemistry,

Rutgers University, New Brunswick, New Jersey 08903

George R. Rossman, Jack Thibeault, and Harry B. Gray

Arthur Amos Noyes Laboratory of Chemical Physics,

California Institute of Technology, Pasadena, California

The ultraviolet absorption spectrum of an isolated metal complex containing the bridging unit  $\text{Fe(III)-O-Fe(III)}$  shows several bands due to the simultaneous electronic excitation of the two  $\text{Fe(III)}$  centers. The band positions are in excellent agreement with calculated sums of one-center d-d transitions.

The simultaneous electronic excitation of a metal ion pair by a single photon was first proposed by Varsanyi and Dieke to explain the fluorescence excitation spectrum of  $\text{PrCl}_3$  crystals<sup>(1)</sup> and later treated theoretically by Dexter.<sup>(2)</sup> More recent studies have established that mixed  $\text{Ni(II)-Mn(II)}$  perovskite fluorides display ultraviolet absorption of a similar nature<sup>(3)</sup> and an apparently related emission process occurs in  $\text{EuAlO}_3$  doped with  $\text{Cr(III)}$ .<sup>(4)</sup> The possibility that simultaneous pair electronic (SPE) excitations occur in discrete polynuclear metal complexes has been suggested previously by Hansen and Ballhausen,<sup>(5)</sup> but hitherto no experimental proof has been offered. Here we show that several prominent ultraviolet



absorption bands exhibited by a binuclear Fe(III) complex are due to SPE transitions.

The ethylenediammonium salt of the dimeric Fe(III) complex ion  $[(\text{HEDTAFe})_2\text{O}]^{2-}$  contains the structural bridging unit Fe(III)-O-Fe(III).<sup>(6,7)</sup> The magnetic moment of this complex decreases with temperature and has been interpreted<sup>(8)</sup> in terms of a pair of antiferromagnetically coupled ( $J = -86 \text{ cm}^{-1}$ ) high-spin ( $S = 5/2$ ) Fe(III) units.

The electronic absorption spectrum of  $[(\text{HEDTAFe})_2\text{O}]^{2-}$  is shown in Figure 1. Except for enhanced band intensities,<sup>(9)</sup> the visible spectrum is characteristic of a monomeric, octahedral  $S = 5/2$  Fe(III) complex. This is reasonable since the ligand field for each metal ion should not be seriously affected by the relatively weak spin-spin interaction. Bands a-d in Figure 1 therefore correspond directly to d-d transitions from a  ${}^6A_1$  one-center ground state to  ${}^4T_1$ ,  ${}^4T_2$ , ( ${}^4A_1$ ,  ${}^4E$ ), and  ${}^4T_2$  excited states, respectively. Using the strong field matrices for an octahedral  $d^5$  system, we have calculated the parameter values  $Dq = 1090$ ,  $B = 950$ , and  $C = 2300 \text{ cm}^{-1}$ , which have been obtained for  $\text{Fe}(\text{H}_2\text{O})_6^{3+}$ .<sup>(10)</sup>

The more intense band (e-h) at higher energies are not found in monomeric Fe(III) complexes and more particularly not in  $[\text{HEDTAFeOH}]^-$  or  $[\text{HEDTAFeOH}_2]$ . The band energies obtained from a concentrated aqueous solution<sup>(11)</sup> of  $[(\text{HEDTAFe})_2\text{O}]^{2-}$  are listed in Table I along with the SPE transition assignments suggested from the calculated sums of the observed, one-center d-d transitions. The fact

Figure 1. Absorption spectrum of 0.20 F aqueous solution of  $\text{enH}_2[(\text{FeHEDTA})_2\text{O}] \cdot 6\text{H}_2\text{O}$  at 296 K. Calculated positions of SPE excitations are indicated by arrows.

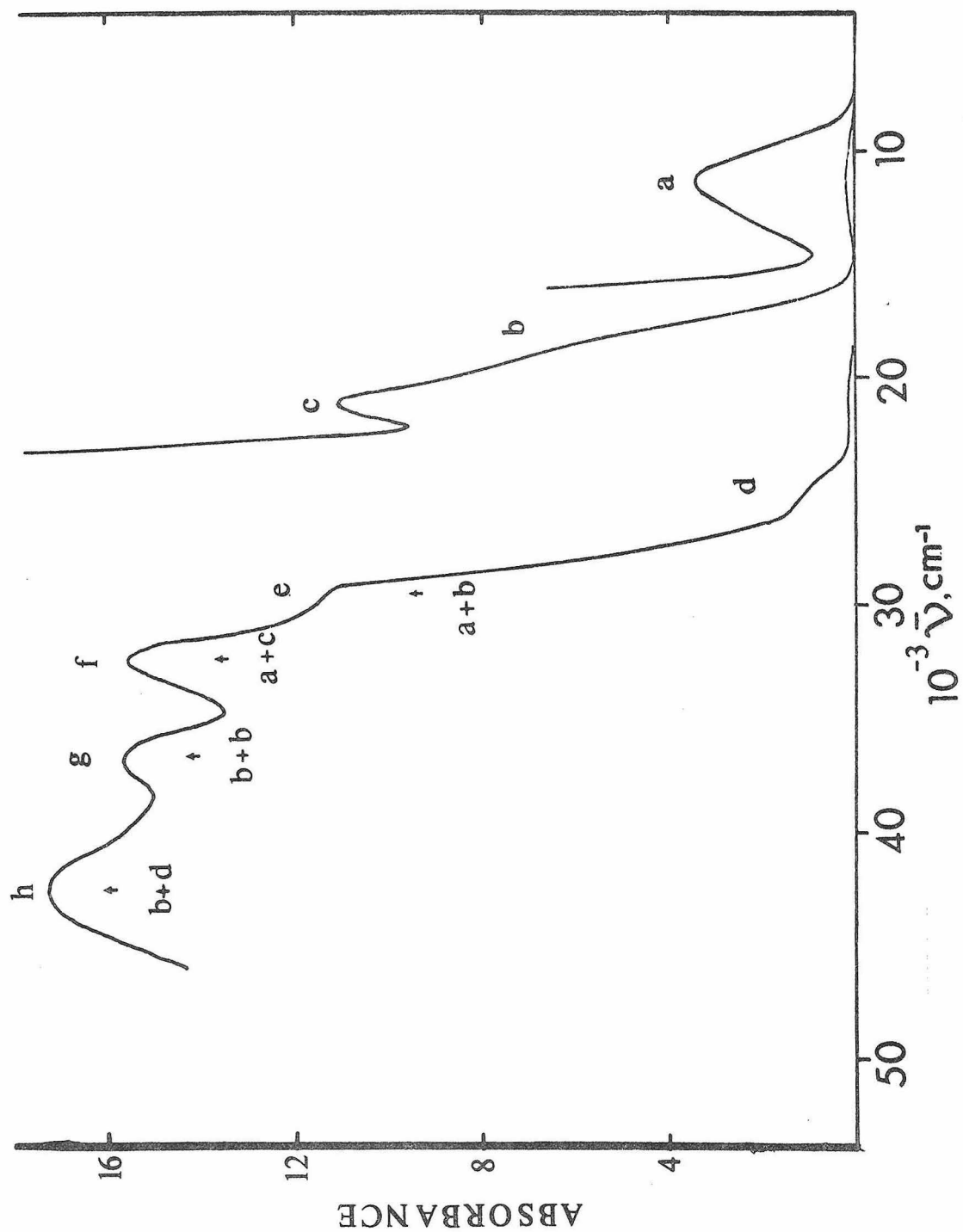


Figure 1

Table I. Electronic Spectral Data for  
 $\text{enH}_2[(\text{HEDTAFe})_2\text{O}] \cdot 6\text{H}_2\text{O}$

<u>Band</u>	<u><math>(10^{-3}) \bar{\nu}_{\text{max}}, \text{cm}^{-1}</math></u>	<u>Assignment</u>
a	11.2	${}^6\text{A}_1 \rightarrow {}^4\text{T}_1$
b	18.2	${}^6\text{A}_1 \rightarrow {}^4\text{T}_2$
c	21.0	${}^6\text{A}_1 \rightarrow ({}^4\text{A}_1, {}^4\text{E})$
d	24.4	${}^6\text{A}_1 \rightarrow {}^4\text{T}_2$
e	29.2	$a + b = 29.4$
f	32.5	$a + c = 32.2$
g	36.8	$b + b = 36.4$
h	42.6	$b + d = 42.6$

that four separate bands are found essentially at the calculated positions for SPE excitations provides compelling support for this interpretation. Bands due to  $a + a$ ,  $a + d$ , and  $c + c$  are predicted to fall in the energy range studied but were not definitely observed. We plan to study the absorption spectra of thin single crystals in an attempt to resolve these three bands.

Similar results were obtained for a closely related dimeric complex,  $[(\text{EDTAFe})_2\text{O}]^{4-}$ . We have also found evidence for SPE excitations in other oxobridged Fe(III) dimers as well as in several binuclear Cu(II) complexes. The latter studies lend strong support to the Hansen-Ballhausen SPE interpretation<sup>(5)</sup> of the  $27,000 \text{ cm}^{-1}$  band in dimeric Cu(II) acetate. Full details will be published in a subsequent paper.

References

1. F. L. Varsanyi and G. H. Dieke, Phys. Rev. Letters, 7, 442 (1961).
2. D. L. Dexter, Phys. Rev., 126, 1962 (1962).
3. J. Ferguson, H. J. Guggenheim, and Y. Tanabe, J. Chem. Phys., 45, 1134 (1966).
4. J. P. van der Ziel and L. G. Van Uitert, Phys. Rev., 180, 343 (1969).
5. A. E. Hansen and C. J. Ballhausen, Trans. Far. Soc., 61, 631 (1965).
6. H. J. Schugar, C. Walling, R. B. Jones, and H. B. Gray, J. Amer. Chem. Soc., 89, 3712 (1967).
7. S. J. Lippard, H. J. Schugar, and C. Walling, Inorg. Chem., 6, 1825 (1967); HEDTA represents the pentadentate ligand  $R'RNCH_2CH_2NR_2$  where  $R = CH_2CO_2^-$ ,  $R' = CH_2CH_2OH$ .
8. H. J. Schugar, G. R. Rossman, and H. B. Gray, J. Amer. Chem. Soc., 91, 4564 (1969).
9. These effects are undoubtedly related to the similar enhancement of the d-d bands of bridged Mn(II) compounds and will not be further considered here. See, for example, J. Ferguson, H. J. Guggenheim, and Y. Tanabe, J. Phys. Soc., Japan, 21, 692 (1966); L. L. Lohr, Jr., and D. S. McClure, J. Chem. Phys., 49, 3516 (1968); D. R. Huffman, J. Appl. Phys., 40, 1334 (1969).

10. G. R. Rossman, unpublished results.
11. A concentrated aqueous solution (thin film) was used to ensure that almost pure dimer was present. Equilibrium data and material preparations are given in reference 6.

F. Electronic Spectra of  $d^5$  Manganese(II) and Iron(III) Compounds

1. Introduction

In order to provide a basis for the detailed discussion of the electronic spectral properties of dimeric and polymeric systems exhibiting spin-spin interaction, it is necessary to first acquire an understanding of the spectroscopy of isolated systems. Although there are a few examples of recent detailed investigations of  $d^5$  systems, most of the more comprehensive survey work is now out of date and needs to be repeated to take advantage of the significant improvement that is realized by using low temperature spectroscopic techniques in higher resolution instruments. For the purposes of providing a better compilation of data regarding the spectroscopy of monomeric  $d^5$  systems and of obtaining a feel for the temperature dependence of  $d^5$  spectra, a series of readily synthesized compounds and shelf reagents were examined by what will be referred to as the 100% pellet technique. This consists of pressing a pellet from several hundred milligrams of the dry powdered solid in a manner analogous to the preparation of a KBr pellet, with the exception that the optical flats of the die are coated with a small drop of mineral oil. Once pressed, the pellet is allowed to soak for about an hour in mineral oil so that it becomes translucent. All of the spectra reported in this section have been obtained at 78°K in a Cary 14RI spectrophotometer. Also included in this section are spectral data for  $d^5$  systems in other than octahedral coordination environments.



## 2. Manganese(II)

N-methyl-1,4-diazabicyclo[2.2.2]octoniumtrichloroaquomanganate(II),  $[\text{Mn}(\text{N}(\text{CH}_2\text{CH}_2)_3\text{N}^+\text{-CH}_3)(\text{OH}_2)\text{Cl}_3]$ .

This compound was prepared according to the literature method<sup>(1)</sup> and recrystallized from a 1:1 H<sub>2</sub>O-ethanol mixture. The compound which displays a yellowish-brown tint in larger crystals has been shown to be isomorphous with the known five-coordinate  $[\text{Ni}(\text{N}(\text{CN}_2\text{CH}_2)_3\text{NCH}_3)(\text{OH}_2)\text{Cl}_3]$  of near trigonal-bipyramidal symmetry.<sup>(2)</sup> Its optical spectrum, obtained by the 100% pellet technique, displays five major bands, four of which show appreciable splitting, plus weaker spikes near 390 nm (Figure 1). Band positions are tabulated in Table I. The approximately 200 cm<sup>-1</sup> spacing of the shoulders and spikes on the 431 nm band is most likely indicative of vibronic fine structure, as is the similar spacing on the 448 nm band. The spectral features are expected and observed to be somewhat different from octahedral complexes. Particularly evident is the low intensity of the first band near 550 nm and the comparatively small separation between the second and third bands at 448 and 431 nm.

Very few data on other five-coordinate manganese(II) compounds exist to which this spectrum might be compared. Two compounds which have been reported,  $[\text{MnBr}(\text{hexamethyl-tren})]\text{Br}$  and  $[\text{MnI}(\text{hexamethyl-tren})]\text{I}$ , have trigonal bipyramidal structure and have published reflectance spectra<sup>(3)</sup> which show considerable similarity between themselves, but which differ in band spacing and relative band

intensities from the 100% pellet spectrum of  $[\text{Mn}(\text{N}(\text{CH}_2\text{CH}_2)_3\text{NCH}_2)(\text{OH}_2)\text{Cl}_3]$ :

cis-dichlorotetraaquomanganese(II),  $\text{cis-MnCl}_2 \cdot 4\text{H}_2\text{O}$

This compound was obtained as a shelf reagent. The 100% pellet  $\text{LN}_2$  optical spectrum of the compound is particularly pleasing in view of the exceptionally good resolution and freedom from scattering (Figure 1). Band positions of this compound with the indicated cis-dichloro grouping in the octahedral structure<sup>(4)</sup> are tabulated in Table I. At low temperature the band at 408 nm displays sharp fine structure dominated by three sharp spikes at 411.1, 408.3, and 406.8 nm, and several other shoulders and weaker bands. These bands can be assigned according to the usual octahedral scheme that is discussed in conjunction with the tetrahedral iron(III), namely in order of increasing energy, bands arising from transitions from the  ${}^6\text{A}_1$  ground state to  ${}^4\text{T}_1$ ,  ${}^4\text{T}_2$  ( ${}^4\text{A}_1$ ,  ${}^4\text{E}$ ),  ${}^4\text{T}_2$ , and  ${}^4\text{E}$ , where the basic octahedral framework is preserved in spite of the non-equivalent ligation.

manganese acetate tetrahydrate,  $\text{Mn}(\text{CH}_3\text{CO}_2)_2 \cdot 4\text{H}_2\text{O}$

This compound was also obtained as a shelf reagent and was studied by the 100% pellet technique. The spectrum displays a close resemblance to that of cis- $\text{MnCl}_2 \cdot 4\text{H}_2\text{O}$  with the exception of the lack of the fine structure in the 400 nm band (Figure 1). The band positions tabulated in Table I, showed very little shift in position upon being warmed to 296°K. The sharp bands at 339, 362, and 404 nm remained unchanged, while the broader bands at 555 and 448 nm shift slightly to 545 and 442 nm at room temperature. It is of interest that higher

resolution studies at lower temperature have shown that the 404 nm band splits into five bands at 4.2°K which have been assigned to the  ${}^6A_1 \rightarrow {}^4A$  transition at  $24496\text{ cm}^{-1}$ , and to four components of the  ${}^6A_1 \rightarrow {}^4E$  transition at 24696, 24710, 24757, and  $24767\text{ cm}^{-1}$ . (5)

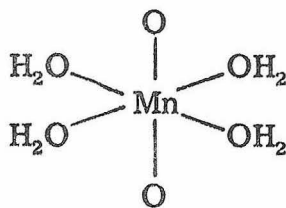
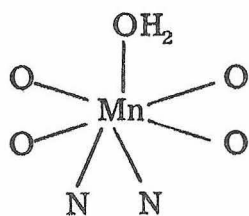
The lesson of this observation is that vibronic fine structure is not necessarily the cause of some of the splittings observed in the spectra of these compounds.



This compound was prepared by reacting a stoichiometric quantity of  $\text{MnCO}_3$  and  $\text{Na}_2\text{H}_2\text{EDTA}$  in  $\text{H}_2\text{O}$  at  $80^\circ\text{C}$ , filtering the solution, and cooling to induce crystallization. Although no structural data are available for this white solid, it is hoped that this compound would be six-coordinate and thereby serve as a model for the mixed six- and seven-coordinate  $\text{Mn}_3\text{H}_2(\text{EDTA})_2 \cdot 10\text{H}_2\text{O}$  discussed below. Spectral data are presented in Figure 1 and Table I. A dominant feature of the spectrum is the width of the band system around 430 nm.



This compound was prepared from  $\text{MnCO}_3$  and  $\text{H}_4\text{EDTA}$  according to the literature method. (6) The x-ray structure of this pale pink material has shown that 2/3 of the manganese atoms are in seven-coordinate sites while the remaining 1/3 are in octahedral sites as pictured below:



It was expected that the optical spectrum would be a superposition of two spectra--one of the six-coordinate Mn(II) and the other from the seven-coordinate atoms. Examination of Figure 1 shows that the spectrum of this compound is considerably more complicated than that of the six-coordinate model systems. Spectral data are tabulated in Table I.

It would be desirable to be able to subtract out the spectrum of an appropriate six-coordinate manganese complex from the spectrum of  $\text{Mn}_3\text{H}_2(\text{EDTA})_2 \cdot 10\text{H}_2\text{O}$  and be left with the spectrum of seven-coordinate Mn(II). For example, subtracting out the spectrum of  $\text{Na}_2\text{MnEDTA} \cdot x\text{H}_2\text{O}$  one would conclude that the band at 477 nm is due to the seven-coordinate manganese. This particular comparison is rendered tenuous by the width of the bands and uncertain coordination number in  $\text{Na}_2\text{MnEDTA} \cdot x\text{H}_2\text{O}$  as well as by the probable differences in ligation of the two six-coordinate species. It is felt that this approach would benefit from a re-examination of these compounds at lower temperatures and under conditions of higher resolution.

### 3. Six-Coordinate Iron(III) Compounds

The general pattern of two weak and comparatively broad bands followed at higher energy by a narrower and more intense band followed in turn by another broader band usually appearing as a shoulder on a

Figure 1. Optical spectra of 100% pellets soaked in mineral oil;

78°K. From top to bottom:

A)  $[\text{Mn}(\text{N}(\text{CH}_2\text{CH}_2)_3\text{NCH}_3)(\text{OH}_2)\text{Cl}_3]$ , five-coordinate.

B) cis- $\text{MnCl}_2 \cdot 4\text{H}_2\text{O}$ , six-coordinate.

C)  $\text{Mn}(\text{acetate})_2 \cdot 4\text{H}_2\text{O}$ , six-coordinate.

D)  $\text{Na}_2\text{Mn}(\text{EDTA}) \cdot x\text{H}_2\text{O}$ , structure unknown.

E)  $\text{Mn}_3\text{H}_2(\text{EDTA})_2 \cdot 10\text{H}_2\text{O}$ , mixed six- and seven-coordinate.

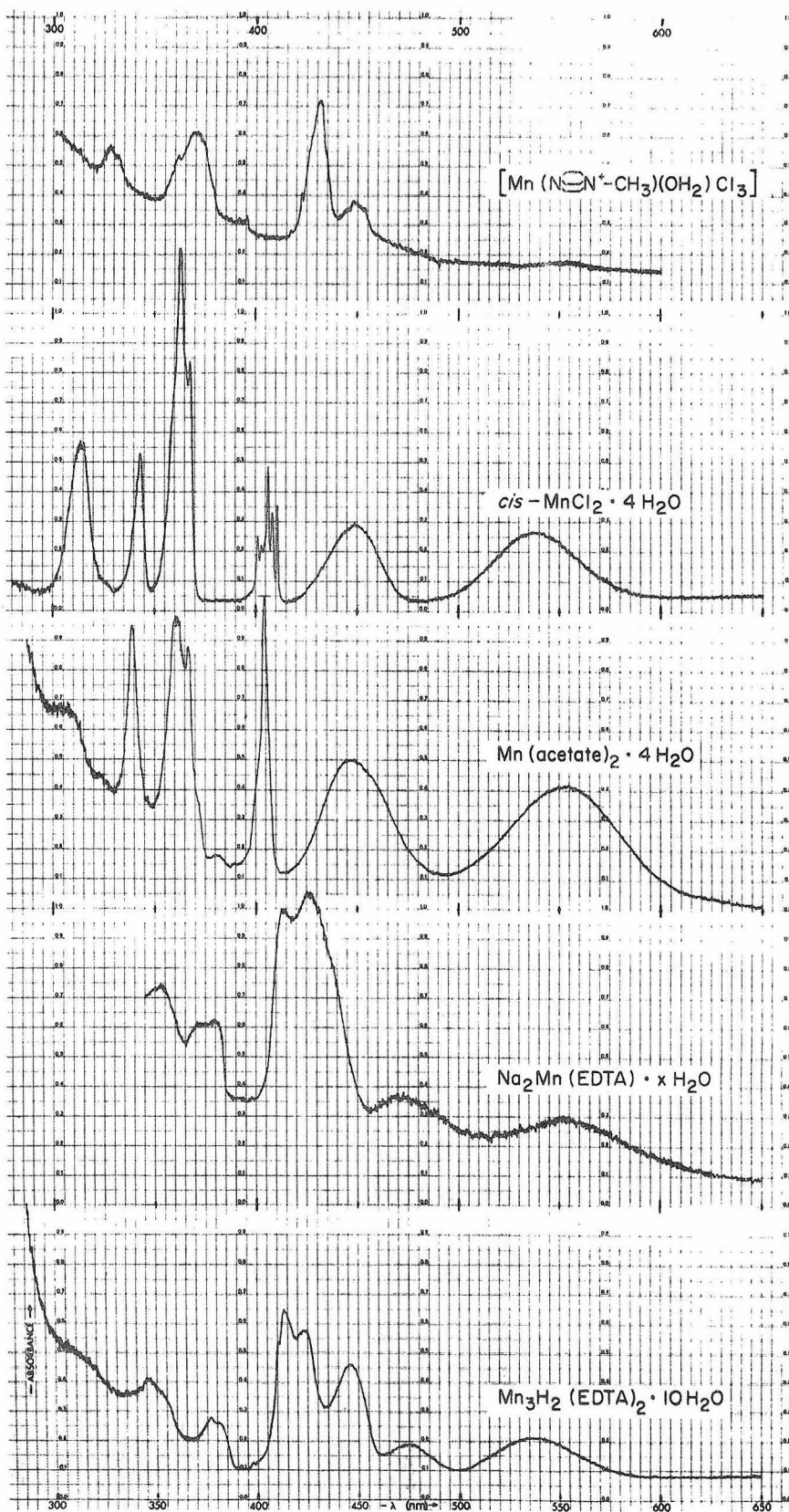
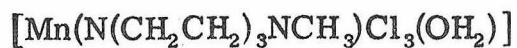


Figure 1

Table I. Optical Spectral Data for  
Manganese(II) Compounds as 100% Pellets plus  
Mineral Oil at 78°K



$\lambda(\text{nm})$	$10^{-3} \bar{\nu} (\text{cm}^{-1})$	
552	18.1	weak band
453	22.1	
448	22.3	
444	22.5	
435	23.0	
431	23.2	main spike
426	23.4	
423	23.6	
420	23.8	
417	24.0	
395	25.3	
392	25.5	
371	27.0	
361	27.7	
332	30.2	
328	30.5	



$\lambda(\text{nm})$	$10^{-3} \bar{\nu} (\text{cm}^{-1})$
536	18.7

Table I (Continued)

<u><math>\lambda</math> (nm)</u>	<u><math>10^{-3} \bar{\nu}</math> (cm<sup>-1</sup>)</u>	
499	22.3	
411.1	24.32	
409.0	24.45	
408.3	24.49	
406.8	24.58	
405.6	24.66	
403.4	24.79	
401.5	24.91	
367.5	27.21	
363.2	27.53	main spike
343	29.2	
314	31.8	
Mn(acetate) <sub>2</sub> · 4H <sub>2</sub> O		
<u><math>\lambda</math>(nm)</u>	<u><math>10^{-3} \bar{\nu}</math> (cm<sup>-1</sup>)</u>	
555	18.0	
448	22.3	
404	24.8	main spike
400	25.0	shoulder
389	25.7	weak
382	26.2	weak



Table I (Continued)

<u><math>\lambda</math> (nm)</u>	<u><math>10^{-3} \bar{\nu}</math> (cm<sup>-1</sup>)</u>	
372	26.9	
367	27.3	
362	27.6	
339	29.5	
310	32.2	
Na <sub>2</sub> Mn(EDTA) · xH <sub>2</sub> O		
<u><math>\lambda</math> (nm)</u>	<u><math>10^{-3} \bar{\nu}</math> (cm<sup>-1</sup>)</u>	
557	17.9	
474	21.1	
439	22.8	shoulder
425	23.6	
413	24.2	
378	26.4	
372	26.9	
352	28.4	
Mn <sub>3</sub> H <sub>2</sub> (EDTA) · 10H <sub>2</sub> O		
<u><math>\lambda</math> (nm)</u>	<u><math>10^{-3} \bar{\nu}</math> (cm<sup>-1</sup>)</u>	
537	18.6	
477	21.0	
447	22.4	

Table I (Continued)

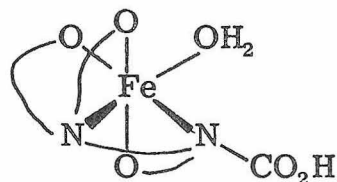
<u><math>\lambda</math> (nm)</u>	<u><math>10^{-3} \bar{\nu}</math> (cm<sup>-1</sup>)</u>	
425	23.6	
413	24.2	main spike
410	24.4	
398	25.1	shoulder
382	26.2	
376	26.7	
355	28.2	
346	28.9	
~ 315	33.9	

charge transfer tail, if detectable at all, is displayed by a wide variety of octahedral, or near octahedral iron(III) compounds. Several examples of this behavior are presented in Figure 2 which were obtained from the solid compounds at 78°K. Band positions are tabulated in Table II. The assignment of these bands has been considered in previous sections dealing with oxobridged dimers and with tetrahedral coordination.

#### 4. Iron(III) EDTA-Type Chelates--Seven-Coordination

Seven-coordination in iron(III) chelates has been established in the calcium salt of trans-1,2-diaminocyclohexane-N,N'-tetraacetatoaquoferrate(III),  $\text{Ca}[\text{Fe}(\text{OH}_2)(\text{CDTA})]_2 \cdot 8\text{H}_2\text{O}$ , and in the lithium and rubidium salts of the iron(III) EDTA aquo complex.<sup>(7,8)</sup> The optical spectra of  $\text{Ca}[\text{Fe}(\text{OH}_2)(\text{CDTA})]_2 \cdot 8\text{H}_2\text{O}$  and  $\text{Na}[\text{Fe}(\text{EDTA})(\text{OH}_2)] \cdot 2\text{H}_2\text{O}$ , which is undoubtedly seven-coordinate like the corresponding Rb and Li salts, display a pattern of bands which is distinctly different from the octahedral complexes previously discussed (Figure 2). Four broad bands, three of which are overlapping, occur at lower energies than the sharp spike (which is presumably related to the  ${}^6\text{A}_1 \rightarrow {}^4\text{A}_1, {}^4\text{E}$  transition in octahedral symmetry). The same type of spectrum is observed for  $\text{FeHEDTA} \cdot 1\frac{1}{2}\text{H}_2\text{O}$  which also is probably seven-coordinate. One would be tempted at this time to say that such a pattern of bands is a characteristic of seven-coordinate iron(III) complexes.

Alas, such temptations must be resisted for upon examination of the spectrum of the known<sup>(9)</sup> six-coordinate compound  $[\text{HFe}(\text{EDTA})(\text{OH}_2)]$ , one finds that it also displays a spectrum which closely resembles the spectrum of the seven-coordinate calcium salt.



Coordination environment of iron in  $[\text{HFe}(\text{EDTA})(\text{OH}_2)]$

Questions then must be raised such as is the non-equivalent ligand field resulting from the carboxyl oxygens, water, and tertiary amine nitrogens of greater importance in determining the electronic structural properties than the coordination number. In view of the pronounced qualitative differences between the spectra of the several model compounds with near equivalent ligation (Figure 2, A-D) and the octahedral aquo-EDTA complex (Figure 2, E) with the non-equivalent ligation, one must answer the proposed question affirmatively.

A curious feature of some of the EDTA-like spectra is the unusual sharpness of the  $22,000 \text{ cm}^{-1}$  spike which is particularly evident in the spectrum of  $\text{NaFeEDTA}(\text{OH}_2) \cdot 2\text{H}_2\text{O}$ . Also included in Figure 2 is the spectrum of an iron complex of diethylenetriaminepentaacetate,  $[\text{H}_2\text{Fe}(\text{DPTA})]$  which has been interpreted as being six-coordinate on the basis of infrared data.<sup>(10)</sup> This spectrum does not fit clearly into the series of spectra. This compound is of added interest because it forms a comparatively stable purple complex with hydrogen peroxide which has an absorption band with  $\lambda_{\text{max}}$  at about

518 ( $19.3 \text{ k cm}^{-1}$ ) with  $\epsilon \geq 240$  and a uv shoulder at 291 nm ( $34.4 \text{ k cm}^{-1}$ ). The low energy d-d bands around  $8\text{-}12 \text{ k cm}^{-1}$  were not observed in the spectrum of a  $0.2 \text{ M}$  aqueous solution at  $0^\circ\text{C}$ .

Figure 2. Optical spectra of six- and seven-coordinate Fe(III) compounds by the 100% pellet technique, 78°K.

- A)  $\text{Fe}_2(\text{SO}_4)_3 \cdot x\text{H}_2\text{O}$
- B)  $\text{K}_3\text{Fe}(\text{oxalate})_3 \cdot 3\text{H}_2\text{O}$
- C)  $\text{K}_3\text{FeF}_6$
- D)  $\text{FeNH}_4(\text{SO}_4)_2 \cdot 12\text{H}_2\text{O}$
- E)  $\text{HFe}(\text{EDTA}) \cdot \text{H}_2\text{O}$ , six-coordinate
- F)  $\text{H}_2\text{FeDTPA}$
- G)  $\text{Na}[\text{Fe}(\text{EDTA})(\text{OH}_2)] \cdot 2\text{H}_2\text{O}$ , seven-coordinate
- H)  $\text{Fe}(\text{HEDTA}) \cdot 1\frac{1}{2} \text{H}_2\text{O}$
- I)  $\text{Ca}[\text{Fe}(\text{OH}_2)(\text{CDTA})]_2 \cdot 8\text{H}_2\text{O}$ , seven-coordinate

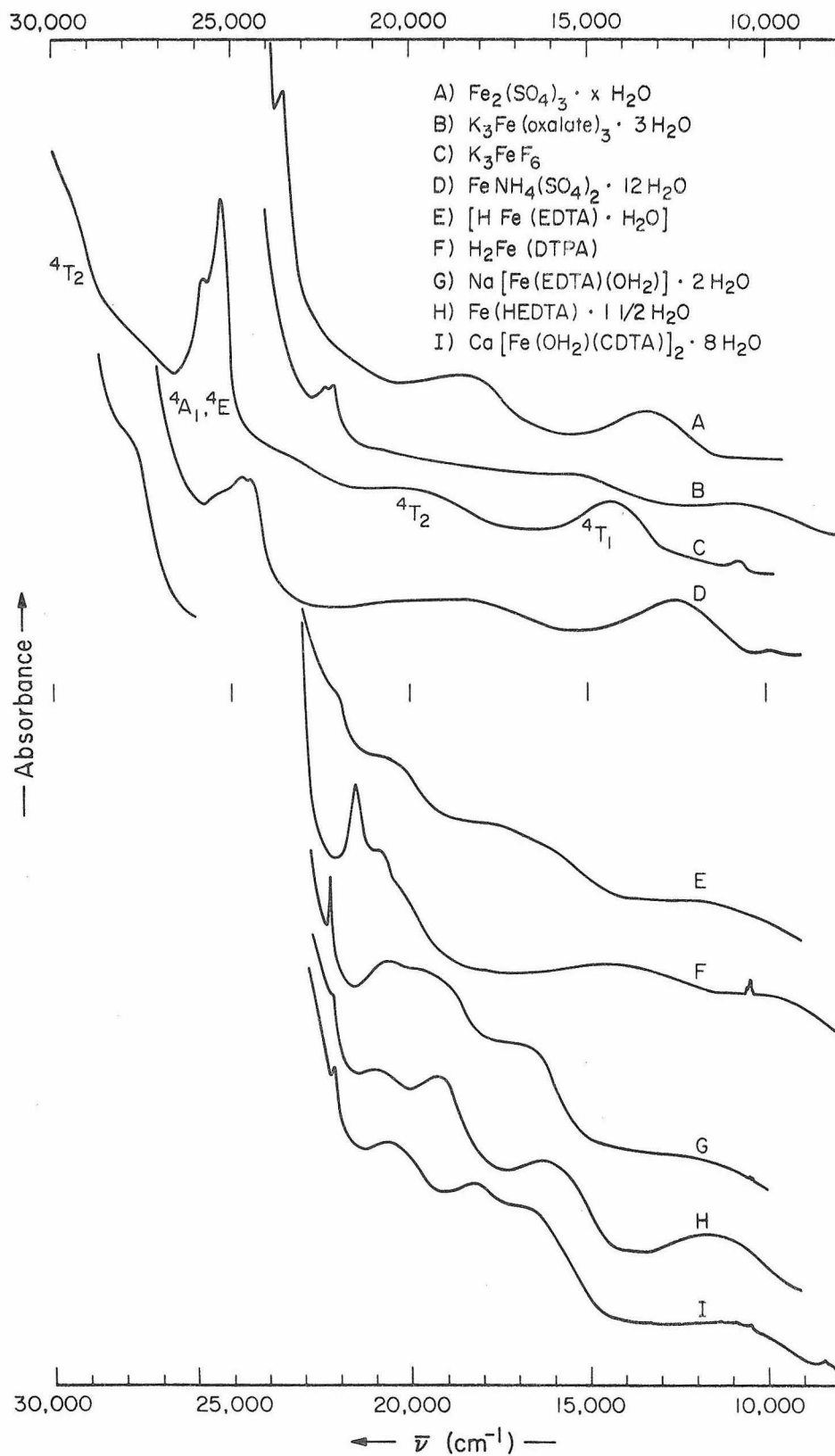


Figure 2

Table II. Optical Spectral Data for  
Iron(III) Compounds

$\text{Fe}_2(\text{SO}_4)_3 \cdot x\text{H}_2\text{O}$	100% pellet + mineral oil	78°K
<u><math>\lambda</math> (nm)</u>	<u><math>10^{-3} \bar{\nu}</math> (cm<sup>-1</sup>)</u>	
752	13.3	
550	18.2	
424.5	23.6	
$\text{K}_3\text{Fe}(\text{oxalate})_3 \cdot 3\text{H}_2\text{O}$	100% pellet + mineral oil	78°K
<u><math>\lambda</math> (nm)</u>	<u><math>10^{-3} \bar{\nu}</math> (cm<sup>-1</sup>)</u>	
964	10.4	
659	15.2	
453	22.1	
448	22.3	
$\text{K}_3\text{FeF}_6$	100% pellet + mineral oil	78°K
<u><math>\lambda</math> (nm)</u>	<u><math>10^{-3} \bar{\nu}</math> (cm<sup>-1</sup>)</u>	
702	14.2	
507	19.7	
396	25.3	main spike
388	25.8	
343	29.2	



Table II (Continued)

$\text{FeNH}_4(\text{SO}_4)_2 \cdot 12\text{H}_2\text{O}$	single crystal slab	room temperature
$\lambda$ (nm)	$10^{-3} \bar{\nu}$ ( $\text{cm}^{-1}$ )	
806	12.4	
550	18.2	
491	20.4	
410	24.4	
405	24.7	
393	25.4	
361	27.7	

5. References

1. V. L. Goedken, J. V. Quagliano, and L. M. Vallarino, Inorg. Chem., 8, 2331 (1969).
2. F. K. Ross and G. D. Stucky, Inorg. Chem., 8, 2734 (1969).
3. M. Ciampolini, Structure and Bonding, 6, 78 (1969).
4. A. Zalkin, J. D. Forrester, and D. H. Templeton, Inorg. Chem., 3, 529 (1964).
5. I. Tsujikawa, J. Phys. Soc. Japan, 18, 1407 (1963).
6. S. Richards, B. Pedersen, J. V. Silverton, and J. L. Hoard, Inorg. Chem., 3, 27 (1964).
7. M. J. Hamor, T. A. Hamor, and J. L. Hoard, Inorg. Chem., 3, 34 (1964).
8. G. H. Cohen and J. L. Hoard, J. Amer. Chem. Soc., 88, 3228 (1966).
9. C. H. L. Kennard, Inorg. Chem. Acta, 1, 347 (1967).
10. R. E. Sievers and J. C. Bailar, Jr., Inorg. Chem., 1, 174 (1962).

### III. SPECTROSCOPIC AND MAGNETIC PROPERTIES OF POLY-MERIC OXO- AND HYDROXOBRIDGED SYSTEMS

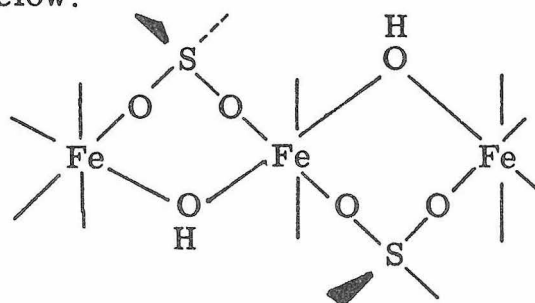
#### A. Extended Lattice Hydroxobridged Iron(III) Systems

##### 1. Introduction

A logical extension of the studies of oxo-, hydroxo-, and alkoxobridged dimers is the study of extended lattice systems containing oxo- or hydroxobridged iron. A number of natural and synthetic minerals and their isoelectronically substituted counterparts provide a wide range of available and often structurally characterized substrates. The initial phases of this work began with the magnetic and infrared study of a series of iron hydroxysulfates and hydroxychromates which were chosen to provide an experimental basis for the comparison of uncharacterized oxo- and hydroxybridged iron polymers.

##### 2. Synthesis of Model Hydroxy-minerals

Fe(OH)SO<sub>4</sub>. This compound was prepared by the high temperature hydrolysis of a ferric sulfate solution. <sup>(1)</sup> The structure consists of chains of iron atoms bridged by hydroxides and sulfates as indicated below:

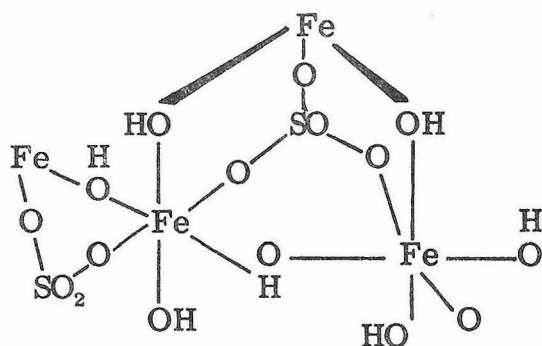


Structure of  
Fe(OH)SO<sub>4</sub> from  
reference 1.

The various chains are then joined to each other by sulfate oxygens coordinated to the remaining octahedral iron positions.

$\text{Fe(OH)CrO}_4$ . This compound, presumably isostructural with  $\text{Fe(OH)SO}_4$ , was prepared by the  $180^\circ\text{C}$ , 24 hour reaction of a  $\text{CrO}_3$  solution upon  $\text{Fe(OH)}_3$ .<sup>(2)</sup>

$\text{KFe}_3(\text{SO}_4)_2(\text{OH})_6$ . Synthetic jarosite was prepared by the  $180^\circ\text{C}$  reaction of  $\text{K}_2\text{SO}_4$  and  $\text{Fe}_2(\text{SO}_4)_3$  in dilute  $\text{K}_2\text{SO}_4$ .<sup>(3)</sup> The material has the alunite structure with iron octahedrally coordinated to two sulfate oxygens and to four OH groups.<sup>(4, 5)</sup>



Coordination structure of iron in jarosite.

$(\text{H}_3\text{O})\text{Fe}_3(\text{SO}_4)_2(\text{OH})_6$ . Hydronium jarosite, isostructural with jarosite<sup>(4)</sup> was prepared by the  $150^\circ\text{C}$  hydrolysis of a 20%  $\text{Fe}_2(\text{SO}_4)_3$  solution.<sup>(6)</sup>

$\text{KFe}_3(\text{CrO}_4)_2(\text{OH})_6$ . This compound, presumably isostructural with jarosite, was prepared by the reaction of  $\text{Fe}(\text{NO}_3)_3$  with a  $\text{K}_2\text{Cr}_2\text{O}_7$  solution at  $180^\circ\text{C}$ .<sup>(2)</sup>

### 3. Magnetic Susceptibility Studies

The magnetic susceptibilities of these extended hydroxobridged minerals show very little temperature dependence. As a result, the magnetic moment per iron steadily decreases as the temperature is

lowered. The top and center portions of Figure 1 show the temperature dependence of the magnetic moments and gram susceptibilities of these compounds. All of these compounds display room temperature magnetic moments in the range 3 to 4 B. M. per iron which is intermediate between Fe-O-Fe and Fe(OH)<sub>2</sub>Fe dimers. The magnetic susceptibility of KFe<sub>3</sub>(CrO<sub>4</sub>)<sub>2</sub>(OH)<sub>6</sub> is exceptional in that at approximately 70°K a magnetic phase transition occurs with a resultant sudden increase in magnetic susceptibility. Down to this temperature, however, it displays normal magnetic behavior typical of this class of polymer (lower right of Figure 1). The deuterated analogue of this compound has been prepared for infrared studies, but has not yet been examined magnetically. In view of the insensitivity of the magnetic behavior of the Fe(OH)<sub>2</sub>Fe unit to replacement of the hydroxides by alkoxides, it is expected that deuteration will not appreciably alter the onset of the magnetic transition.

#### 4. Infrared Spectra

One of the objectives of this work was to identify the bridging hydroxide bands and to compare them to the known oxobridged and dihydroxobridged dimers. It was hoped that these systems would provide models for comparison to other condensed polymeric forms of iron such as aquo-polymers and the inorganic core of the protein ferritin.

The infrared bands near 3500 and 1000 cm<sup>-1</sup> in KFe<sub>3</sub>(CrO<sub>4</sub>)<sub>2</sub>(OH)<sub>6</sub> and Fe(OH)(CrO<sub>4</sub>)<sub>2</sub> are easily identified as originating from OH modes through comparison with their corresponding deuterated species

Figure 1. Magnetic susceptibility of synthetic iron(III) minerals.

Top: Temperature dependence of the magnetic moment of

- a)  $\text{Fe(OH)SO}_4$
- b)  $\text{KFe}_3(\text{SO}_4)_2(\text{OH})_6$
- c)  $(\text{H}_3\text{O})\text{Fe}_3(\text{SO}_4)_2(\text{OH})_6$
- d)  $\text{KFe}_3(\text{CrO}_4)_2(\text{OH})_6$
- e)  $\text{Fe(OH)CrO}_4$

Center: Temperature dependence of the gram susceptibility of:

- a)  $\text{Fe(OH)SO}_4$
- b)  $\text{KFe}_3(\text{SO}_4)_2(\text{OH})_6$
- c)  $\text{H}_3\text{OFe}_3(\text{SO}_4)_2(\text{OH})_6$
- d)  $\text{KFe}_3(\text{CrO}_4)_2(\text{OH})_6$
- e)  $\text{Fe(OH)CrO}_4$

Bottom right: Temperature dependence of the gram susceptibility of  $\text{KFe}_3(\text{CrO}_4)_2(\text{OH})_6$ .

Bottom left: Comparison of the temperature dependence of the magnetic moments of:

- a) typical monomeric high-spin octahedral Fe(III) compounds
- b) dihydroxobridged Fe(III) dimer
- c) jarosite type minerals with extended lattice OH bridging of Fe(III)
- d) oxobridged Fe(III) dimers

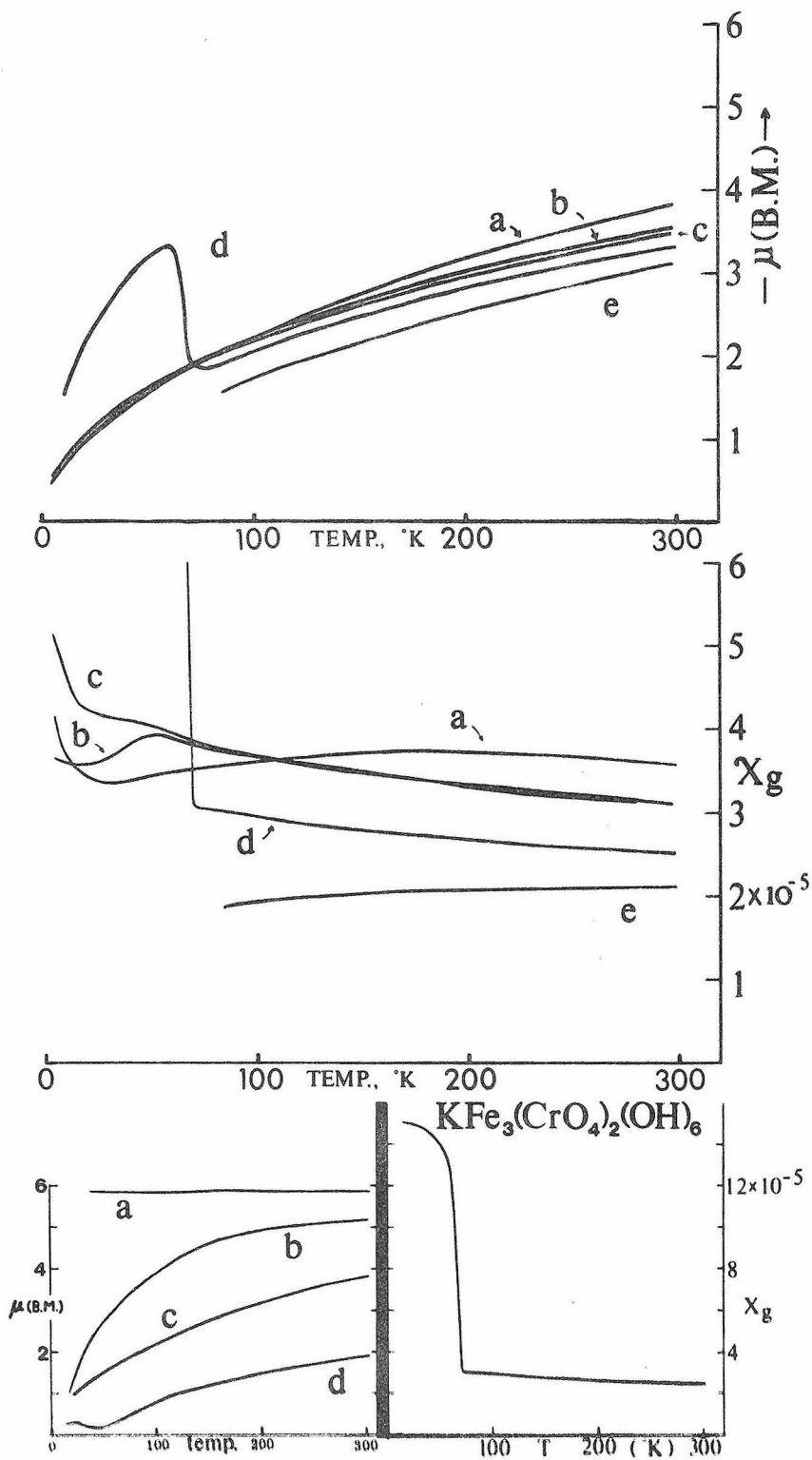


Figure 1

(Figure 2). The bands in comparable locations in the sulfate analogues are similarly assigned to OH modes. The relative sharpness of the OH bands near  $3400\text{ cm}^{-1}$  compared to the width of free water bands arising from adsorbed surface water or as solvated water is indicative of definite order in the OH unit. Also of significance is the fact that the OH bands near  $1100\text{ cm}^{-1}$  are comparatively intense and sharp. These bands which arise from bridging OH groups are found at higher energies than the bridging OH band found at  $950\text{ cm}^{-1}$  in the picolinate-dihydroxobridged iron dimer.



Figure 2. Infrared spectra of synthetic iron(III) minerals:

- A)  $\text{Fe}(\text{OH})\text{CrO}_4$ , 0.95 mg/400 mg KBr pellet, ambient temperature. Two inserts show new bands that appear in the spectrum of deuterated  $\text{Fe}(\text{OD})\text{CrO}_4$ .
- B)  $\text{Fe}(\text{OH})\text{SO}_4$ , 1.07 mg/400 mg KBr pellet, ambient temperature.
- C)  $\text{KFe}_3(\text{CrO}_4)_2(\text{OH})_6$ , 0.46 mg/400 mg TiBr pellet, ambient temperature. From left to right, the inserts show a 78°K spectrum of the OH region of the compound; the 310° and 78°K spectrum of the OD region deuterated compound,  $\text{KFe}_3(\text{CrO}_4)_2(\text{OD})_6$ ; two inserts of the room temperature spectrum of the low energy region of the deuterated compound.
- D)  $\text{KFe}_3(\text{SO}_4)_2(\text{OH})_6$ , 1.55 mg/400 mg KBr pellet, ambient temperature.

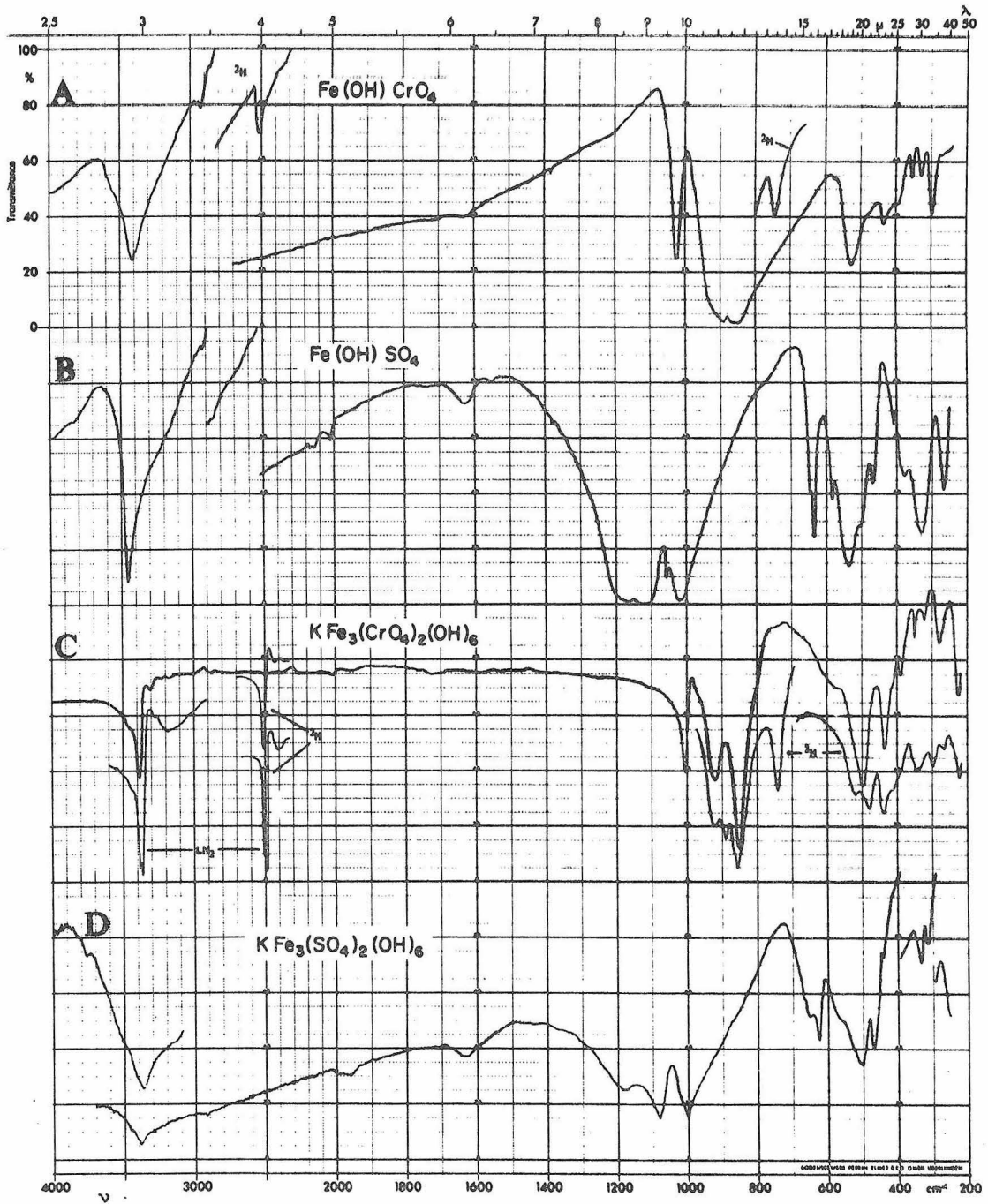


Figure 2

5. References

1. G. Johansson, Acta Chem. Scand., 16, 1234 (1962).
2. A. Bonnin and A. Lecerf, Compt. Rend., ser. c, 262, 1782 (1966).
3. J. G. Fairchild, Amer. Mineralogist, 18, 543 (1933).
4. S. B. Hendricks, Amer. Mineralogist, 22, 773 (1937).
5. R. Wang, W. F. Bradley, and H. Steinfink, Acta Cryst., 18, 249 (1965).
6. G. Brauer, Ed., "Handbook of Preparative Inorganic Chemistry," 2nd ed., 1507 (1965).

## B. Metal Oxides and Hydrous Oxides

### 1. Introduction

Several naturally occurring and synthetic minerals of formulation  $MO(OH)$  and  $M_2O_3$  were also studied to provide data regarding the infrared spectral properties of condensed oxo- and hydroxobridged systems with particular emphasis upon the iron minerals. A specific objective of these studies was to determine if information regarding the structural constitution of the inorganic core of the protein ferritin could be obtained.

### 2. Source of Materials

Diaspore,  $\alpha\text{-AlO(OH)}$ , was obtained from the Caltech geology reference collection (No. 1567).

Boehmite,  $\gamma\text{-AlO(OH)}$ . Several spectra were provided by Dana Powers.

Groutite,  $\alpha\text{-MnO(OH)}$ , was obtained from the Caltech geology reference collection (No. 6048).

Manganite,  $MnO(OH)$ , was obtained from the Caltech geology reference collection (No. 2402). Spectral data on a synthetic sample were also furnished by Dana Powers.

Goethite,  $\alpha\text{-FeO(OH)}$ , was obtained from the Smithsonian Institute (No. 117395) and as a synthetic sample furnished by Dana Powers.

Lepidocrocite,  $\gamma\text{-FeO(OH)}$ , was obtained from the Smithsonian Institute and as a synthetic sample furnished by Dana Powers.

Hematite,  $\alpha$ -Fe<sub>2</sub>O<sub>3</sub>, was obtained from the Smithsonian Institute.

Maghemite,  $\gamma$ -Fe<sub>2</sub>O<sub>3</sub>, was furnished by Pfizer, Inc., (MO-2035).

Magnetite, Fe<sub>3</sub>O<sub>4</sub>, was obtained from the Smithsonian Institute.

$\delta$ -FeO(OH) was prepared by very rapid oxidation of freshly prepared Fe(OH)<sub>2</sub> with excess 30% H<sub>2</sub>O<sub>2</sub>.<sup>(1)</sup>

"Ferric Hydroxide" was prepared by adding a 0.1F KOH solution to a 0.1F Fe(NO<sub>3</sub>)<sub>3</sub> solution, washing the precipitate with H<sub>2</sub>O, and allowing it to air dry at room temperature for the specified times.

The Towe Hydrolyzate was a sample furnished by John Webb which had been obtained from Ken Towe.<sup>(2)</sup>

The Ferric Nitrate polymer was a sample provided by John Webb which had been obtained from Paul Saltman.<sup>(3)</sup>

The Horse Ferritin Micelles were obtained from John Webb who in turn obtained them from Ken Towe.<sup>(2)</sup>

### 3. Infrared Spectra

The bridging OH bands would be expected to occur in the vicinity of 1000 cm<sup>-1</sup> for the various MO(OH) species. In the  $\alpha$ -series of compounds a pair of bands at 968 and 1080 cm<sup>-1</sup> in  $\alpha$ -AlO(OH) and at 796 and 890 cm<sup>-1</sup> in  $\alpha$ -FeO(OH) have been previously assigned to OH absorptions.<sup>(4,5)</sup> In a  $\alpha$ -MnO(OH) a distinctive three band pattern appears with peaks at 1083, 1113, and 1147 cm<sup>-1</sup> (Figures 1 and 2). This pattern is also undoubtedly due to an OH absorption. In the  $\gamma$ -series, a sharp band at 1071 cm<sup>-1</sup> in  $\gamma$ -AlO(OH) and a sharp band at

Figure 1. Infrared spectra of aluminum and manganese oxyhydroxides.

- A)  $\alpha$ -AlO(OH), diaspore, 1.12 mg/400 mg KBr pellet, ambient temperature.
- B)  $\gamma$ -AlO(OH), boehmite, 0.55 mg/ 400 mg KBr pellet, ambient temperature.
- C)  $\alpha$ -MnO(OH), groutite, 0.71 mg/400 mg TlBr pellet, ambient temperature.
- D) MnO(OH), manganite, 0.47 mg/400 mg TlBr pellet, ambient temperature.

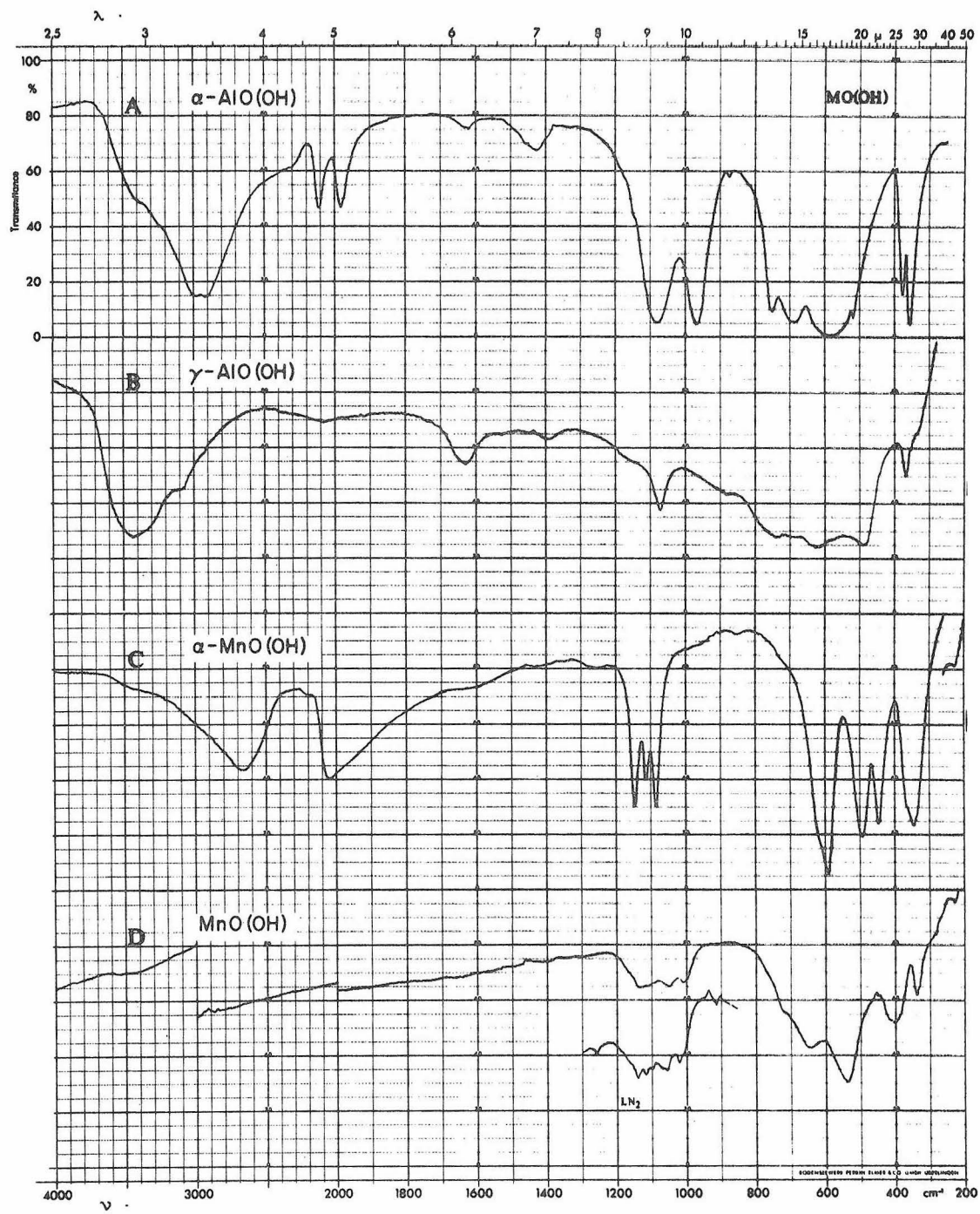


Figure 1

Figure 2. Infrared spectra of iron(III) oxyhydroxides

- A)  $\alpha$ -FeO(OH), goethite, 0.91 mg/400 mg KBr pellet, ambient temperature.
- B)  $\beta$ -FeO(OH), akagonite, 0.46 mg/400 mg TlBr pellet, ambient temperature.
- C)  $\gamma$ -FeO(OH), lepidocrocite, 0.92 mg/400 mg KBr pellet, ambient temperature. Insert shows a 0.50 mg/400 mg TlBr pellet at 78°K in the OH region.
- D)  $\delta$ -FeO(OH), 0.48 mg/400 mg TlBr pellet, ambient temperature.



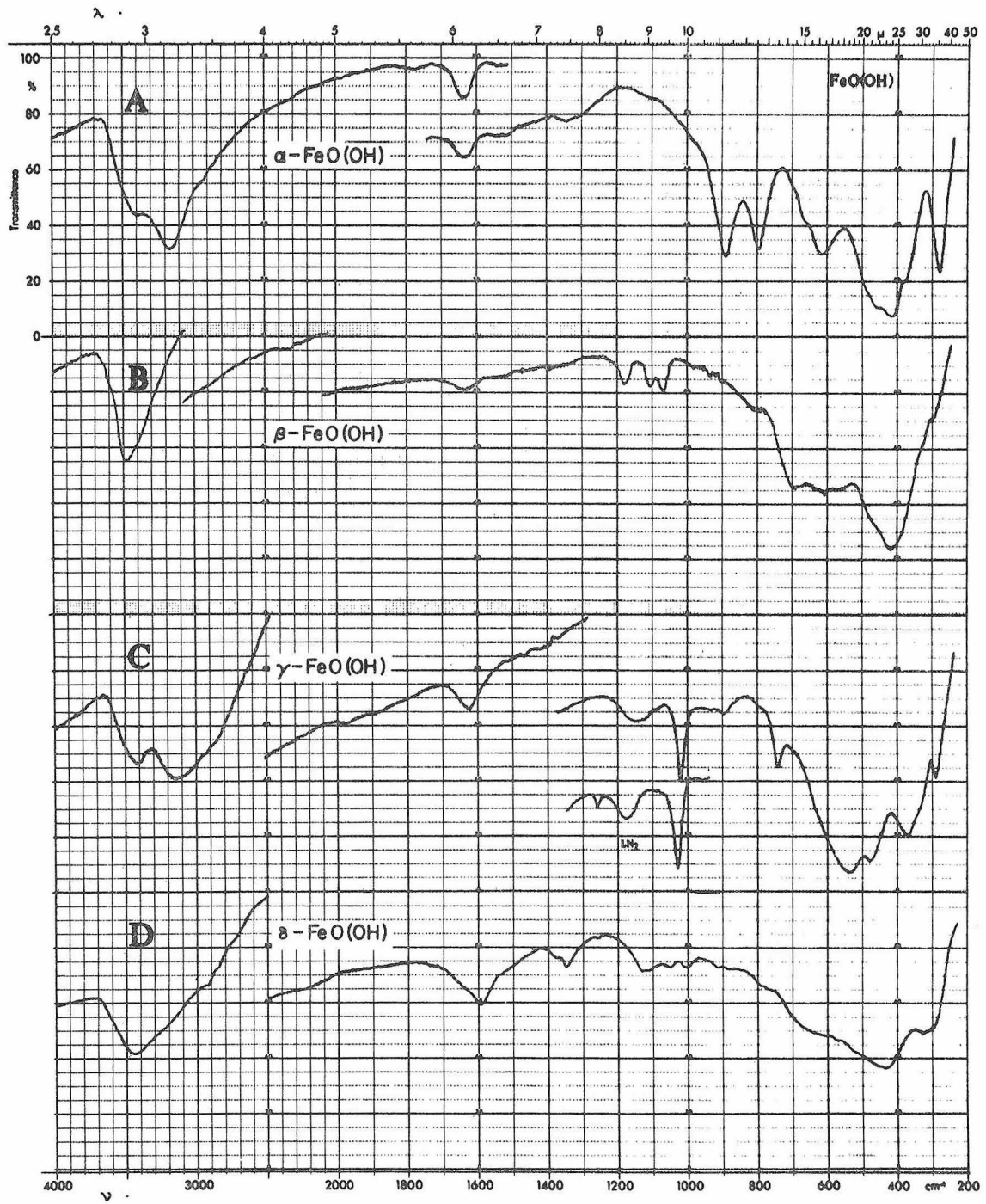


Figure 2

1019  $\text{cm}^{-1}$  in  $\gamma\text{-FeO(OH)}$  are likewise assigned to OH absorption. A high energy shoulder which also may be OH absorption appears near 1170  $\text{cm}^{-1}$  in  $\gamma\text{-AlO(OH)}$  and at 1148  $\text{cm}^{-1}$  in  $\gamma\text{-FeO(OH)}$ . A similar shoulder on the high energy side of a sharp OH band has been reported in the spectrum of  $\gamma\text{-ScO(OH)}$ .<sup>(6)</sup> Band systems which can be assigned to OH also occur in manganite,  $\text{MnO(OH)}$ , from 1000 to 1150  $\text{cm}^{-1}$ , in  $\beta\text{-FeO(OH)}$  from 1050 to 1190  $\text{cm}^{-1}$ , and in  $\delta\text{-FeO(OH)}$  from 980 to 1140  $\text{cm}^{-1}$ .

Most of these hydrous oxides show infrared absorption bands in the vicinity of 2000  $\text{cm}^{-1}$  which can be satisfactorily explained as overtones of the OH bands near 1000  $\text{cm}^{-1}$ . A pair of bands appear in the spectrum of  $\alpha\text{-AlO(OH)}$  at 1982 and 2113  $\text{cm}^{-1}$ . In the same region in the spectrum of  $\alpha\text{-MnO(OH)}$  a broad asymmetric band is present. Low temperature studies discussed below indicate that this band is not the overtone of the OH absorption near 1100  $\text{cm}^{-1}$ . In the spectrum of  $\alpha\text{-GaO(OH)}$ , the first harmonic of the OH band has been assigned to a similar pair of bands at 1940 and 2028  $\text{cm}^{-1}$ .<sup>(4,7)</sup> This system of bands is not well defined in the spectrum of  $\alpha\text{-FeO(OH)}$ . Two weak and fairly broad bands are present at about 1645 and 1760  $\text{cm}^{-1}$  which are in about the right positions to be overtones of the 796 and 890  $\text{cm}^{-1}$  bands.

In analogy to the large temperature dependence of the 960  $\text{cm}^{-1}$  OH band in the spectrum of the dihydroxobridged dimer it was anticipated that the position of these bands would show a comparatively large temperature dependence. To examine this possibility, the infrared spectra of a couple of representative extended lattice compounds

were studied at liquid nitrogen temperatures. Lepidocrocite at room temperature has a sharp OH absorption at  $1019\text{ cm}^{-1}$  and a broader but weaker band at  $1148\text{ cm}^{-1}$  which is also attributed to OH. As is shown in the insert in Figure 2-C, at  $\sim 78^\circ\text{K}$  the sharp band moves  $10\text{ cm}^{-1}$  to higher energy to  $1029\text{ cm}^{-1}$  and the broader higher energy band shifts  $27\text{ cm}^{-1}$  up to  $1175\text{ cm}^{-1}$ . The origin of the weak  $1259\text{ cm}^{-1}$  band at  $\sim 78^\circ\text{K}$  is unknown. These shifts must be compared to the shifts that occur in other spectral regions. The Fe-O band at  $478\text{ cm}^{-1}$  has an apparent shift of only  $+2$  and no change could be observed in the shoulder at  $510\text{ cm}^{-1}$ . On the other hand, the band at  $742\text{ cm}^{-1}$  shifted  $12\text{ cm}^{-1}$  to  $754\text{ cm}^{-1}$ . The higher energy OH stretch at  $3160\text{ cm}^{-1}$  shifted down to about  $3130\text{ cm}^{-1}$ .

Data for  $\alpha\text{-FeO(OH)}$  have also been obtained. <sup>(8)</sup> The  $885\text{ cm}^{-1}$  band shifts  $6\text{ cm}^{-1}$  to  $891\text{ cm}^{-1}$  and the  $792\text{ cm}^{-1}$  band shifts  $7\text{ cm}^{-1}$  to  $799\text{ cm}^{-1}$ , the overtone at about  $1755\text{ cm}^{-1}$  shifts  $45\text{ cm}^{-1}$  to about  $1800\text{ cm}^{-1}$ , the  $636\text{ cm}^{-1}$  band shifts  $9\text{ cm}^{-1}$  to  $645\text{ cm}^{-1}$ , and additional band structure is revealed between  $1000$  and  $1100\text{ cm}^{-1}$ .

In  $\alpha\text{-MnO(OH)}$ , the OH bands at  $1083$ ,  $1113$ , and  $1146\text{ cm}^{-1}$  shift to  $1089$ ,  $1125$ , and  $1158\text{ cm}^{-1}$  respectively. The broad band near  $2050\text{ cm}^{-1}$  sharpens slightly and moves to about  $2075\text{ cm}^{-1}$ . More significantly, the shoulder at  $2210\text{ cm}^{-1}$  sharpens to reveal two weak bands at about  $2245$  and  $2205\text{ cm}^{-1}$  which are more likely to be the overtones of the OH bands around  $1100\text{ cm}^{-1}$  than the broad band near  $2000\text{ cm}^{-1}$  of comparable density to the  $1100\text{ cm}^{-1}$  bands. The asymmetric band at  $2665\text{ cm}^{-1}$  also shifts to lower energy to about  $2610\text{ cm}^{-1}$ .

In the manganite spectrum, low temperature improves resolution in the 1000-1200  $\text{cm}^{-1}$  region and produces shifts of about 10 to 20  $\text{cm}^{-1}$  to higher energy (insert in Figure 1-D). This contrasts with the small shifts (1 to 3  $\text{cm}^{-1}$ ) observed for bands in the 400-800  $\text{cm}^{-1}$  region.

The spectra of three iron oxides are presented in Figure 3. Although the spectrum of magnetite was obtained with a high concentration of sample in a TlBr pellet, bands are weak and overall quality is low due to the extreme scattering from the high refractive-index material.

#### 4. Relationship of Ferritin to Hydrous Iron Oxides

An important feature of the infrared spectra is that each of these various species has a distinctive spectrum which should prove useful in characterizing the iron polymers derived from natural systems. Comparison of the infrared spectrum of horse ferritin micelles (Figure 4) with the spectra of the numerous iron oxides and hydrous oxides shows that while there is little similarity between the ferritin spectrum and the well-established oxides and hydrous oxides, there is a definite similarity in the spectrum of the micelles to that of dried "ferric hydroxide". Furthermore, this same resemblance also extends to one of the two synthetic polymers, namely, Towe's hydrolyzate.

The problem of determining the structure of ferritin thus appears to be associated with the problem of determining the structure of "ferric hydroxide". At best this is a complicated problem to which no single solution may exist. Two additional points need to be noted

Figure 3. Infrared spectra of iron oxides.

- A)  $\alpha$ -Fe<sub>2</sub>O<sub>3</sub>, hematite, 0.91 mg/400 mg KBr pellet, ambient temperature.
- B)  $\gamma$ -Fe<sub>2</sub>O<sub>3</sub>, maghemite, 0.60 mg/400 mg TlBr pellet, ambient temperature.
- C) Fe<sub>3</sub>O<sub>4</sub>, magnetite, 2.09 mg/400 mg TlBr pellet, ambient temperature.

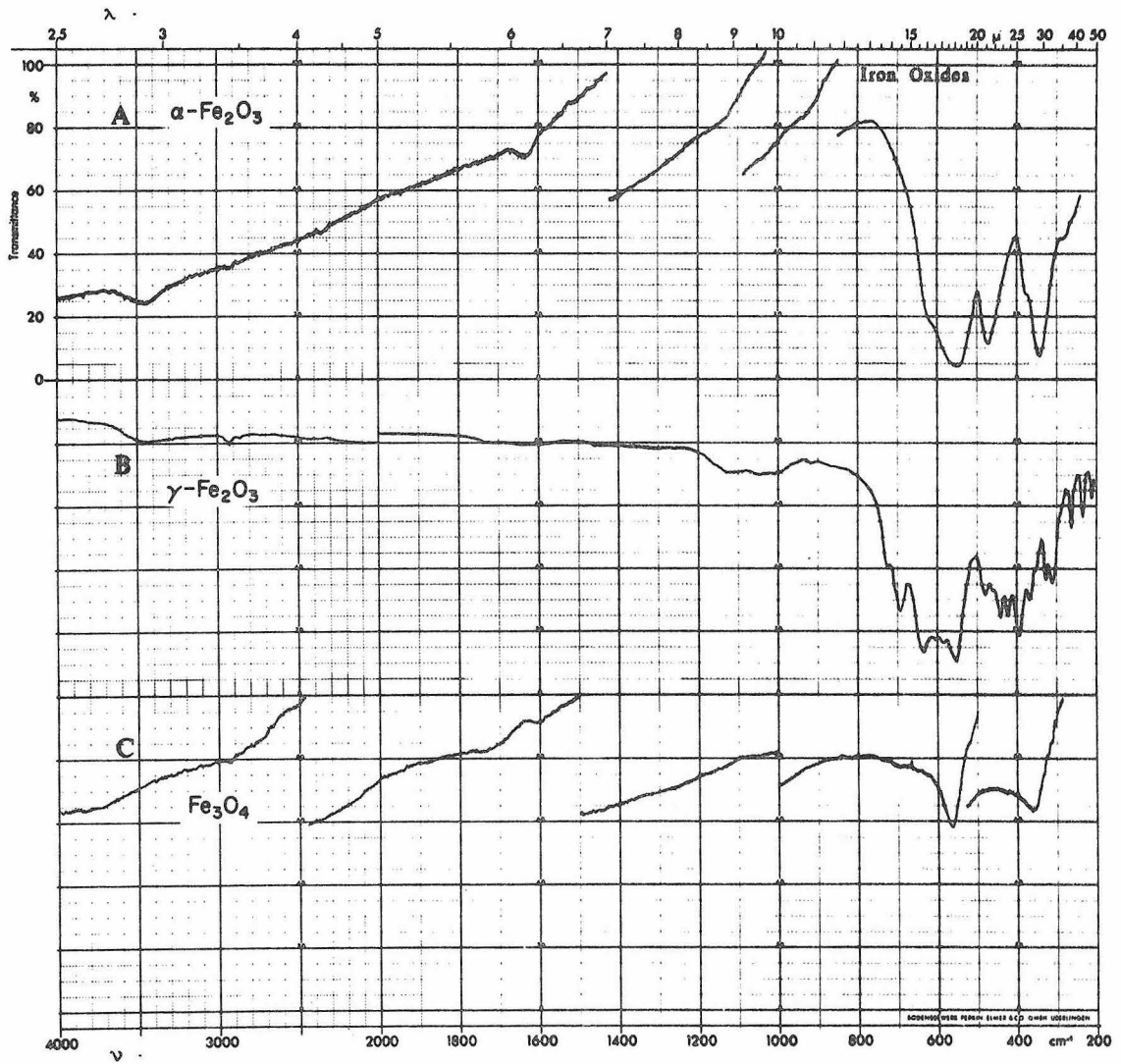


Figure 3

**Figure 4. Infrared spectra of ferritin models**

- A) "Ferric hydroxide" air-dried overnight. 3.85 mg/400 mg TlBr pellet, ambient temperature.
- B) Saltman-Spiro polymer,  $\text{Fe}_4\text{O}_3(\text{OH})_4(\text{NO}_3)_2 \cdot 1\frac{1}{2}\text{H}_2\text{O}$ , 0.86 mg/400 mg KBr pellet, ambient temperature
- C) Towe hydrolyzate, 0.49 mg/400 mg KBr pellet, ambient temperature.
- D) Horse ferritin micelles, 0.64 mg/400 mg KBr pellets, ambient temperature.

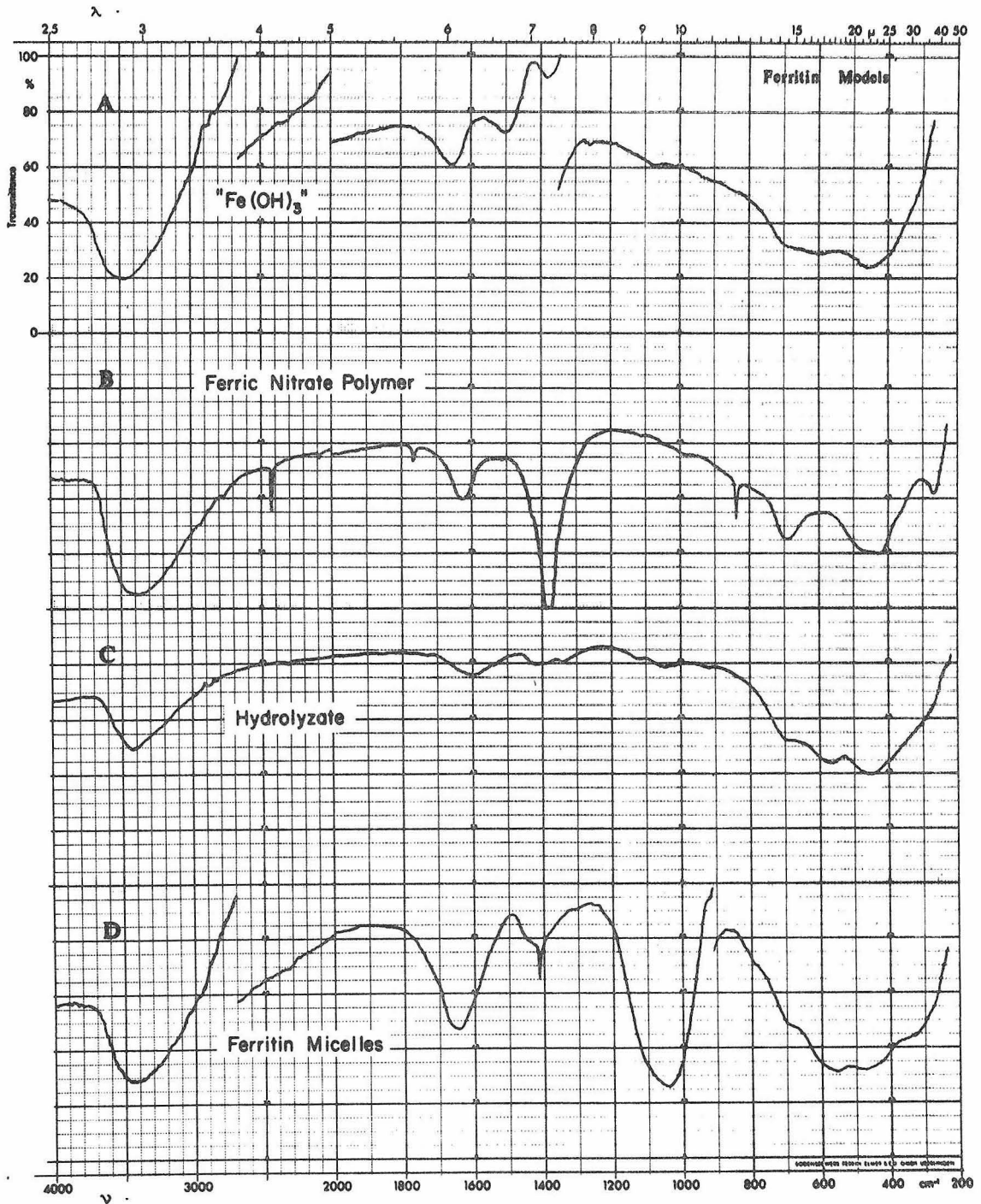


Figure 4



from the infrared studies. The first is that in ferritin and "ferric hydroxide" the bands below  $1000\text{ cm}^{-1}$  are all broad and overlapping in contrast to the sharper bands and consequent improved definition of this region in the model oxides and hydrous oxides. This arises from substantial disorder in the lattice (in fact it is questionable if the term lattice with its implication of long range order is even appropriate in discussions of this material). X-ray evidence clearly indicates that  $\text{Fe}(\text{OH})_3$  does not exist as such, but rather is a non-crystalline material which upon dehydration is slowly converted into mixtures of oxides and hydrous oxides. Powder pattern lines are broad and diffuse in the hydrolyzate, ferric hydroxide, and the micelles, a fact in agreement with the disorder indicated by the infrared evidence. The second point is that in the spectra of the micelles, synthetic polymers, and ferric hydroxide, there are no comparatively sharp bands in the infrared around  $3500\text{ cm}^{-1}$  which could be assigned to discrete OH. This fact again points to the lack of crystallographically ordered OH and argues for a hydrous oxide formulation as opposed to a definite hydroxide. This point will be further elaborated below.

Ferritin contains phosphate in the ratio of one phosphorus atom per eight irons. Although it has been argued that the phosphate is associated with the surface and therefore is not a structural component of the interior of the core, it was deemed appropriate to examine the infrared spectra of several representative ferric phosphates to see if a similarity did indeed exist between ferritin and naturally occurring phosphates. Figure 5 presents the infrared spectra of three naturally occurring ferric phosphates and an aluminum hydroxyphosphate. The

Figure 5. Infrared spectra of phosphate minerals.

- A)  $2\text{Fe}_2\text{O}_3 \cdot \text{P}_2\text{O}_5 \cdot 9\text{H}_2\text{O}$ , Delvauxite, 0.53 mg/400 mg KBr pellet, ambient temperature.
- B)  $2\text{Fe}_2\text{O}_3 \cdot \text{P}_2\text{O}_5 \cdot 3\text{H}_2\text{O}$ , Dufrenite, 0.51 mg/400 mg TlBr pellet, ambient temperature.
- C)  $(\text{Fe}, \text{Mn})\text{PO}_4 \cdot \frac{1}{2}\text{H}_2\text{O}$ , Purpurite, 0.52 mg/400 mg KBr pellet, ambient temperature.
- D)  $\text{NaAl}_3(\text{PO}_4)_2(\text{OH})_4$ , Brazilianite, 0.81 mg/400 mg KBr pellet, ambient temperature.

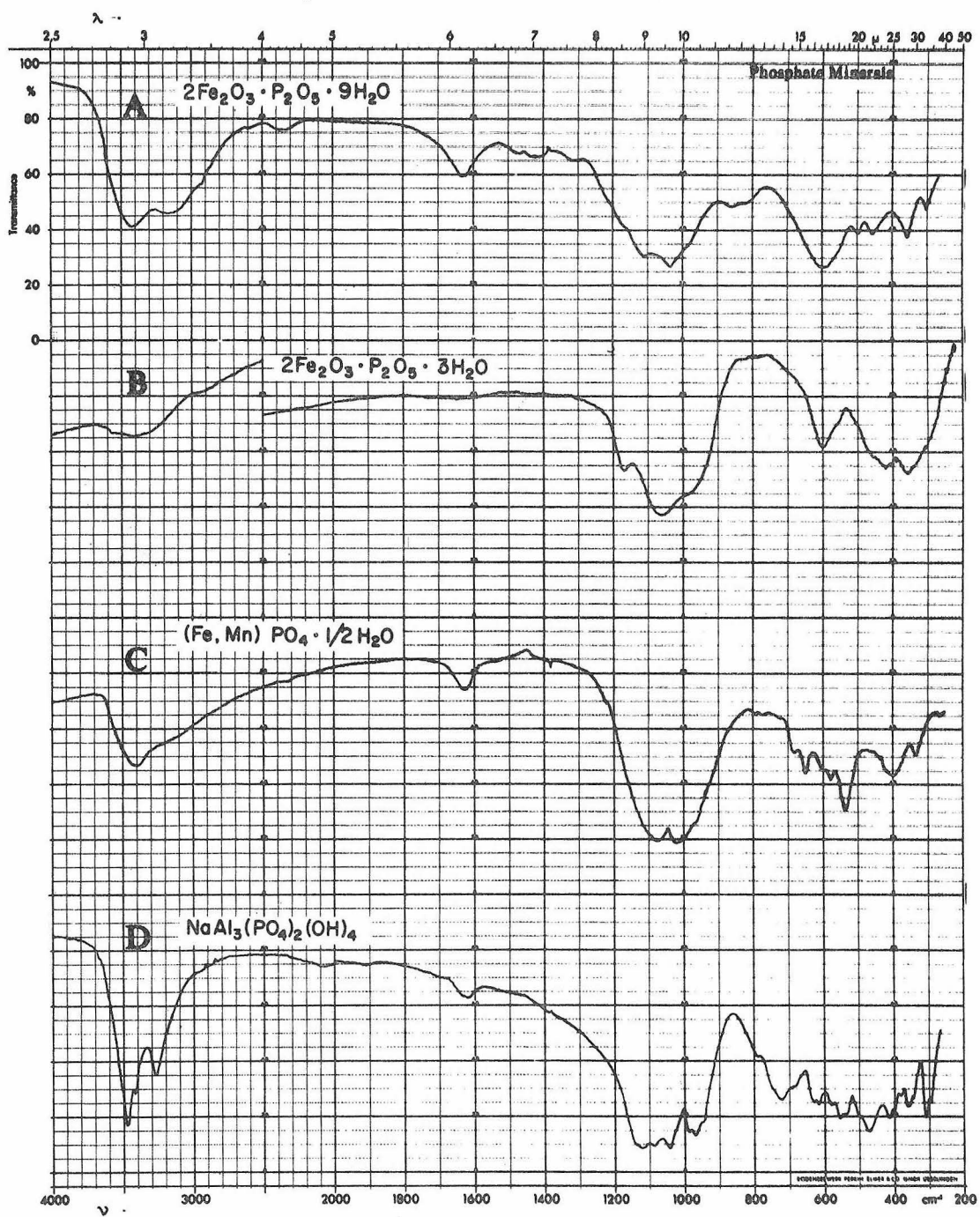


Figure 5

samples of brazilianite,  $\text{NaAl}_3(\text{PO}_4)_2(\text{OH})_4$ , chosen because of its formulation as a hydroxyphosphate; and delvauxite -  $2\text{Fe}_2\text{O}_3 \cdot \text{P}_2\text{O}_5 \cdot 9\text{H}_2\text{O}$ , dufrenite -  $2\text{Fe}_2\text{O}_3 \cdot \text{P}_2\text{O}_5 \cdot 3\text{H}_2\text{O}$ , and purpurite -  $\text{Fe}(\text{Mn})\text{PO}_4 \cdot \frac{1}{2}\text{H}_2\text{O}$ , three minerals chosen as representing various degrees of hydration of the ferric phosphate, were obtained from the Caltech geology reference collection (Nos. 5920, 1618, 7590, and 7560, respectively).

The main feature to note is the comparative sharpness of the bands in the  $200\text{-}800\text{ cm}^{-1}$  region as compared to the ferritin micelles. Substances such as these are not appropriate models of ferritin. Although there are no x-ray data to confirm that brazilianite is a true hydroxo-containing species, the sharpness of the infrared bands in the  $3200\text{-}3500\text{ cm}^{-1}$  region conclusively demonstrate the presence of OH as formulated. While it is also likely that at least one of the bands in the  $950\text{-}1150\text{ cm}^{-1}$  region is an OH band, phosphate absorption in this region interferes with the observation of the OH bands. Observe however, that among the phosphate minerals only brazilianite has a noticeable absorption near  $2000\text{ cm}^{-1}$ . This is conveniently attributed to the overtone of an OH absorption near  $1000\text{ cm}^{-1}$  as occurred in the  $\text{MO}(\text{OH})$  compounds. The absence of such bands near  $2000\text{ cm}^{-1}$  in the other phosphate minerals makes phosphate overtones an unlikely explanation. Returning to the ferritin micelles, it is seen that no overtones exist near  $2000\text{ cm}^{-1}$ , confirming again the absence of ordered OH.

References

1. J. D. Bernal, D. R. Dasgupta, and A. L. Mackay, Clay Minerals Bull., 4, 15 (1959).
2. K. M. Towe and W. F. Bradley, J. Colloid and Interface Sci., 24, 384 (1967).
3. T. G. Spiro, S. E. Allerton, J. Renner, A. Terzis, R. Bils, and P. S. Saltman, J. Amer. Chem. Soc., 88, 2721 (1966).
4. E. Schwarzmam and H. Sparr, Z. Naturforschg., 24b, 8 (1969).
5. E. Schwarzmam and H. Marsmann, Naturwissenschaften, 53, 349 (1966).
6. A. N. Christensen, Acta Chem. Scand., 21, 121 (1967).
7. A. Cornelis-Benoit, Spectrochim. Acta, 21, 623 (1965).
8. Dana Powers, private communication of unpublished data.

### C. Optical Spectra of Selected Iron Polymers with an Eye for SPE Transitions

A logical extension of the study of SPE bands in the dimeric oxobridged systems is the study of SPE-related bands in polymeric materials involving a number of metal-oxygen-metal bridges and various magnitudes of magnetic exchange interactions. A major experimental difficulty arises, however, from the high refractive indices of most of these materials which results in low quality spectra due to excessive scattering. This problem can be largely obviated with many substrates through the use of TiCl pellets for absorption spectroscopy in the visible and near-infrared portion of the spectrum. In a few instances it has been possible to extend these studies into the uv by the use of chemically prepared thin films of the sample on a quartz substrate. A survey of the preliminary results follows.

Natural samples of  $\alpha$ -FeO(OH),  $\gamma$ -FeO(OH), and  $\alpha$ -Fe<sub>2</sub>O<sub>3</sub> display several bands in the near-infrared and visible portions of the spectrum (Figure 1). Synthetic  $\delta$ -FeO(OH) also displays a much stronger absorption near 900 nm. Several features emerge from these spectra. First of all, the pattern of broad-broad-sharp so prevalent in the spectra of model iron(III) octahedral compounds does not appear in these compounds in testimony to their distorted structures. Instead these spectra consist of a series of broad, and often poorly resolved, bands riding an intense tail of steadily increasing absorption. The second feature is the intensity of the bands. Pellets can provide a lower bound for the  $\epsilon$  of compounds. The absorbances of the lowest energy band observed for Fe<sub>2</sub>O<sub>3</sub>,  $\alpha$ -, and  $\beta$ -FeO(OH) correspond to  $\epsilon$

Figure 1. Optical spectra of iron(III) oxides and oxyhydroxides.

- A)  $\alpha$ -FeO(OH), goethite, 4.0 mg/400 mg TiCl<sub>3</sub> pellet, 78°K.
- B)  $\alpha$ -Fe<sub>2</sub>O<sub>3</sub>, hematite; left: thin film on SiO<sub>2</sub>, 78°K, prepared by heating thin film of lepidocrocite in air; right: 4.0 mg/400 mg TiCl<sub>3</sub> pellet, 78°K.
- C)  $\gamma$ -FeO(OH), lepidocrocite; left: thin film on SiO<sub>2</sub>, 78°K, prepared by letting water from a rusty steam line drip on a SiO<sub>2</sub> plate; right: 4.0 mg/400 mg TiCl<sub>3</sub> pellet, 78°K.

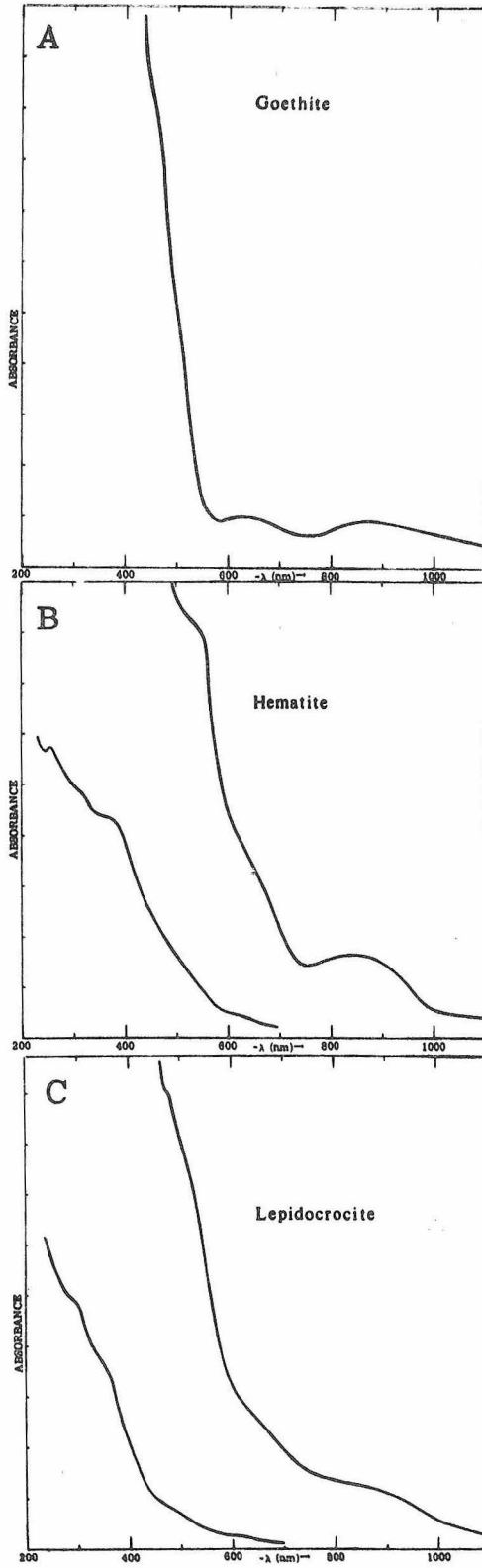


Figure 1



on the order of 3, while the first band in  $\delta$ -FeO(OH) has an  $\epsilon$  on the order of 30. In comparing  $\delta$ -FeO(OH) with  $\alpha$ - and  $\gamma$ -FeO(OH) it is interesting to note that the apparently higher intensity of absorption coincides with a greater magnetic exchange which is also present in the  $\delta$ -FeO(OH). Recall that  $\delta$ -FeO(OH) sticks to weakly magnetized spatulas. Theoretical considerations referred to in the discussion of SPE excitations (Section II-E) have indicated that the intensification of d-d bands should accompany increased magnetic interaction between metal atoms. The third feature is the series of bands in the ultraviolet. The number and positions of these bands are suggestive of an origin related to SPE bands. Although the additivity of energies does not apply, this is not unexpected in view of the strong magnetic coupling and the complexity of the structures wherein interaction among three or more metal atoms may be as important as two metal, nearest neighbor interactions. The occurrence of SPE related bands in condensed metal oxides seems certain to become widely recognized. Such band systems have already been intensively investigated in  $\text{Cr}_2\text{O}_3$  which shows a series of new bands in the near ultraviolet region when compared to dilute  $\text{Cr}^{3+}$  ion in  $\text{Al}_2\text{O}_3$ . (1,2)

Table I. Optical Absorption Bands in  
Iron Oxide and Hydrrous Oxides

$\alpha$ -Fe <sub>2</sub> O <sub>3</sub>	natural Hematite,	4.0 mg/400 mg TlCl, 78°K	
<u><math>\lambda</math>(nm)</u>		<u><math>10^{-3} \bar{\nu}</math> (cm<sup>-1</sup>)</u>	
876		11.4	
~680		14.7	faint shoulder
550		18.2	
441		22.7	faint shoulder
rust film heated in air			
<u><math>\lambda</math> (nm)</u>		<u><math>10^{-3} \bar{\nu}</math> (cm<sup>-1</sup>)</u>	
387		25.8	
317		31.5	
261		38.3	
$\alpha$ -FeO(OH)	natural Goethite,	4.0 mg/400 mg TlCl, 78°K	
<u><math>\lambda</math> (nm)</u>		<u><math>10^{-3} \bar{\nu}</math> (cm<sup>-1</sup>)</u>	
887		11.3	
648		15.4	
510		19.6	faint shoulder
466		21.4	

Table I (Continued)

$\gamma$ -FeO(OH)	natural Lepidocrocite	4.0 mg/400 mg TiCl <sub>3</sub> , 78°K	
	<u><math>\lambda</math> (nm)</u>	<u><math>10^{-3} \bar{\nu}</math> (cm<sup>-1</sup>)</u>	
	902	11.1	
	665	15.0	
	~534	18.7	
	482	20.8	
	rust film on quartz, 78°K		
	<u><math>\lambda</math>(nm)</u>	<u><math>10^{-3} \bar{\nu}</math> (cm<sup>-1</sup>)</u>	
	486	20.6	
	360	27.8	
	302	33.1	
	256	39.1	weak shoulder
$\delta$ -FeO(OH)	synthetic preparation, TiCl <sub>3</sub> pellet, 296°K		
	<u><math>\lambda</math> (nm)</u>	<u><math>10^{-3} \bar{\nu}</math> (cm<sup>-1</sup>)</u>	
	~900	~11.1	difficult to locate precisely
	no other band observed to 570 nm		

References

1. D. S. McClure, J. Chem. Phys., 38, 2289 (1963).
2. H. L. Schafler, J. Chem. Phys., 42, 504 (1965).

## PROPOSITION I

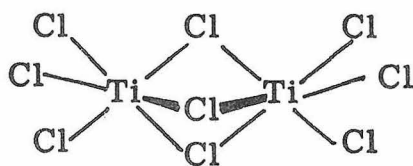
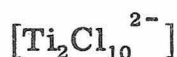
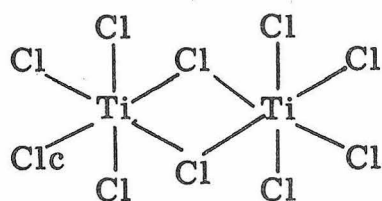
The Synthesis of a Vanadium(IV) Dimer  
for Experimental Testing of Theories of Simultaneous  
Pair Electronic Excitations

It is proposed that  $VCl_4$  will react with  $PCl_5$  to form dimeric compounds analogous to  $[PCl_4]_2[Ti_2Cl_{10}]$  and  $[PCl_4][Ti_2Cl_9]$  examples of  $d^1$  antiferromagnetic dimers. These dimers would be examined spectroscopically for simultaneous pair electronic excitations.

Examples of molecules and crystal systems continue to be discovered which experimentally exhibit the phenomenon of simultaneous pair electronic (SPE) excitations and emissions (also referred to as cooperative effects).<sup>(1-5)</sup> These systems have been confined to multi-d-electron systems such as  $d^5$  Mn(II) and Fe(III), and to rare earth f-electron systems. While providing a multitude of absorption bands, the f-electron systems are not sensitive to chemical environmental effects and have yet to be reported in a discrete dimeric system. While experimentally fascinating, the d-electron systems have not been well suited to theoretical studies due to the inherent complexity of multi d-electron theory, and due to the presence of numerous spin-forbidden bands in the SPE region. A vital theoretical question that has yet to be satisfactorily answered is whether or not SPE bands are intensified spin forbidden bands, higher energy spin allowed d-d bands, true simultaneous pair excitations of d-d bands, or admixtures of the various possibilities. Ideally, a dimeric  $d^1$  first-row system should be examined since the theory is simple, and with just one d-d band the ambiguities which arise from higher energy d-d bands occurring in the

region where SPE bands are predicted to be do not occur. However, first one must make such a system.

Taking a cue from the recent report<sup>(6)</sup> of the crystal structures of bis(tetrachlorophosphonium) di- $\mu$ -chloro-octachlorodititanate(IV),  $[\text{PCl}_4]_2[\text{Ti}_2\text{Cl}_{10}]$ , and tetrachlorophosphonium tri- $\mu$ -chloro-hexachlorodititanate(IV),  $[\text{PCl}_4][\text{Ti}_2\text{Cl}_9]$ , prepared respectively from the reaction of  $\text{PCl}_5$  with  $\text{TiCl}_4$  in  $\text{POCl}_3$  and  $\text{SOCl}_2$  solvents, it is proposed that an attempt be made to synthesize the analogous vanadium(IV) compounds using analogous procedures. The two titanium dimers both contain octahedral titanium with the structures indicated below:



A precedent for the reactions with vanadium(IV) halides has been established. A dark violet powdery precipitate was obtained when tetramethylammonium chloride was added to a solution of  $\text{VCl}_4$  in  $\text{AsCl}_3$ .<sup>(7)</sup> It was formulated as a 1:1 adduct, namely  $[(\text{CH}_3)_4\text{N}][\text{VCl}_5]$ . In a survey of the reactions of anhydrous halides with phosphorous pentachloride in a phosphorous oxychloride solvent, the formation of a 1:1 adduct,  $\text{PCl}_5 \cdot \text{VCl}_4$ , has been reported.<sup>(8)</sup> More recently, vanadium oxytrichloride has been found to react with phosphorous

pentachloride to form a compound of the same stoichiometry,

$\text{PCl}_5 \cdot \text{VCl}_4$ .<sup>(9)</sup> The 1:1 adduct is consistent with a dimeric structure:  
 $2[\text{PCl}_5 \cdot \text{VCl}_4] = [\text{PCl}_4]_2[\text{V}_2\text{Cl}_{10}]$ .

The potential advantages of this system are the availability of the dichloro- and the trichlorobridged dimers which should exhibit different degrees of antiferromagnetic spin-spin coupling, and the possibility of synthesizing these dimers with different halides. The potential disadvantages are the likelihood of intense charge transfer bands of annoyingly low energy, and the possibility of monomer rather than dimer formation as occurs in  $[\text{PCl}_4][\text{FeCl}_4]$ .<sup>(10)</sup> The first disadvantage may be offset by the possibility of obtaining fluoro-dimers which would provide minimal charge transfer problems, and secondly by the fact that the d-d band is spin allowed and consequently should provide a more favorable case than occurs in the  $d^5$  systems which have been studied whose one-center bands are spin forbidden to begin with.

## REFERENCES

1. F. L. Varsanyi and G. H. Dicke, Phys. Rev. Letters, 7, 442 (1961).
2. J. M. Marrs and M. Kasha, Chem. Phys. Letters, 6, 235 (1970).
3. J. Ferguson, H. J. Guggenheim, and Y. Tanabe, J. Chem. Phys., 45, 1134 (1966).
4. H. J. Schugar, G. R. Rossman, J. Thibeault, and H. B. Gray, Chem. Phys. Letters, 6, 26 (1970).
5. J. S. Margolis, O. Stafsudd, and E. Y. Wong, J. Chem. Phys., 38, 2045 (1963).
6. T. J. Kistenmacher and G. D. Stucky, Inorg. Chem., 10, 122 (1971).
7. V. Gutmann, Z. anorg. allg. Chem., 266, 331 (1951).
8. W. L. Groeneveld, Rec. Trav. Chim., 71, 1152 (1952).
9. L. Kolditz, V. Neumann, and G. Kilch, Z. anorg. allg. Chem., 325, 275 (1963).
10. T. J. Kistenmacher and G. D. Stucky, Inorg. Chem., 7, 2150 (1968).



## PROPOSITION II

An Investigation of the Structural Status of  
OH in Extended Lattice Compounds

High resolution infrared and raman studies of OH-containing extended lattice compounds are proposed for the purpose of better identifying and characterizing the various forms of OH which can exist in these systems. Definitive criteria need to be established for such forms as  $\text{H}_3\text{O}^+$ , "lattice" water, "surface" water, and the several forms of bridging OH.

One of the most difficult features to obtain from x-ray crystallographic study of large molecules is the position of protons. There are numerous basic salts, hydrated silicates, and extended lattice compound which are formulated as containing either water of hydration, lattice water, constitutional water, or OH in some form. Vibrational spectroscopy is one of the best means of probing the hydrogen atom in these systems. Raman spectroscopic studies of these systems are almost entirely lacking, and most of the few which have been done suffer from the multiple disadvantages of being old, published in obscure places, and confined to simple systems such as  $\text{Mg}(\text{OH})_2$  and  $\text{CaSO}_4 \cdot 2\text{H}_2\text{O}$ .<sup>(1, 2)</sup> More data is available from infrared studies, particularly with regard to simple systems. Studies of the more complicated systems have been generally non-critical, low resolution, survey studies which have not concentrated upon structural aspects.<sup>(3, 4)</sup>

Infrared studies have been conducted on a variety of hydrous metal oxides. For example, using the correlations of Nakamoto, et al.<sup>(5)</sup> which show that for linear  $\text{O}-\text{H} \cdots \text{X}$  hydrogen bonds there is

a nearly linear relationship between the displacement of the OH stretching band and the O-H...X distance, Benoit<sup>(6)</sup> determined the hydrogen bond distance in  $\alpha$ -GaO(OH) and identified the low energy OH bands through deuteration studies. The perpendicular orientation of the OH group with respect to the basal cleavage plane of mica has been determined through polarized single crystal infrared studies of muscovite<sup>(7)</sup> and the presence of bridging OH has been verified in jarosite and several dimeric systems.

It is proposed that a detailed raman and infrared investigation be begun on a variety of OH-containing extended lattice compounds of known structure for the purpose of better establishing the spectroscopic characteristics of the various forms of OH in these systems. Several specific problems come to mind.

The status of water in amorphous metal "hydroxides" such as Al(OH)<sub>3</sub>, Si(OH)<sub>4</sub>, etc., is generally unclear. While it is easily established that neither ionic OH<sup>-</sup> nor discrete M(OH)<sub>x</sub> molecules exist by examining the 3500 cm<sup>-1</sup> region of the spectrum, little effort has been directed toward establishing the presence or absence of various forms of bridging OH. This would be accomplished through careful examination of the lower energy portions of the spectrum. The course of the dehydration of iron, aluminum, and silicon "hydroxides" to their respective oxides and hydrous oxides has yet to be adequately described at the molecular level.

Hydronium ion is occasionally postulated as a discrete cation in compounds, usually on the basis of stoichiometry and packing considerations. Definite spectroscopic criteria have not been presented for

identifying  $\text{H}_3\text{O}^+$ . There also is much uncertainty as to lattice water, coordinated water, and surface water inclusions in mineral systems.

A combined infrared raman study of these systems and deuterated models of known structure with particular attention to the low energy region and to low temperature spectra should prove valuable for elucidating the structural role of OH in extended lattices.

#### REFERENCES

1. Shashanka S. Mitra, Univ. Microfilm (Ann Arbor, Mich), L.C. Card No. Mic 58-3713; Dissertation Abstr. 19, 841 (1958).
2. A. J. Stekhanov, Doklady Akad. Nauk. S. S. S. R., 106, 433 (1956).
3. J. M. Hunt, M. P. Wisherd, and L. C. Bonham, Anal. Chem., 22, 1478 (1950).
4. K. Omori, Sci. Rept. Tohoku Univ., Third. Ser., 9, 65 (1964).
5. K. Nakamoto, M. Margoshes, and R. E. Rundle, J. Amer. Chem. Soc., 77, 6480 (1955).
6. A. C. Benoit, Spectrochim. Acta, 21, 623 (1965).
7. D. K. Arkhipenko, Doklady Mezhuuz. Nauch Konf. po Spektroskopii i Spekr. Analizu, Tomsk. Univ., 1960, 81. CA 56: 117b.

## PROPOSITION III

An Investigation of the Color Effects in  
Potassium and Cesium Tetrafluoroborate Solutions

Solutions of  $\text{KBF}_4$  in  $\text{HBF}_4$  have previously been observed to display temperature dependent colors. These systems should be re-examined and the cause of the colors established.

In the late 1920's it was reported<sup>(1-4)</sup> that a saturated aqueous solution of  $\text{KBF}_4$  gave color effects upon heating if a small excess of solid  $\text{KBF}_4$  were present in solution. A light blue color was present in a 10% aqueous solution at  $100^\circ$  which turned green at  $90^\circ$  and yellow at  $60^\circ$ . Precipitates of  $\text{CsBF}_4$  obtained by reacting  $\text{CsCl}$  with  $\text{HBF}_4$  were jelly-like and also showed color effects. In a slurry of  $\text{KBF}_4$  in concentrated  $\text{HBF}_4$ , the color changes occurred at room temperature. The explanation given for these color changes was that the refractive index of the solids was close to water ( $n_D = 1.3563 - 1.3502$  for  $\text{CsBF}_4$ ), but the dispersion was different. Both properties being temperature dependent interacted appropriately to give the observed color effects.

Maybe the effect is not so simply explained. When a saturated solution of commercial  $\text{KBF}_4$  is heated with excess solid, no color changes occur. When  $\text{KBF}_4$  is saturated in commercial  $\text{HBF}_4$ , the resulting solution does not display color changes. When an aqueous  $\text{CsCl}_2$  solution is mixed with a  $\text{HBF}_4$  solution, the jelly-like  $\text{CsBF}_4$  precipitate does not show color effects. Possibly the effect that was originally observed was due to impurities in the chemicals, or alternately, the conditions necessary to make it happen are much more

critical than the original articles would lead one to believe.

The effect must be physical in origin since both alkali metal cations and the  $\text{BF}_4^-$  anion have no accessible low-lying electronic states to which visible absorptions could occur. The possibility of an inorganic cholesteric liquid crystal comes to mind as does opalescence of the type observed in the gemstone opal.

It is proposed that this system be reinvestigated by first reproducing the phenomenon following exactly the procedure of de Boer and then systematically eliminating the possibility of impurities.

#### REFERENCES

1. J. H. de Boer, Physica, 7, 99 (1927).
2. J. H. de Boer, Verslag. Akad. Wetenschappen Amsterdam, 36, 161 (1927).
3. J. H. de Boer and J. A. M. van Liempt, Rec. Trav. Chim., 46, 124 (1927).
4. The earlier work is summarized in H. S. Booth and D. R. Martin, "Boron Trifluoride and its Derivatives," J. H. Wiley and Sons, New York, 1949, p. 99.

## PROPOSITION IV

## Molybdenum Cyanide-Sulfide

## Complexes

A molybdenum compound containing cyanide and sulfide ligands has been prepared which has an infrared spectrum which indicates the compound also contains a hydride unit. This compound should be investigated for catalytic properties and the whole field of molybdenum cyanosulfides should be investigated.

For decades the chemistry of "hydroxocyano" molybdates was astir with  $\text{Mo(OH)}_4(\text{CN})_4^{4-}$ ,  $\text{Mo(OH)}_3(\text{CN})_5^{4-}$ , the corresponding Mo(V) compounds, deprotonated derivatives, and rarely, a proposal for a six-coordinated formulation. The fury has ended with the determination of the x-ray structure of six-coordinate  $\text{NaK}_3\text{MoO}_2(\text{CN})_4 \cdot 6\text{H}_2\text{O}$  which had been presumed to contain eight coordinate  $\text{Mo(OH)}_4(\text{CN})_4^{4-}$ . With simple deprotonations of  $\text{MoO}_2(\text{CN})_4^{4-}$ , a large amount of data can be explained by the formation of  $\text{MoO(OH)(CN)}_4^{3-}$  and  $\text{Mo(OH)}_2(\text{CN})_4^{2-}$ . It is proposed that it is now appropriate to replace the oxygen by sulfur and delve into the meager quagmire of data regarding cyanothiomolybdates.

In 1896, Heide<sup>(1)</sup> reacted  $\text{MoS}_2$  with KCN under various conditions and obtained a variety of red-brown to dark green materials which he formulated as  $\text{K}_2\text{MoS}_2(\text{CN})_4$ ,  $\text{K}_6\text{Mo}_2\text{S}_3(\text{CN})_6$ ,  $\text{K}_4\text{MoOS}(\text{CN})_6 \cdot 4\text{H}_2\text{O}$ , and  $\text{K}_5\text{Mo}_3\text{S}_4(\text{CN})_8 \cdot 7\text{H}_2\text{O}$ . In 1928, Crepaz<sup>(2)</sup> dissolved  $\text{MoO}_3$  in KOH + KCN and bubbled  $\text{H}_2\text{S}$  gas into the solution. After undergoing a series of color changes, the solution turned light blue. From this solution a compound formulated as  $\text{K}_3[\text{MoS}(\text{CN})_4] \cdot 2\text{H}_2\text{O}$  was isolated. The solutions of this blue salt, which has come to be called Crepaz's salt,

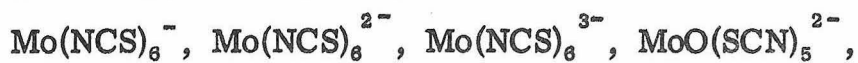
turn violet upon air oxidation. From the violet solution, a violet salt formulated as  $K_3[MoS(OH)(CN)_4(H_2O)_2] \cdot 2H_2O$  has been isolated. (3)

The latest addition to the literature of this subject recently came about when it was reported that a sulfur bridged dimer of formulation  $K_6[(CN)_5Mo-S-Mo(CN)_5] \cdot 4H_2O$  was isolated from the intense green solution resulting from the reaction of  $H_2S$  with  $MoO_3$  dissolved in strongly basic KCN. (4) This proposed dimer was also prepared as the anhydrous salt by drying over  $P_4O_{10}$ . None of these compounds is adequately structurally characterized, and even the accuracy of the earlier elemental composition data is questionable.

An added complication to these studies is the existence of a variety sulfur-containing species that could occur as coproducts in these preparations. At one time or another, the following ions have been claimed to have been isolated from reaction mixtures of molybdates and  $H_2S$ (5):

red-orange	$MoS_4^{2-}$
yellow	$MoS_5^{2-}$
blood-red	$HMoS_5^-$
black	$MoS_6^-$
dark grey	$Mo_2S_7^{2-}$
	$MoOS_3^{2-}$
golden yellow	$MoO_2S_2^{2-}$
golden yellow	$MoO_3S^{2-}$
dark red	$H_2(MoS_4)_6^{10-}$

Thiocyanate complexes are also possible coproducts. The following ions appear frequently in the literature:



One aspect of molybdenum-sulfur-cyanide chemistry looks particularly promising for research. While attempting to repeat the preparation of  $\text{K}_6[(\text{CN})_5\text{Mo-S-Mo}(\text{CN})_5] \cdot 4\text{H}_2\text{O}$  by the reaction of 40g  $\text{MoO}_3$  dissolved in 250 ml 25%  $\text{KOH}$  with 90g  $\text{KCN}$  and  $\text{H}_2\text{S}$  gas, at least ten different substances were isolated from the reaction mixture during work-up. They ranged from orange-red  $\text{K}_2\text{MoS}_4$ , and blue Crepaz's salt, to black, tarry thiocyanate complexes. One compound, obtained as small red-brown crystals by  $-20^\circ\text{C}$  cooling of the filtrate obtained after filtering the initial reaction mixture after cooling to  $0^\circ\text{C}$ , has an infrared spectrum which has strong cyanide stretches at 2100 and  $2088\text{ cm}^{-1}$ ; a triplet of medium intensity bands at 2043, 2032, and  $2019\text{ cm}^{-1}$ , which, although of unusually low energy, could be cyanide; and of greatest interest, a medium intensity band at  $1955\text{ cm}^{-1}$ .

The  $1950\text{ cm}^{-1}$  region is appropriate for a metal hydride stretch. If this is the case, this particular compound should be ideally suited for catalysis studies since it combines the backbone of much of transition metal catalysis, the hydride unit, with high field cyanide ligands, a soft and polarizable sulfide group which is also obviously present as judged by the stench of the compound, all put on a metal, molybdenum, which has a multitude of accessible oxidation states.



This moderately stable compound (the solid decomposed completely within one week at room temperature) could possibly be made in reasonable yields by the reaction of  $\text{BH}_4^-$  with other cyanothiomolybdates such as Crepaz's salt. Once synthesized, it could be studied by a variety of standard techniques from both the structural and the reactivity points of view.

## REFERENCES

1. K. von der Heide and K. A. Hofmann, Z. anorg. Chem., 12, 288 (1896).
2. E. Crepaz, Gazz. Chem. Ital., 58, 391 (1928).
3. K. N. Mikhalevich and A. N. Sergeeva, Nauch. Zapiski L'vov. Politekh. Inst., 22, 11 (1956). CA:52:13509<sup>b</sup> (1958).
4. A. Müller and P. Christophlien, Angew. Chem., Eng. ed., 8, 753 (1969).
5. J. W. Mellor, "A Comprehensive Treatise on Inorganic and Theoretical Chemistry," Vol. XI, Longmans, Green and Co., London, 1931.

## PROPOSITION V

## An Examination of Infrared Intensities of Coordination Compounds

The intensities of infrared bands in coordination compounds have not been adequately investigated for use as a practical tool. Cyano- and carbonyl-complexes which show large variations in band intensities are proposed as suitable compounds for examination of band intensities as a function of structural variables.

It is proposed that a detailed investigation of infrared epsilons and oscillator strengths be conducted on a large group of cyano- and carbonyl complexes to determine if quantitative measurement of infrared absorption intensity could develop into as useful a technique as band intensity data is for optical spectroscopy. The cyano and carbonyl complexes would be particularly convenient for these initial studies since water has sufficient transparency around  $2000\text{ cm}^{-1}$  to allow studies of solutions of cyanocomplexes and numerous solvents are available for carbonyl complexes

Since most spectra are taken in mulls or pellets, and since when solution spectra are taken, it is not a common practice to report either  $\epsilon$ 's or sufficient experimental details to allow  $\epsilon$  to be evaluated, very few data are available for comparisons at this time. The scattering of data which are available serve to indicate the wide range of band intensities encountered in cyano and carbonyl systems. Tabulated below are  $\epsilon$ 's for a few carbonyls. The hemoglobin data were obtained in water, while the others were obtained in iso-octane.

Compound	$\nu$ (cm <sup>-1</sup> )	$\epsilon$	$\epsilon/\text{CO}$
W(CO) <sub>6</sub> <sup>(1)</sup>	1983	100,000	16,700
	1950	2100	( <sup>13</sup> C)
Mo(CO) <sub>6</sub> <sup>(1)</sup>	1989	50,000	8300
	1957	780	( <sup>13</sup> C)
Cr(CO) <sub>6</sub> <sup>(1)</sup>	1987	30,000	5000
	1955	500	( <sup>13</sup> C)
W(CO) <sub>5</sub> (acetone) <sup>(1)</sup>	1933	1556	311
Carbonylhemoglobin	1951		≥ 800

A moderate amount of work has been done on organic carbonyl compounds, most of it relating to solvent effects. In one extensive study of intensities of N-methyl-benzamides and acetanilides<sup>(2)</sup> it was found that inductive effects controlled the position of the carbonyl bands, while mesomeric effects primarily controlled the intensity. In a similar study of aliphatic nitriles,<sup>(3)</sup> it was found that the intensity of the CN stretch was more sensitive to structural influence than was the position of the band. Significantly, the intensity of the CN stretch was found to increase to a limiting value for a six carbon chain, and remained at that limit for a series of longer chain nitrites. The same limit per CN was also found in a variety of dinitriles of the type (CH<sub>2</sub>)<sub>n</sub>(CN)<sub>2</sub> for six or more carbon atoms.

Much less work has been done on inorganic cyano complexes. The free cyanide ion has  $\epsilon = 29$  in aqueous solution. Coordinated cyanide, on the other hand, is usually much higher. A summary of available data is tabulated below.

<u>ion</u>	<u><math>\nu(\text{cm}^{-1})</math></u>	<u><math>\epsilon</math></u>	<u><math>\epsilon/\text{CN}</math></u>	<u>Ref</u>
$\text{CN}^-$	2080	29	29	4
$[\text{Ag}(\text{CN})_2]^-$	2135	264	132	4
$[\text{Ag}(\text{CN})_3]^{2-}$	2105	379	126	4
$[\text{Ag}(\text{CN})_4]^{3-}$	2092	556	139	4
$[\text{Cu}(\text{CN})_2]^-$	2125	165	83	5
$[\text{Cu}(\text{CN})_3]^{2-}$	2094	1090	363	5
$[\text{Cu}(\text{CN})_4]^{3-}$	2076	1657	414	5
$[\text{Zn}(\text{CN})_4]^{2-}$	2149	113	28	6
$[\text{Cd}(\text{CN})_4]^{2-}$	2140	75	19	6
$[\text{Hg}(\text{CN})_3]^-$	2161	26	9	6
$[\text{Hg}(\text{CN})_4]^{2-}$	2143	113	28	6
$[\text{Ni}(\text{CN})_4]^{2-}$	2124	1068	267	7
$[\text{Ni}(\text{CN})_5]^{3-}$	2102	1730	346	7
$[\text{Mo}(\text{CN})_7]^{4-}$	2080	930	130	
	2040	880	126	

$[\text{MoO}(\text{ON})(\text{CN})_4]^{3-}$	2169	38	10
	2088	1930	470
	2052	17	4
$[\text{Fe}(\text{CN})_5\text{NO}]$	1936	1580	316
	2142	659	132

Note that while Zn, Cd, and Hg tetracyanides have about the same  $\epsilon/\text{CN}$ , they differ greatly from  $\text{Cu}(\text{CN})_4^{3-}$  and  $\text{Ag}(\text{CN})_4^{3-}$  which differ between themselves.

An extremely interesting example of unusual intensity variations in cyanide stretching modes is provided by iron(III) ortho-phenanthroline-cyanide complexes.  $\text{K}[\text{Fe}(\text{o-phen})(\text{CN})_4]$  has the expected strong cyanide absorption near  $2100 \text{ cm}^{-1}$ , but in  $[\text{Fe}(\text{o-phen})_2(\text{CN})_2]\text{ClO}_4$  the CN stretch is so weak as to be unobservable at ordinary concentrations in KBr pellets. (8, 9) A similar effect is observed in the analogous bipyridyl complexes.

Several papers have appeared which have dealt with the theory of band intensities including a fairly detailed review. (10) Generally these discussions deal with the more fundamental, but practically less useful, integrated band intensity, and fail to establish useful correlations for the practicing spectroscopist.

## REFERENCES

1. Mark Wreighton, unpublished data, 1970.
2. H. W. Thompson and D. A. Jameson, Spectrochim. Acta, 13, 236 (1958).
3. J. P. Jesson and H. W. Thompson, Spectrochim. Acta, 13, 217 (1958).
4. L. H. Jones and R. A. Penneman, J. Chem. Phys., 22, 965 (1964).
5. R. A. Penneman and L. H. Jones, J. Chem. Phys., 24, 293 (1956).
6. R. A. Penneman and L. H. Jones, J. Inorg. Nucl. Chem., 20, 19 (1961).
7. R. L. McCullough, L. H. Jones, and R. A. Penneman, J. Inorg. Nucl. Chem., 13, 286 (1960).
8. A. A. Schilt, Inorg. Chem., 3, 1324 (1964).
9. Sadtler Research Laboratories, Inc., Philadelphia, Pa., "Infrared Spectra Collection: Inorganics and Related Compounds," Spectra Y615K and Y616K.
10. K. S. Seshadri and R. N. Jones, Spectrochim. Acta, 19, 1013 (1963).